

AUGMENTATION OF BOILING HEAT TRANSFER
BY INTERNALLY FINNED TUBES

by

VISWANATHAN SIVAKUMAR

B.E. (Hons.), University of Madras, Madras, India, 1980

A MASTER'S THESIS

submitted in partial fulfillment of

requirements for the degree

MASTER OF SCIENCE


Department of Mechanical Engineering

KANSAS STATE UNIVERSITY

Manhattan, Kansas

1982

Approved by:


Major Professor

SPEC
COLL
LD
2668
.T4
1982
S57
C.2

A11202 312713

TABLE OF CONTENTS

	Page
CHAPTER I. INTRODUCTION	1
CHAPTER II. LITERATURE SURVEY	5
CHAPTER III. EXPERIMENTAL INVESTIGATION	10
3.1 EXPERIMENTAL FACILITY	10
3.2 TEST SECTION	12
3.3 OPERATION OF EXPERIMENTAL FACILITY AND DATA ACQUISITION	20
CHAPTER IV. EXPERIMENTAL RESULTS	22
4.1 INTRODUCTION	22
4.2 HEAT TRANSFER RESULTS	24
4.3 PRESSURE DROP RESULTS	32
CHAPTER V. CORRELATION OF EXPERIMENTAL DATA	40
5.1 INTRODUCTION	40
5.2 HEAT TRANSFER	40
5.2.1 Smooth Tube Correlations	40
5.2.2 Existing Finned Tubes Correlations	55
5.2.3 New Finned Tubes Correlations	58
5.3 PRESSURE DROP	74
5.3.1 Smooth Tube Correlations	74
5.3.2 Existing Finned Tubes Correlations	77
5.3.3 New Finned Tubes Correlations for Saturated Boiling	79
CHAPTER VI. PERFORMANCE EVALUATION OF AUGMENTED TUBES	85
6.1 INTRODUCTION	85
6.2 PERFORMANCE INDICES	85
CHAPTER VII. SUMMARY, CONCLUSIONS AND RECOMMENDATIONS	89
Recommendations for Future Studies	90
ACKNOWLEDGEMENTS	91
SELECTED BIBLIOGRAPHY	92
NOMENCLATURE	96
APPENDIX A: SAMPLE OF DATA REDUCTION AND CALCULATION PROCEDURE OF HEAT TRANSFER COEFFICIENT	100

TABLE OF CONTENTS (cont.)

	Page
APPENDIX B: COMPUTER PROGRAM FOR DATA REDUCTION	103
APPENDIX C: REDUCED DATA	107
APPENDIX D: ADDITIONAL INFORMATION ON THE INSTRUMENTATION AND COMPONENTS USED IN THIS STUDY	116
1. R-113 FLOW CIRCUIT	116
A. Components	116
B. Instrumentation	117
2. WATER FLOW CIRCUIT	119
APPENDIX E: STATISTICAL INFORMATION FOR THE CURVE FITS TO THE EXPERIMENTAL DATA	120
APPENDIX F: UNCERTAINTY ANALYSIS IN EXPERIMENTAL MEASUREMENTS OF AVERAGE HEAT TRANSFER COEFFICIENTS	122
APPENDIX G: CALIBRATION OF PRESSURE TRANSDUCER	126

LIST OF FIGURES

Figure Number	Title	Page
1.1	Regions of Heat Transfer for Convective Boiling.	3
3.1	A Schematic Diagram for the R-113 Flow Circuit.	11
3.2	Photographic View of the Entire Test Facility.	13
3.3	Photograph of All the Tubes.	14
3.4	A Schematic Diagram of the Heating and Boiling Test Section.	16
3.5	Construction Details of One Transparent Section.	18
3.6	Pressure Tap Construction Details.	19
4.1	Experimental Overall Average Heat Transfer Coefficient Versus Mass Flux ($X_{out} = 0.17 - 0.231$).	26
4.2	Experimental Overall Average Heat Transfer Coefficient Versus Mass Flux ($X_{out} = 0.243 - 0.285$).	27
4.3	Experimental Overall Average Heat Transfer Coefficient Versus Mass Flux ($X_{out} = 0.295 - 0.332$).	28
4.4	Experimental Overall Average Heat Transfer Coefficient Versus Mass Flux ($X_{out} = 0.35 - 0.512$).	29
4.5	Experimental Overall Average Heat Transfer Coefficient Versus Mass Flux ($X_{out} = 0.576 - 0.815$).	30
4.6	Experimental Pressure Drop Versus Mass Flux ($X_{out} = 0.17 - 0.231$).	33
4.7	Experimental Pressure Drop Versus Mass Flux ($X_{out} = 0.243 - 0.285$).	34
4.8	Experimental Pressure Drop Versus Mass Flux ($X_{out} = 0.295 - 0.332$).	35
4.9	Experimental Pressure Drop Versus Mass Flux ($X_{out} = 0.35 - 0.512$).	36
4.10	Experimental Pressure Drop Versus Mass Flux ($X_{out} = 0.576 - 0.815$).	37
5.1	Comparison of Experimental Overall Average Heat Transfer Coefficients with Predictions of Pierre's Correlation, Eq. (5.3), Tube 1.	47

LIST OF FIGURES (cont.)

Figure Number	Title	Page
5.2	Comparison of Experimental Overall Average Heat Transfer Coefficients with Predictions of Dengler and Addoms Correlation, Eq. (5.4), Tube 1.	48
5.3	Comparison of Experimental Overall Average Heat Transfer Coefficients with Predictions of Guerrieri and Talty Correlation, Eq. (5.7), Tube 1.	49
5.4	Comparison of Experimental Overall Average Heat Transfer Coefficients with Predictions of Bennett et al. Correlation, Eq.(5.10), Tube 1.	50
5.5	Comparison of Experimental Overall Average Heat Transfer Coefficients with Predictions of Chen's Correlation, Eq.(5.12), Tube 1.	51
5.6	Comparison of Experimental Overall Average Heat Transfer Coefficients with Predictions of Shah's Correlation, Eq. (5.17), Tube 1.	52
5.7	Comparison of Experimental Overall Average Heat Transfer Coefficients with Predictions of Schrock and Grossman Correlation, Eq. (5.29), Tube 1.	53
5.8	Comparison of Experimental Overall Average Heat Transfer Coefficients with Predictions of Sani's Correlation, Eq. (5.30), Tube 1.	54
5.9	Cross Section of Internally Finned Tube.	57
5.10	Nusselt Number Versus the Pierre Parameter ($Re^2 Kf$).	59
5.11	Comparison of Experimental Values of Nusselt Number with Predictions of Modified Pierre's Type of Correlation, Eq. (5.46), Tube 2.	61
5.12	Comparison of Experimental Values of Nusselt Number with Predictions of Modified Pierre's Type of Correlation, Eq. (5.46), Tube 3.	62
5.13	Comparison of Experimental Values of Nusselt Number with Predictions of Modified Pierre's Type of Correlation, Eq. (5.46), Tube 4.	63
5.14	Comparison of Experimental Overall Average Heat Transfer Coefficients with Predictions of Modified Sani's Correlation, Eq. (5.48), Tube 2.	65

LIST OF FIGURES (cont.)

Figure Number	Title	Page
5.15	Comparison of Experimental Overall Average Heat Transfer Coefficients with Predictions of Modified Sani's Correlation, Eq. (5.48), Tube 3.	66
5.16	Comparison of Experimental Overall Average Heat Transfer Coefficients with Predictions of Modified Sani's Correlation, Eq. (5.48), Tube 4.	67
5.17	Comparison of Experimental Overall Average Heat Transfer Coefficients with Predictions of Eq. (5.51), Tube 1.	69
5.18	Comparison of Experimental Overall Average Heat Transfer Coefficients with Predictions of Eq. (5.55), Tube 2.	70
5.19	Comparison of Experimental Overall Average Heat Transfer Coefficients with Predictions of Eq. (5.55), Tube 3.	71
5.20	Comparison of Experimental Overall Average Heat Transfer Coefficients with Predictions of Eq. (5.55), Tube 4.	72
5.21	Comparison of Experimental Pressure Drop with Predicted Values Obtained from Pierre's Correlation, Eq. (5.56), Tube 1.	75
5.22	Comparisons of Experimental Pressure Drop with Predicted Values of Martinelli and Nelson's Correlation, Eq. (5.61), Tube 1.	78
5.23	Comparison of Experimental Values of Pressure Drop with Predicted Values of Modified Pierre's Correlation, Tube 1.	81
5.24	Comparison of Experimental Values of Pressure Drop with Predicted Values of Eq. (5.73), Tube 2.	82
5.25	Comparison of Experimental Values of Pressure Drop with Predicted Values of Eq. (5.73), Tube 3.	83
5.26	Comparison of Experimental Values of Pressure Drop with Predicted Values of Eq. (5.73), Tube 4.	84
6.1	Pumping Power per Unit Heat Transfer Rate Versus the Reynolds Number at $T_{in} = 120^{\circ}\text{F}$ (49°C).	87
G.1	Calibration Curve for Pressure Drop.	127

LIST OF TABLES

Table Number	Title	Page
3.1	Geometric Parameters of the Tubes Under Study	15
4.1	Ranges of Experimental Parameters Covered	23
4.2	Summary of Heat Transfer Enhancements of Finned Tubes Over Smooth Tubes	31
4.3	Summary of Increases in Pressure Drop	39
5.1	Computed Values of F_1 , F_2 , F_3 , and F_4	58
C.1	Reduced Data	108
C.2	Reduced Data	112
E.1	Tabulation of Statistical Information for the Curve Fits to the Experimental Overall Heat Transfer Coefficient	120
E.2	Tabulation of Statistical Information for the Curve Fits to the Experimental Overall Pressure Drop	121

CHAPTER I

INTRODUCTION

Vertical tube evaporators have been used in numerous industrial equipment since 1877. A number of investigators have explored the use of different techniques to augment the heat transfer of evaporators and therefore improve their performance. Augmentation of heat transfer in these evaporators leads to a reduction in their size and hence a reduction in their cost. According to a survey conducted by Bergles [1], it was estimated that investment in heat exchanger equipment in the U.S. would approach 1 billion dollars annually in the next few years and savings in the 10 million dollar range could be obtained with 10-20% reduction in capital cost.

In general, a lot of emphasis is being placed these days on optimizing the performance of heat exchangers. Therefore, an accurate knowledge of the heat transfer coefficients and pressure drop is mandatory, before optimization can be achieved. The following factors have to be taken into consideration when choosing a particular augmentation technique: capital cost, development cost, operating cost, safety, reliability, and maintenance cost.

The number of augmentation techniques, which are being investigated is increasing. These include fluid vibration, electrostatic fields, surface vibration, fluid additives, surface promoters, swirl flow generators and displaced promoters. Heat transfer enhancement by surface promoters and swirl flow generators, has been found to be most promising. The displaced promoters have an inherent disadvantage, in that they are

difficult to install inside tubes and produce large pressure drops. Swirl flow can be achieved by using coiled tubes, propellers, spiral fins and twisted tapes. It has been realized in recent years that spiral fins produce a better fin effect when compared to twisted tape inserts.

The main concern of the present study was to investigate the augmentation of saturated boiling heat transfer by internally finned tubes.

Flow Regimes for Boiling Heat Transfer

Figure 1.1 shows the various heat transfer regimes encountered in a vertical tube, heated uniformly over its length and fed with subcooled liquid at its base. In region A the process of heat transfer is single phase convective heat transfer to the liquid phase. In this region, the liquid is being heated up to the saturation temperature and the wall temperature remains below that necessary for nucleation. The heat transfer mechanism in region B is known as subcooled nucleate boiling, with vapor formation taking place in the presence of subcooled liquid. In this region, the mean bulk fluid temperature is increasing to the saturation temperature, whilst the wall temperature remains essentially constant, a few degrees above the saturation temperature. The liquid reaches the saturation temperature in the transition region between B and C, where subcooled nucleate boiling regions exist. The quality increases through the saturated nucleate boiling region and a point may be reached where a transition in the mechanism of heat transfer occurs. The process of "evaporation" replaces the process of "boiling". A change in flow pattern from bubbly or slug flow to annular flow takes place before the transition can occur, as represented by regions E and F. Evaporation occurs in the liquid film-vapor core interface, due to heat transfer by forced convection from the wall. In the forced convective region, nucleation is

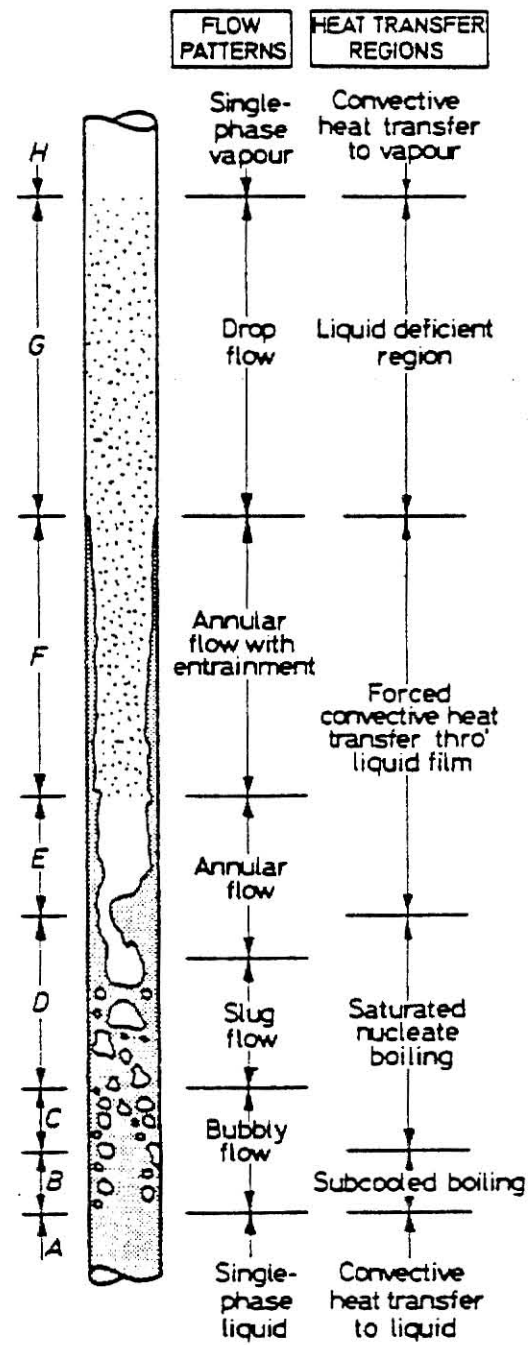


Fig.1.1 Regions of heat transfer for convective boiling

completely suppressed and the regions E and F are referred to as the two phase forced convective region of heat transfer.

The complete evaporation of the liquid film occurs at some critical value of the quality. This region is termed the liquid deficient region, corresponding to region G in Fig. 1.1 and is accompanied by a rise in the wall temperature for channels operating with a controlled surface heat flux. A transition to dry saturated vapor takes place in region H. A condition known as "dryout" occurs in the liquid deficient region. It often limits the amount of evaporation that can take place in a tube at a particular value of heat flux. "Dryout" is an extremely important phenomenon in the design of pipe stills, evaporators, nuclear reactors and boilers.

It is an established fact the heat transfer characteristics depend on the flow regime. The heat transfer regime encountered in the present experimental investigation was chosen to be in the saturated nucleate boiling region.

CHAPTER II

LITERATURE SURVEY

A bibliography of world literature on augmentation was published by Bergles et al. [2] in 1979. Over 1900 references were cited in this bibliography. A similar bibliography was published by Bergles and Webb [3] in 1970. It included 472 references. For the purpose of the present study, only the references relevant to augmentation of single phase and boiling heat transfer by internally finned tubes will be reviewed.

Boling et al. [4] reported that evaporator performance could be considerably improved by using fins within the refrigerant flow passage.

Bernstein et al. [5] investigated the performance of once through zero gravity boiler tubes, with two phase water flow. The different tube configurations used in the experiment, included internally finned tubes. It was reported that the boiler tubes with some device to turbulate or baffle the fluid, displayed a remarkable improvement in heat transfer, over a straight round tube. Most of the boiler pressure drop was found to occur in the high quality regime.

Kidd [6] analysed the heat transfer and pressure drop characteristics of gas flow inside spirally corrugated tubes. The results showed that spirally corrugated tubes were very effective in enhancing the heat transfer.

Lipets [7] analysed the hydraulic resistance and the temperature regime of tubes with internal longitudinal fins. Experiments proved the efficiency of internal fins in reducing the wall temperatures of superheaters.

Watkinson et al. [8] investigated the heat transfer and pressure drop

characteristics of integral inner fin tubes, in turbulent water flow. Based on inside tube diameter and nominal area, the heat transfer was enhanced up to 170% over the smooth tube values, at constant Reynolds number in the range of 100,000 to 150,000. Fin spiralling was reported to have led to a considerable improvement in performance, under both constant flow and constant pumping power conditions.

Wither and Habdas [9] investigated the heat transfer characteristics of helically corrugated tubes for in-tube boiling of refrigerant-12, in the temperature range of 30° to 50°F and over the full vaporization range. They reported that the integral, internal helical ridging resulted in doubling or tripling of the in-tube boiling film coefficient of heat transfer, and increased full vaporization heat flux by up to 200% over the peak burnout flux for the plain tube.

Ornatskiy et al. [10] presented a method for calculating the temperature of a pipe with internal fins, trapezoidal or rectangular. This method also helped in rationally selecting the geometry of the finned surfaces.

Watkinson et al. [11] reported heat transfer and pressure drop measurements for eighteen internally finned tubes in turbulent air flow. Heat transfer enhancements varied from 17 to 95%, over smooth tube values, at a Reynolds number of 50,000, based on the inside diameter. At constant pumping power, the performance of spiral fin tubes increased with the inter fin spacing to pitch ratio. For straight fin tubes, the performance was relatively insensitive to the inter fin spacing to equivalent diameter ratio.

Masliyah and Nandakumar [12, 13, 14] analytically studied the heat transfer characteristics for laminar forced convection, fully developed flow in an internally finned circular tube, with axially uniform heat

flux and with peripherally uniform temperature, using finite element method. The Nusselt number based on inside tube diameter was higher than that for a smooth tube. They reported that, for maximum heat transfer, there exists an optimum fin number for a given fin configuration.

Soliman and Feingold [15] investigated the performance of quintuplex internally finned tubes. They reported that remarkably compact heat transfer equipment could be produced with quintuplex tubes, when compared with similar smooth tube heat exchangers. However, this would be possible only at the expense of increasing the pumping power. The authors recommended quintuplex tubes when the size of the heat transfer equipment is to be kept to a minimum. But for applications where a certain amount of heat is to be transferred with minimum pumping power expenditure, the single finned tube proved to be the best choice.

Vander Mast et al. [16] used sea water in falling film evaporators and reported that the boiling mechanism is one of evaporation at the continuous liquid-vapor interface, with little nucleation. It was found that spirally corrugated tubes had better heat transfer characteristics than smooth tubes.

Van Rooyen and Kröger [17] investigated the heat transfer and pressure drop characteristics for laminar flow of oil in smooth and internally finned tubes with twisted tape inserts. The heat transfer coefficients in finned tubes with twisted tape inserts were found to be as much as four times the smooth tube values, when cooling at the same pumping power, and three times in the case of heating.

Marner and Bergles [18] carried out experimental studies on augmenting the heat transfer in horizontal tubes under laminar flow conditions. Tests were conducted with twisted tape inserts, internally finned tubes

and static mixer assemblies. Based on constant pumping power performance, the internally finned tube looked especially promising for cooling as well as heating.

Patankar et al. [19] analysed the turbulent flow and heat transfer characteristics of circular tubes and annuli with longitudinal internal fins. The analysis was based on the differential equations for momentum and energy conservation, in the flowing fluid, supplemented by a turbulence model having an adjustable constant. Average Nusselt numbers and friction factors were evaluated for a range of Reynolds numbers, fin heights and number of fins. The results were found to be quite insensitive both to fin height and to the number of fins.

Minchenko and Shvartsman [20] presented the results of an experimental investigation of the optimum geometry of internally helical finned steam generator tubes. They demonstrated the high thermal efficiency of the finned tubes in sub and supercritical pressure steam generators. The study showed that the placing of helical fins with optimum geometries in steam generating tubes allowed the designer to reduce the mass flow rate by approximately a factor of two, with corresponding reduction in pumping losses.

Kubanek and Milette [21] conducted heat transfer and pressure drop studies on three spiral finned tubes with two phase flow of R-22 under evaporating conditions. They compared the results with and without a star shaped insert. Heat transfer enhancements for internally finned tubes ranged from 30 to 760% over those for the smooth tubes and increased with mass velocity. Pressure drop increases ranged from 10 to 290%. It was concluded that internally finned tubes should prove beneficial in the design of compact direct expansion water chillers and other equipment in which the refrigerant is evaporated inside the tube to cool a fluid on

the outside.

Carnavos [22] determined experimentally the heat transfer performance for heating water in turbulent flow, having integral internal spiral and longitudinal fins. The best performers were the tubes with the higher helix angles and internal heat transfer surface relative to a smooth tube. Also, Carnavos [23, 24] investigated the heat transfer performance for cooling air in turbulent flow with 21 tubes having integral spiral and longitudinal fins. The finned tubes were found to perform better by factors of 1.2 - 2.0.

Soliman et al. [25] presented an analysis for fully developed, laminar, convective heat transfer in tubes with internal longitudinal fins and uniform outside temperature. They reported that the various fins were more effective than the unfinned surfaces, based on average heat transfer per unit area.

The literature survey revealed that the effect of internally finned tubes in augmenting the saturated boiling heat transfer was not fully investigated. The present study was directed towards this objective.

CHAPTER III

EXPERIMENTAL INVESTIGATION

The primary objectives of this experimental investigation were:

- i) To obtain experimental heat transfer and pressure drop data during forced flow of saturated boiling inside vertical tubes with and without internal fins.
- ii) To develop design correlations for predicting the heat transfer and pressure drop during boiling for the finned tubes.

The test fluid used was R-113.

3.1 EXPERIMENTAL FACILITY

Figure 3.1 shows a schematic diagram of the R-113 flow loop. It included the following main components:

- i) Gear pump for circulating the liquid.
- ii) Preheaters.
- iii) Observation section located at inlet to test section.
- iv) Four, parallel, vertically mounted, electrically heated boiler tubes. One tube was smooth, the second had straight fins on the inside, the third and fourth tubes had spiral fins.
- v) Condenser.
- vi) Liquid receiver.
- vii) Liquid flow meters.

R-113 was pumped from the liquid receiver to the test section through the preheater, which was used to control the inlet temperature to the test section. The test sections were electrically heated, well instrumented to measure the outside wall temperatures, at different locations along the test section.

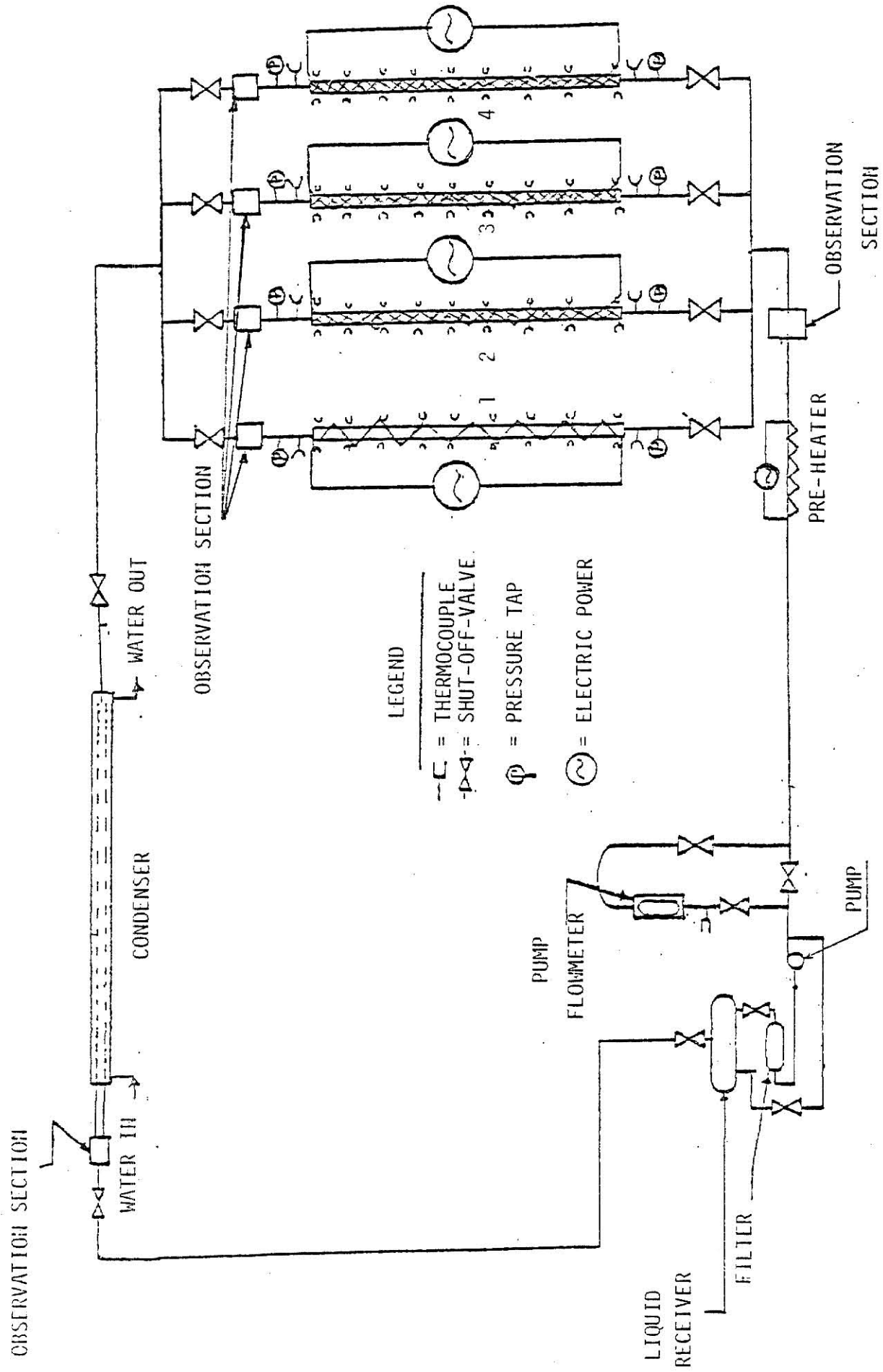


Fig. 3.1 A Schematic Diagram for the R-113 Flow Circuit.

The flow meter was used to measure the total flow rate of the R-113 entering the test section.

All temperatures were measured by copper constantan thermocouples of type RIP-24. All wall thermocouples were connected to a data acquisition system which gave a printout of the readings along the test section. A Honeywell Electronic-18, multichannel potentiometer was also used to measure separately the inlet and exit temperatures of R-113 to each test section.

The pressure drop across the test section was measured by a pressure transducer along with a digital voltmeter. A photographic view of the entire test facility is given in Fig. 3.2.

3.2 TEST SECTION

The following tubes were tested: a smooth tube, tube 1, a straight finned tube, tube 2, and two spiral finned tubes with different helix angles and outside diameters, tubes 3 and 4. The geometric parameters of these tubes are given in Table 3.1. A photographic view of all the tubes tested is given in Fig. 3.3.

The four tubes were mounted vertically, in parallel, in the test facility as shown in Fig. 3.1. Each test tube was instrumented to measure the wall surface temperatures at equidistant axial locations. At each location two thermocouples were silver-brazed to the surface opposite each other. The distance between the two thermocouple stations at the top and the bottom was half the distance between the intermediate stations. The test tube was also instrumented to measure the inlet and outlet temperature of R-113 and the pressure drop along its length. Figure 3.4 gives additional details about the construction of each test tube. After attaching the thermocouples each tube was wrapped with teflon

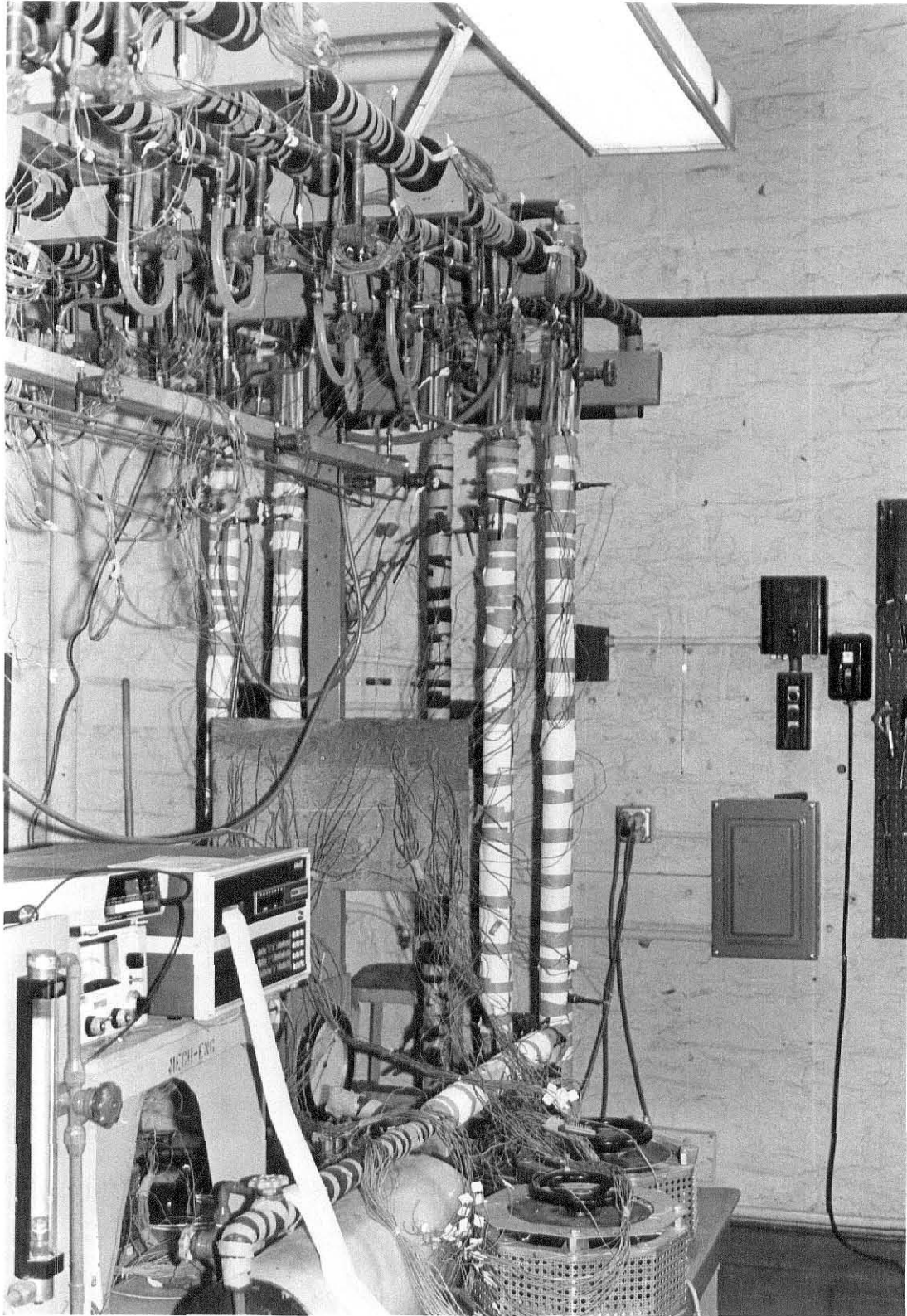


Fig. 3.2 Photographic View of the Entire Test Facility.

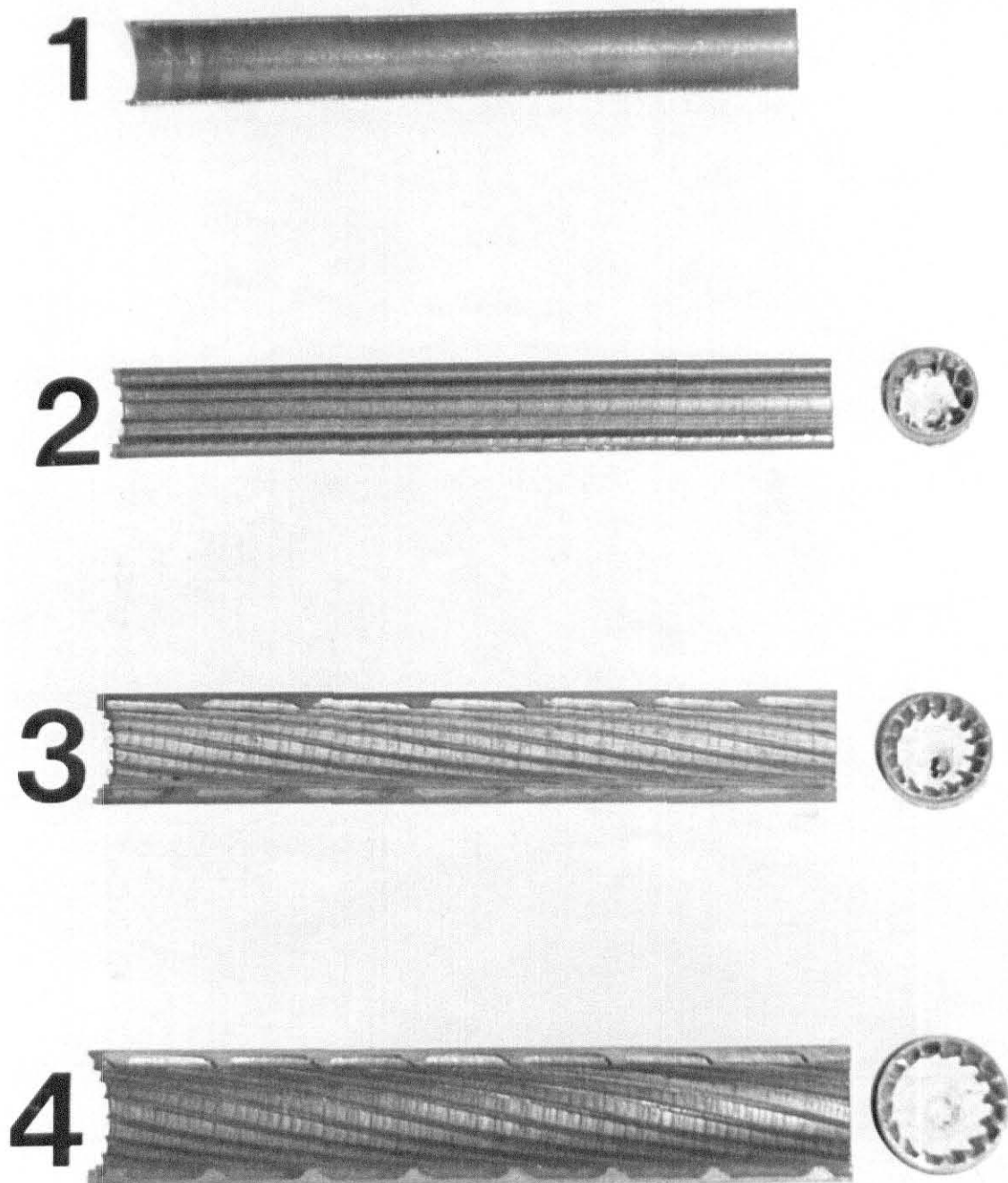


Fig. 3.3 Photograph of all the Tubes.

TABLE 3.1. Geometric Parameters of the Tubes Under Study
(All Values in Cm.)

Tube No.	1	2	3	4
Type	Smooth	Straight Finned	Spiral Finned	Spiral Finned
Material	Cu	Cu	Cu	Cu
Length	133.5	135.89	134.62	133.5
No. of fins, n	-	10	32	16
Outside diameter, D_o	1.5875	1.5850	1.5875	2.2162
Inside diameter, D_i	1.3843	1.4199	1.4707	2.0384
Equivalent diameter, D_e	1.3843	1.3600	1.4028	1.9870
Hydraulic diameter, D_h	1.3843	0.8530	0.6772	1.1300
Fin Height, b	-	0.1575	0.0686	0.1981
Wall thickness	0.1016	0.0826	0.0463	0.0889
Fin Height/Inside diameter	-	0.1109	0.0466	0.0972
Actual flow area, A_{fa}^{**}	1.5050	1.4527	1.5455	3.1009
Nominal flow area, A_{fn}^{**}	1.5050	1.5835	1.6988	3.2634
Core flow area, A_{fc}^{**}	-	0.9588	1.3966	2.1181
Actual area, A_a^{**}	4.3489	6.6800	9.1292	11.3000
Nominal Area, A_n^{**}	4.3489	4.4607	4.6203	6.4038
Inter-fin spacing, W	-	0.297	0.102	0.305
Helix Angle, α	-	0^0	16.2^0	12.34^0
Pitch, cm/360 0	-	ST	30.48	20.3

* all lengths and areas are in cm and cm² respectively, as appropriate.

** area in cm²

** area in cm²/cm

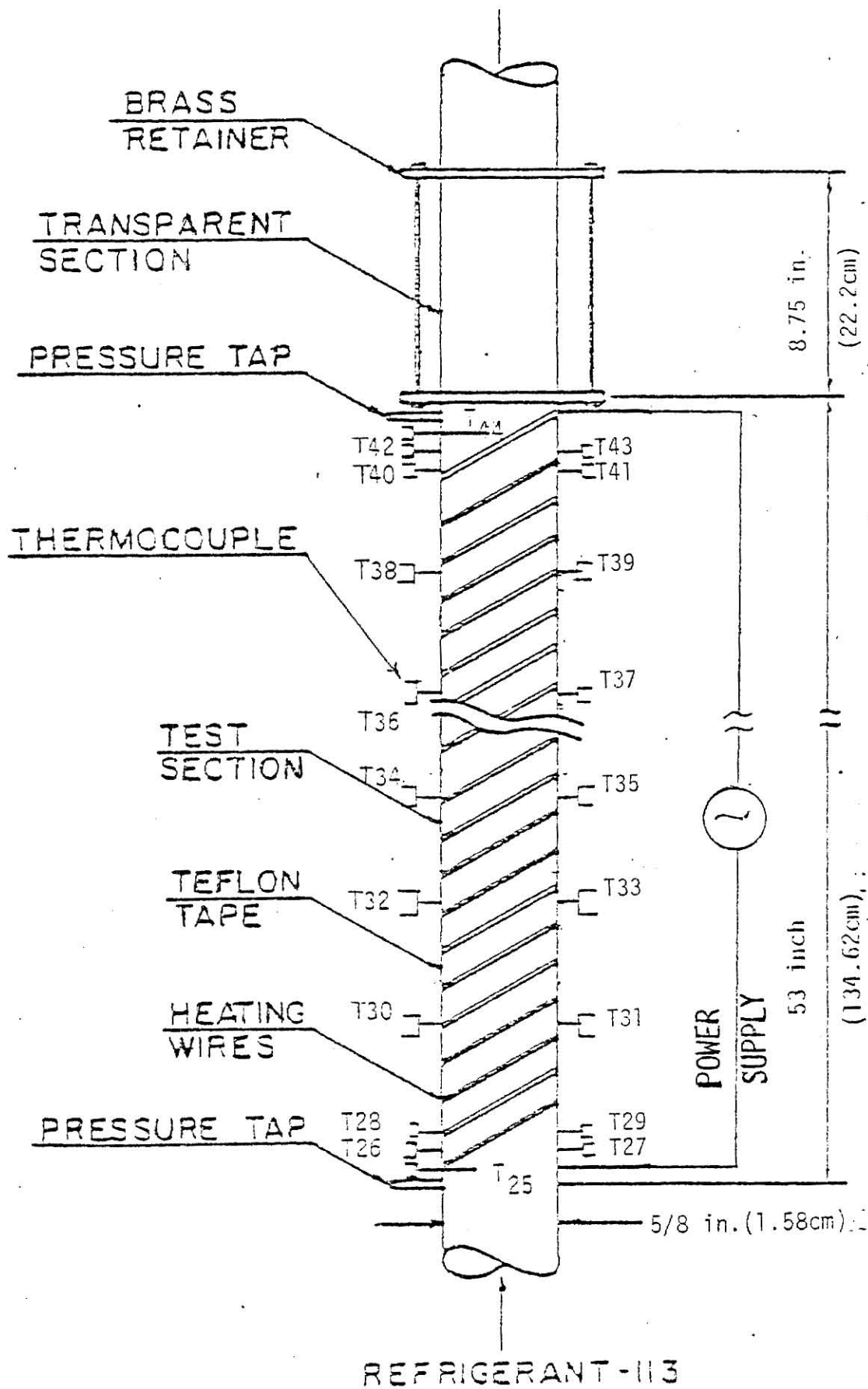


Fig. 3.4 A Schematic Diagram of the Heating and Boiling Test Section.

tape on the outside, in order to insulate the heating element from the surface of the tube. Heating was accomplished by a ribbon-type Chromel heating element, which was wound uniformly on the teflon tape. The heating element was then coated with a layer of epoxy resin to hold it onto the tube, and a second layer of teflon tape was again wound over the resin. The entire test section was then insulated with 6.25 cm thick fiberglass insulation to prevent any heat losses to the atmosphere. The exit of each test section had a transparent glass section attached to it. There was also another transparent observation section at the inlet to the test sections, which was used in observing the flow regime of R-113 as it entered the test section. The transparent sections were made of standard, clear, high pressure glass tubing. The construction details of the transparent section are shown in Fig. 3.5.

The construction details of the pressure taps are shown in Fig. 3.6. Four holes $1/16$ in (0.002m) diameter each and spaced 90° apart, around the circumference of the tube, were drilled in the test section. The holes were then covered with a copper sleeve, whose inner diameter was approximately equal to the outside diameter of the boiler tube plus $3/16$ in (0.005m). The copper sleeve was silver brazed to the tube and a hole was drilled in it to accommodate a short copper tube $1/8$ in (0.003m) I.D. The two pressure taps, at the top and the bottom, were connected to the pressure transducer by means of two separate pieces of tubing which were connected to the short copper tubes. There existed the possibility that the hole drilled for the pressure tap either went through a fin or the space between the fins. The above arrangement minimized this possibility and produced an averaging effect at the pressure taps.

The pressure drop across the pressure taps was measured by a Pace

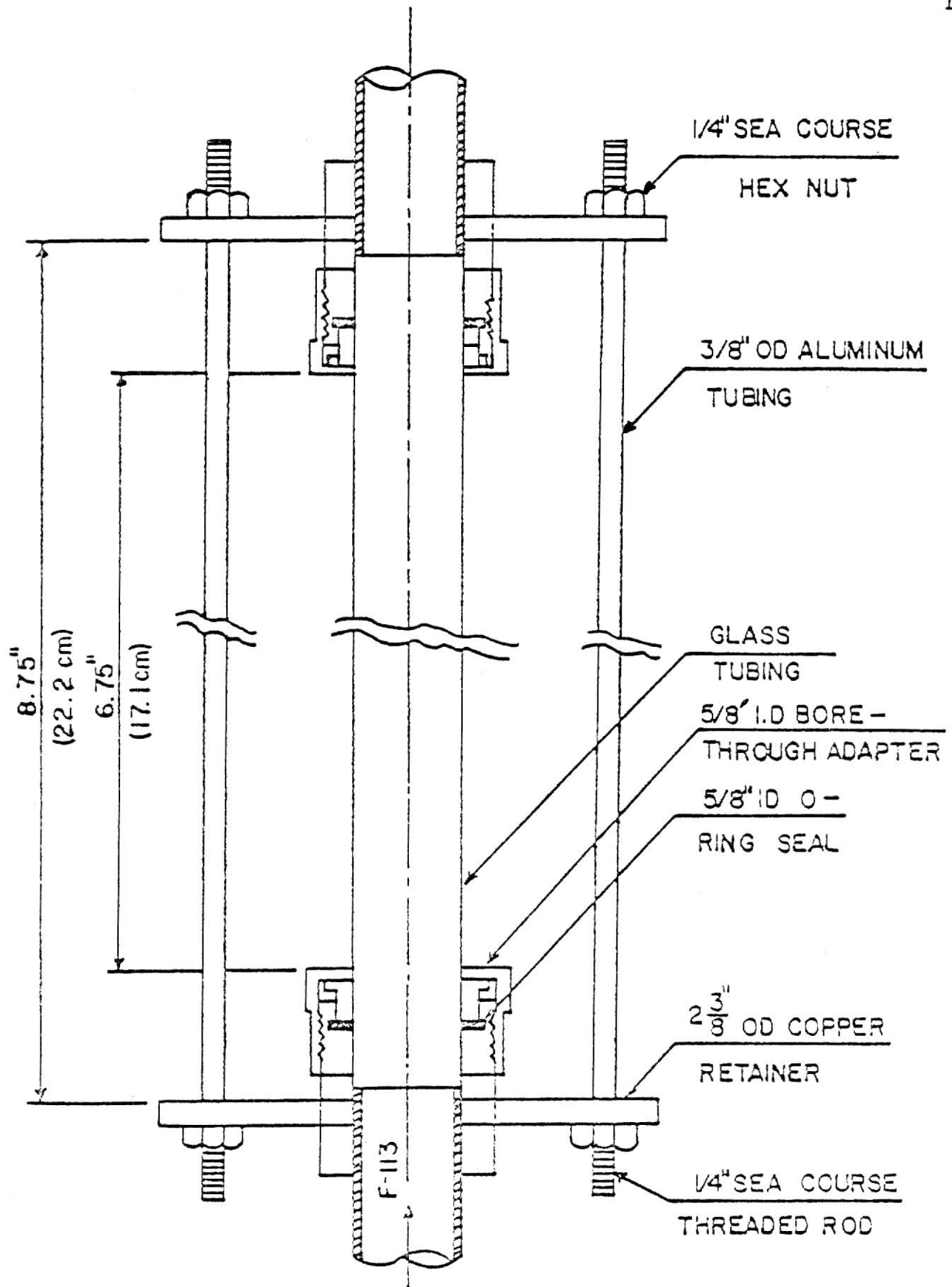


Fig. 3.5 Construction Details of One Transparent Section.

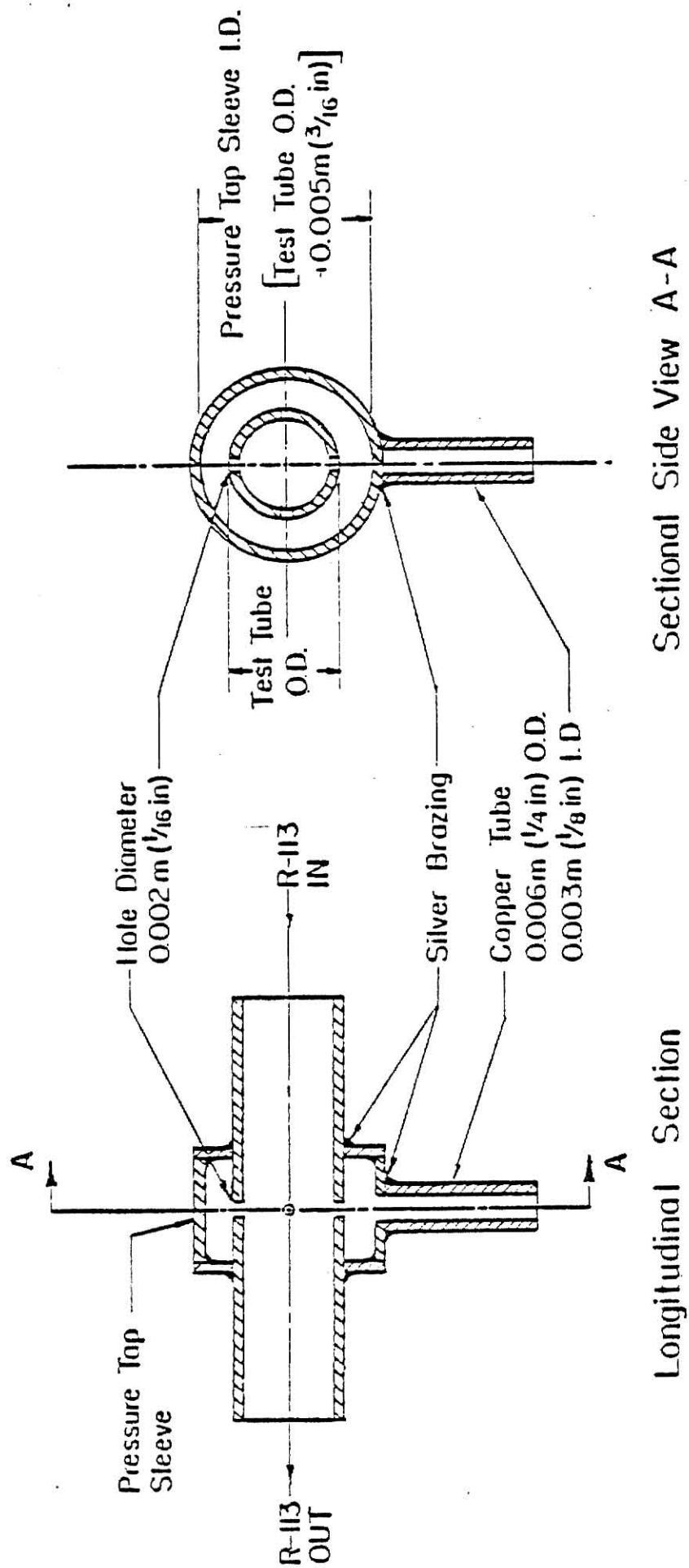


Fig. 3.6 Pressure Tap Construction Details

Wianco pressure transducer model KP15, which was connected to a Pace Wianco digital indicator, model CD25. It was calibrated using a dead weight tester. The calibration curve for the pressure transducer is given in Appendix G, Fig. G.1.

The flow rate of the refrigerant was measured by two Fisher and Porter variable area flow meters, which were mounted vertically in parallel, to be used individually or simultaneously to measure the flow rate.

The power input to the boiling test section and the preheaters was controlled by means of a variable transformer and the voltage and current across each heating circuit were measured by a digital voltmeter and a digital clamp-on ammeter, respectively. Additional details about the instrumentation used is given in Appendix D.

3.3 OPERATION OF EXPERIMENTAL FACILITY AND DATA ACQUISITION

After installation, the system was checked for leaks under pressurized and evacuated conditions. It was then evacuated down to 1000 microns of Hg by a vacuum pump. The liquid receiver was then filled to the top with R-113 before the final evacuation process was started. It was then isolated from the rest of the system. The system was then evacuated down again to 1000 microns of Hg.

The water pump was then put into operation and the flow rate adjusted to any desired level. The liquid freon was pumped from the liquid receiver through the flow meter and the preheater to the test section, by adjusting the proper valves. The flow rate of R-113 was adjusted to the desired value and the electrical power was then gradually and simultaneously applied to the preheater and the test section until equality of the inlet and outlet temperatures of R-113 in the test tube was achieved. The equality of the inlet and outlet temperature was accompanied by single phase

liquid entering and boiling fluid leaving the test section. This procedure ensured that saturated conditions were maintained throughout the test tube. For each experimental run, steady state condition was established when the readings of all temperatures, pressures and flow rates remained steady for a period of at least two hours.

During each experimental run, the following measurements were taken:

i) The inlet and outlet temperatures of R-113 in the test section, in m.v. $^{\circ}\text{C}$ ($^{\circ}\text{F}$).

ii) The temperatures of the eighteen thermo couples attached to the outer wall of the boiling section in $^{\circ}\text{C}$ ($^{\circ}\text{F}$).

iii) The flow rate of refrigerant into the test section in gpm.

iv) Inlet gauge pressure of R-113, entering the test section, in psig.

v) Pressure drop across the test section in m.v. (psi).

vi) The readings of the voltmeter and ammeter connected to the test section in volts and amps, respectively.

vii) The atmospheric temperature, in $^{\circ}\text{F}$.

Before the saturated boiling experiments were run, it was felt essential to carry out a heat balance test for single phase flow, for every flow rate tested, to test the performance of the test facility. The heat balance calculation was based on the heat input and the heat gained by the freon, taking into consideration the conduction losses at the top and bottom. If the heat balance error was within $\pm 6\%$, data for saturated boiling were taken for this particular flow rate. In such runs, the electrical power input, adjusted for the conduction end losses of the tube, was used to calculate the boiling heat transfer coefficient.

CHAPTER IV

EXPERIMENTAL RESULTS

4.1 INTRODUCTION

Experimental data were obtained for the smooth and the three finned tubes. Thirty-two readings were taken with the smooth tube (tube 1); twenty-eight with the straight finned tube (tube 2); nineteen with the spiral finned tube (tube 3); and seventeen with the spiral finned tube (tube 4). The heat transfer and pressure drop results formed the major focus of the study. The main parameters that were varied were the mass flow rate, the heat flux input, and the saturated boiling temperature. The ranges of experimental parameters are given in Table 4.1.

The average heat transfer coefficient for the entire test section for all the tubes, was calculated from

$$h_i = \frac{Q}{A\Delta T} = \frac{Q}{(\pi * D_i * L) * (T_{WL} - T_{av})} \quad (4.1)$$

where Q represents the electric input to the test section; D_i represents the inner diameter of the test tube; L represents the length of the test section between the points, where the electrical heat input was supplied; T_{WL} represents the average inside wall temperature along the test section and T_{av} is the average of the inlet and outlet temperatures of R-113. The average inside wall temperature T_{WL} was obtained from the average outside surface temperature of the test tube (= arithmetic average of all outside surface thermocouples) and the temperature drop across the tube wall. This temperature drop was obtained from the one dimensional heat conduction equation for a cylinder.

TABLE 4.1. Ranges of Experimental Parameters Covered

Refrigerant's Mass Flux (based on nominal inside area)	44.48(32850.46) - 183.94(135847.10) $\frac{\text{KG}}{\text{s-m}^2}$ (lbm/hr - ft ²)
Overall Heat Transfer Coefficient	1716.27(302.27) - 9511.13(1675.08) W/m ² °C (Btu/hr ft ² °F)
Overall Heat Flux	5073.27(1614.51) - 13217.90(4206.44) W/m ² (Btu/hr ft ²)
Saturation Temperature	47.20(116.96) - 63.21(145.77) °C (°F)
Outlet Quality	0.1114 - 0.8150

As was mentioned earlier, the heat input to the preheater and the test section were adjusted, such that the inlet and outlet temperatures were the same and no boiling was observed at the inlet observation section, while boiling was observed at the exit section. This guaranteed that R-113 entered as saturated liquid and left as partially boiled at the same temperature.

A sample of the calculation procedure is given in Appendix A.

4.2 HEAT TRANSFER RESULTS

The overall average heat transfer coefficients at various exit quality ranges are plotted versus the mass flux in Figs. 4.1 through 4.5 for all tubes tested. The heat transfer coefficient was found to increase with mass flux, in all the ranges of exit conditions, for all the tubes. The results were correlated by the following equation:

$$\bar{h} = c G^n \quad (4.2)$$

where c and n are constants obtained using the least square regression analysis. Their values are given in Table E.1 in Appendix E.

With the increase in mass flow rate it can be seen that the heat transfer coefficient increased at a faster rate in the spiral finned tube 3, when compared to the other tubes.

The enhancements in heat transfer obtained with tubes 2 and 3 compared to tube 1, at three selected values of mass flux and different ranges of exit dryness fraction, are given in Table 4.2. Tube 4 was not included in this comparison due to the fact the mass fluxes in the table could not be covered.

The percentage enhancement was calculated from the following ratio:

LEGEND

TUBE 1 --(*)-----> SMOOTH TUBE(.624in.O.D)

TUBE 2 --(+)-----> STRAIGHT FINNED TUBE(.624in.O.D)

TUBE 3 --(o)-----> SPIRAL FINNED TUBE(.625in.O.D)

TUBE 4 --(^)-----> SPIRAL FINNED TUBE(.8725in.O.D)

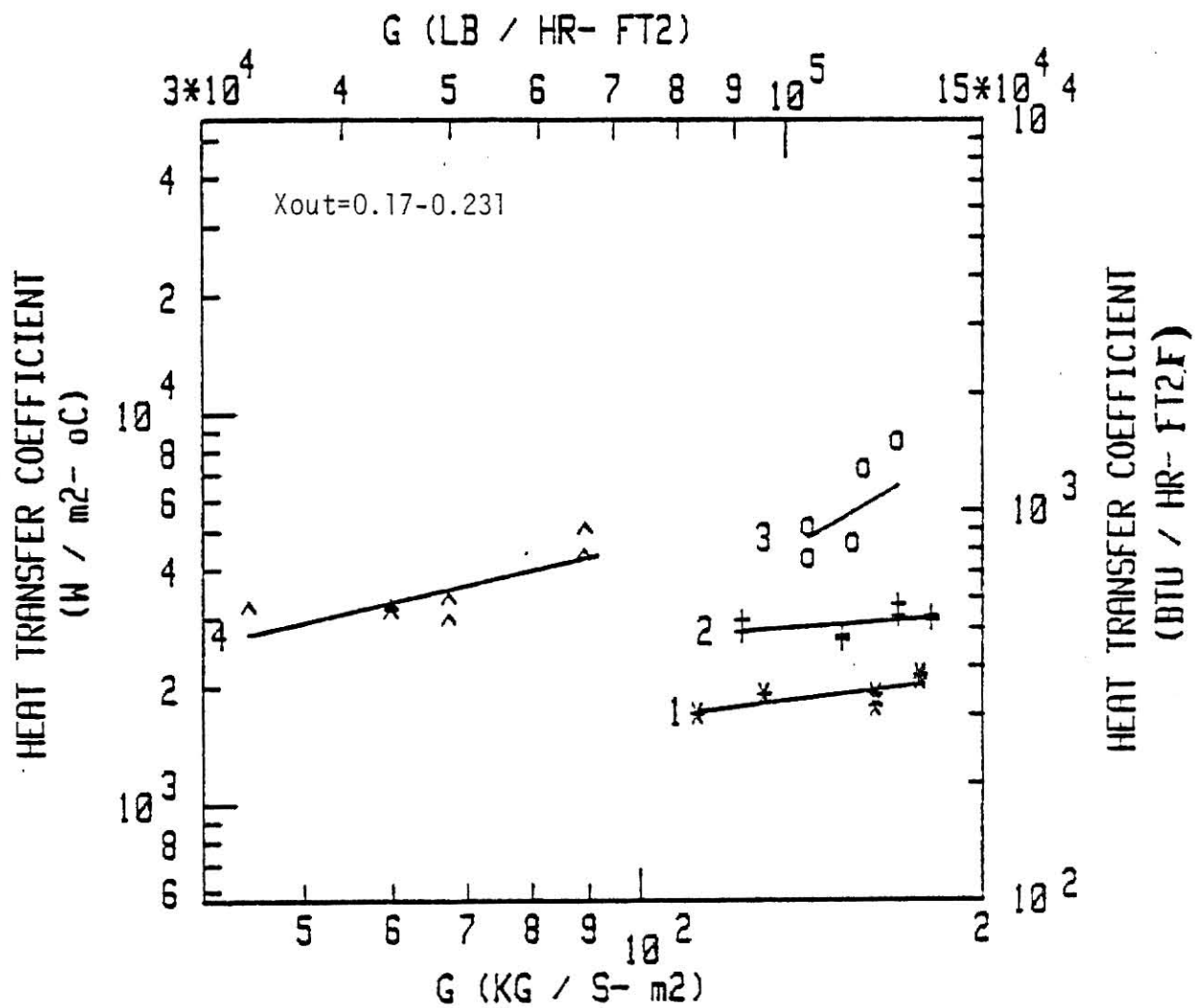


Fig. 4.1 Experimental Overall Average Heat Transfer Coefficients Versus Mass Flux, (Xout=0.17-0.231).

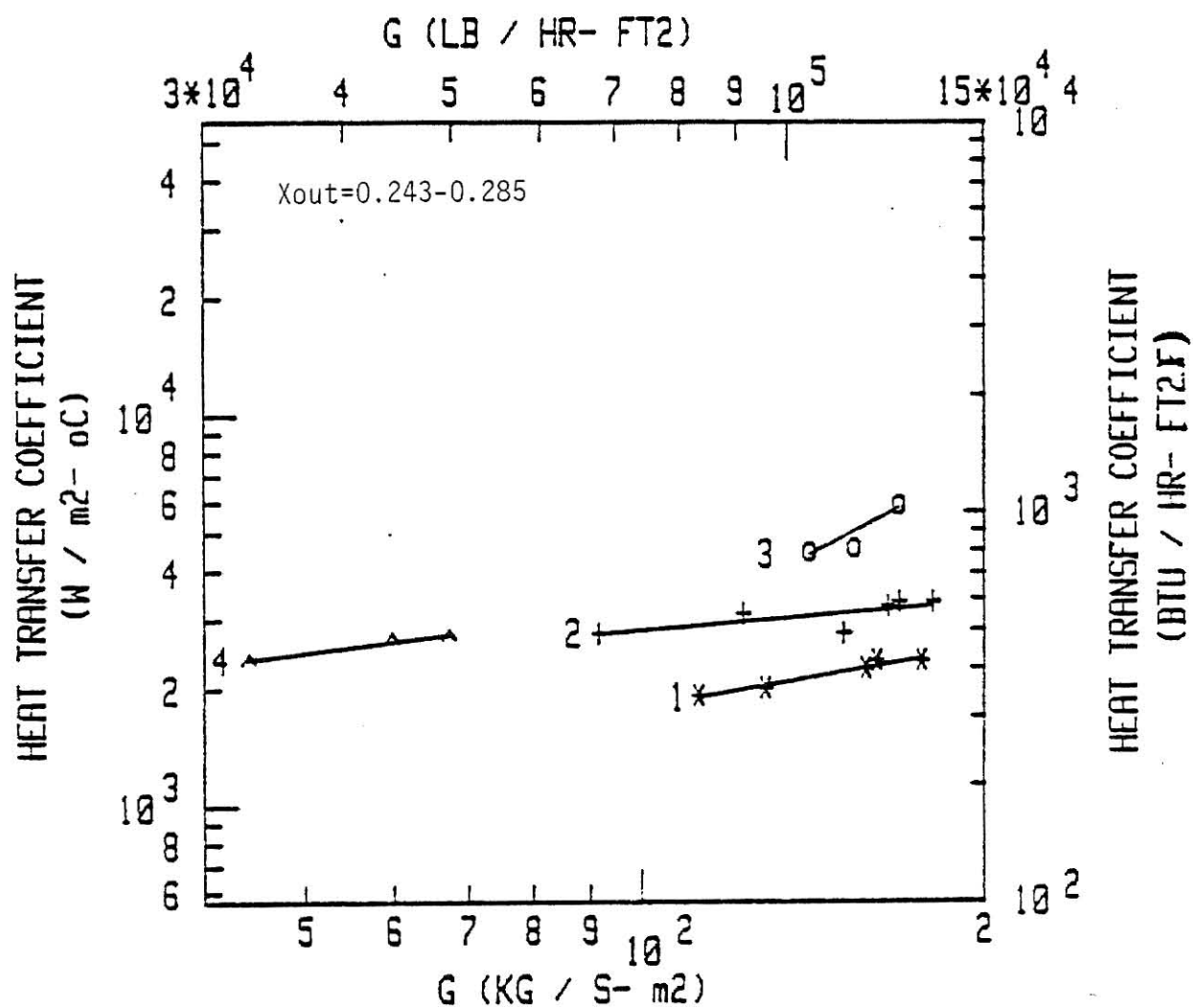


Fig. 4.2 Experimental Overall Average Heat Transfer Coefficients Versus Mass Flux, (X_{out}=0.243-0.285).

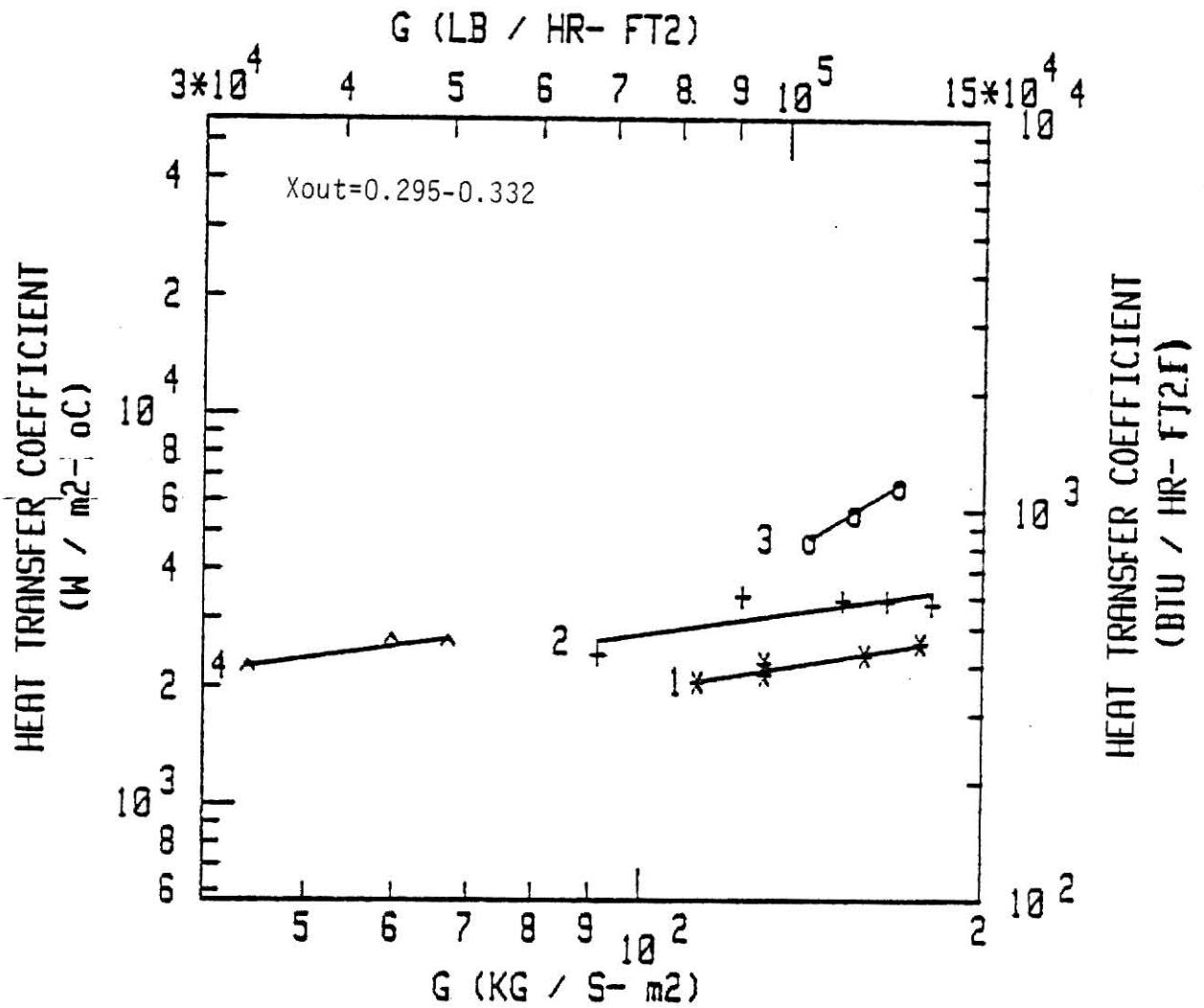


Fig. 4.3 Experimental Overall Average Heat Transfer Coefficients Versus Mass Flux, ($X_{out}=0.295-0.332$).

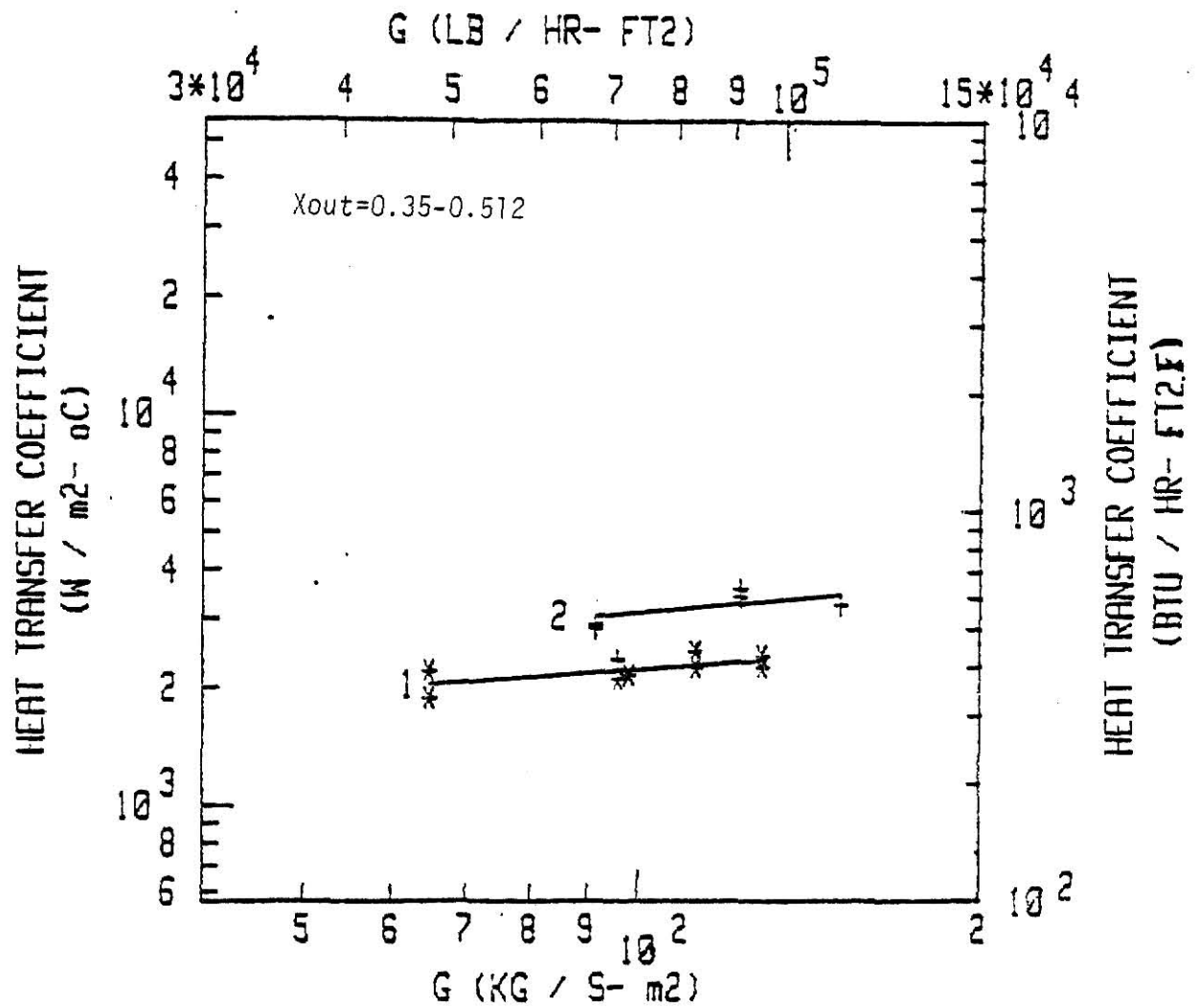


Fig. 4.4 Experimental Overall Average Heat Transfer Coefficients Versus Mass Flux, ($X_{out}=0.35-0.512$).

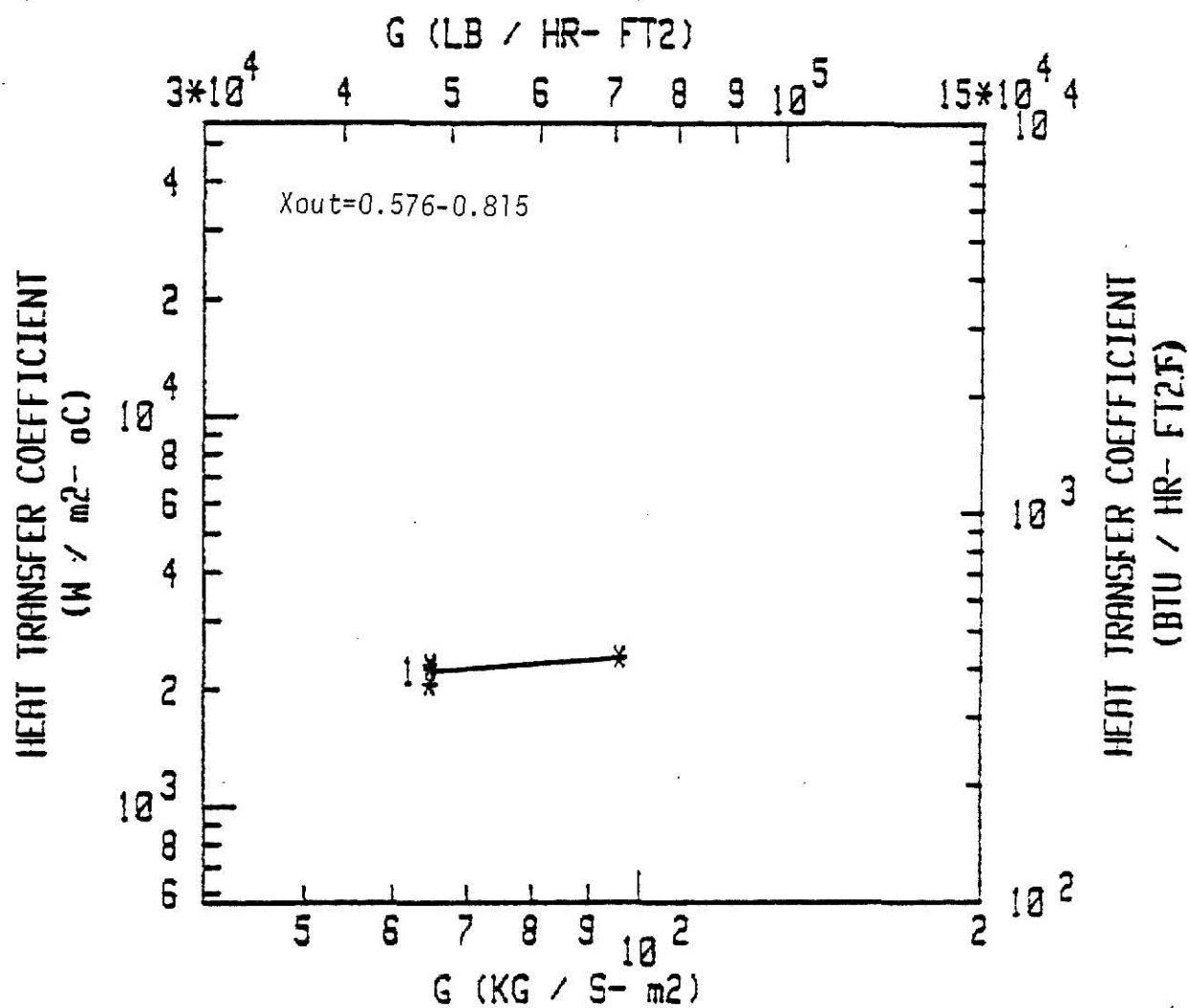


Fig. 4.5 Experimental Overall Average Heat Transfer Coefficients Versus Mass Flux, ($X_{out} = 0.576 - 0.815$).

TABLE 4.2. Summary of Heat Transfer Enhancements of
Finned Tubes Over Smooth Tubes

Tube No.	Refrigerant's Quality Change ΔX	% Heat Transfer Enhancement at Different Mass Velocities, lb/hr ft ²		
		80,000	100,000	130,000
1) Tube 2	0.17 - 0.231	59	54	48
Tube 3		75	134	230
2) Tube 2	0.243 - 0.285	53	45	35
Tube 3		57	97	156
3) Tube 2	0.295 - 0.332	39	37	35
Tube 3		48	97	175

$$\% \text{ Enhancement} = \frac{(\bar{h} \text{ finned tube} - \bar{h} \text{ smooth tube}) \times 100\%}{\bar{h} \text{ smooth tube}} \quad (4.3)$$

Straight finned tube (tube 2)

The enhancement in heat transfer decreased with increase in mass flow rate and the above trend was found to hold true for all the exit dryness fraction ranges covered.

There was a maximum enhancement of 59% and a minimum value of 35%.

Spiral finned tube (tube 3)

The heat transfer enhancement increased with increase in mass flow rate. A maximum enhancement of 230% was attained with the minimum value being 48%.

The highest enhancements in heat transfer coefficients were obtained with the spiral finned tube (tube 3).

Thus it can be seen that the enhancement of heat transfer by tube 3 was better than the enhancement of the straight finned tube (tube 2), despite the fact that both had the same outside diameter and length. However, tube 3 had 32 fins compared to 10 for tube 2. Also, the fins of tube 3 were spiral and resulted in vortex flow which caused a considerable increase in heat transfer.

4.3 PRESSURE DROP RESULTS

The two phase pressure drop, which includes both friction and acceleration pressure drop terms, is plotted versus the mass flux in Figs. 4.6 through 4.10, for different ranges of exit qualities.

The pressure drop was found to increase with mass flux in all the tubes considered, over the different exit quality ranges.

The maximum pressure drop values were obtained in the straight finned

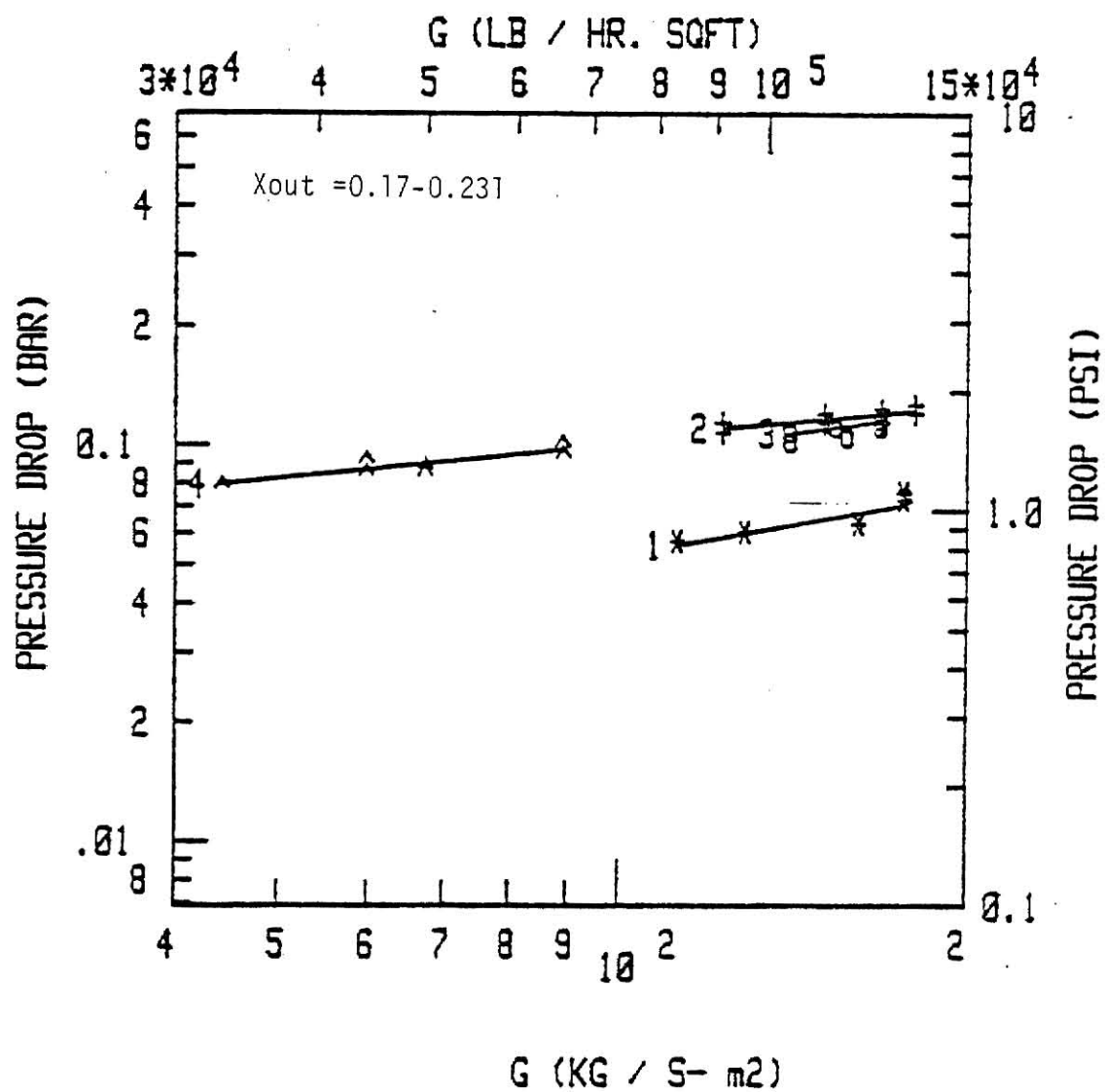


Fig. 4.6 Experimental Pressure Drop Versus Mass Flux ,
($X_{out} = 0.17-0.231$).

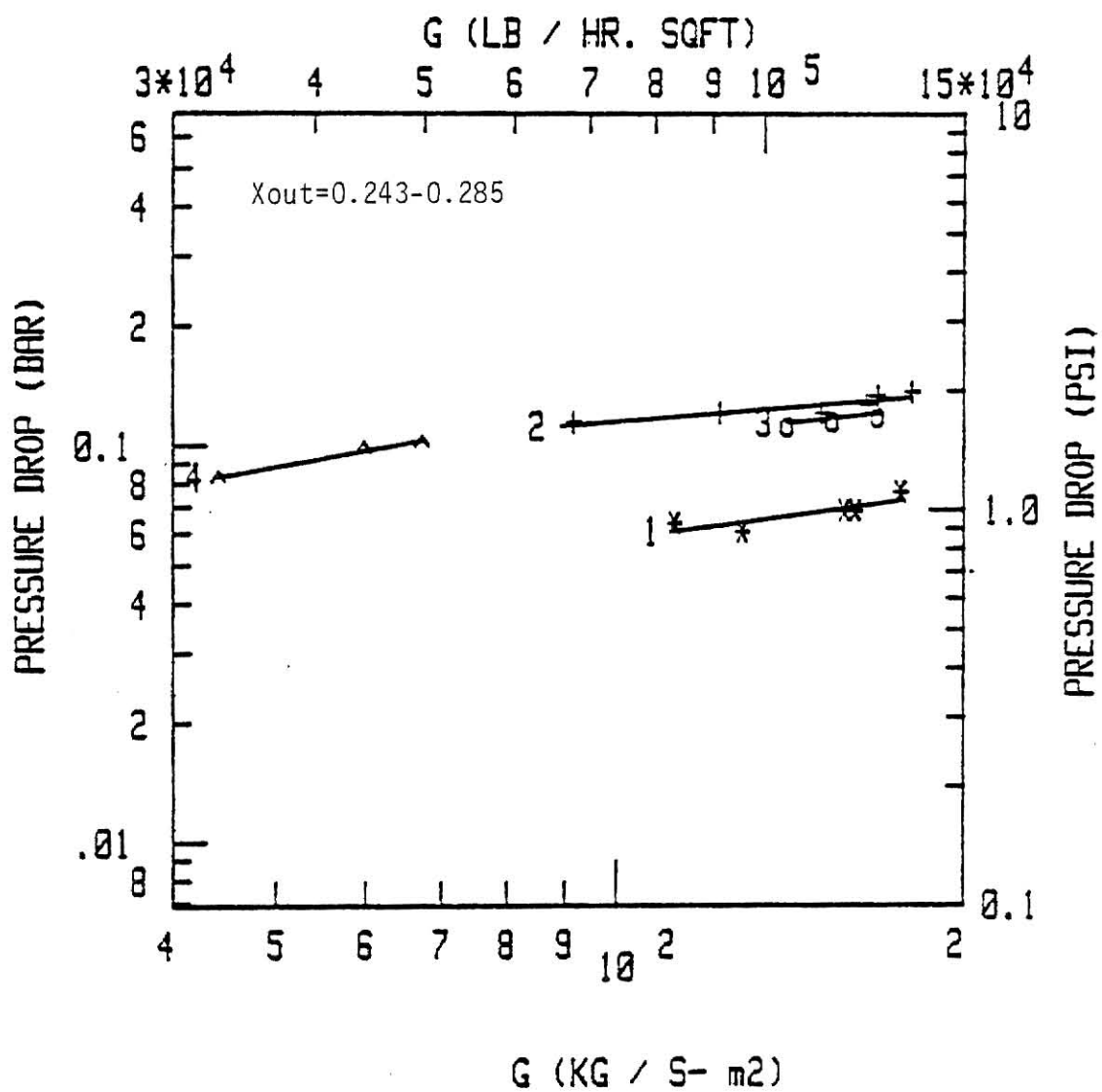


Fig. 4.7 Experimental Pressure Drop Versus Mass Flux,
($X_{out} = 0.243-0.285$).

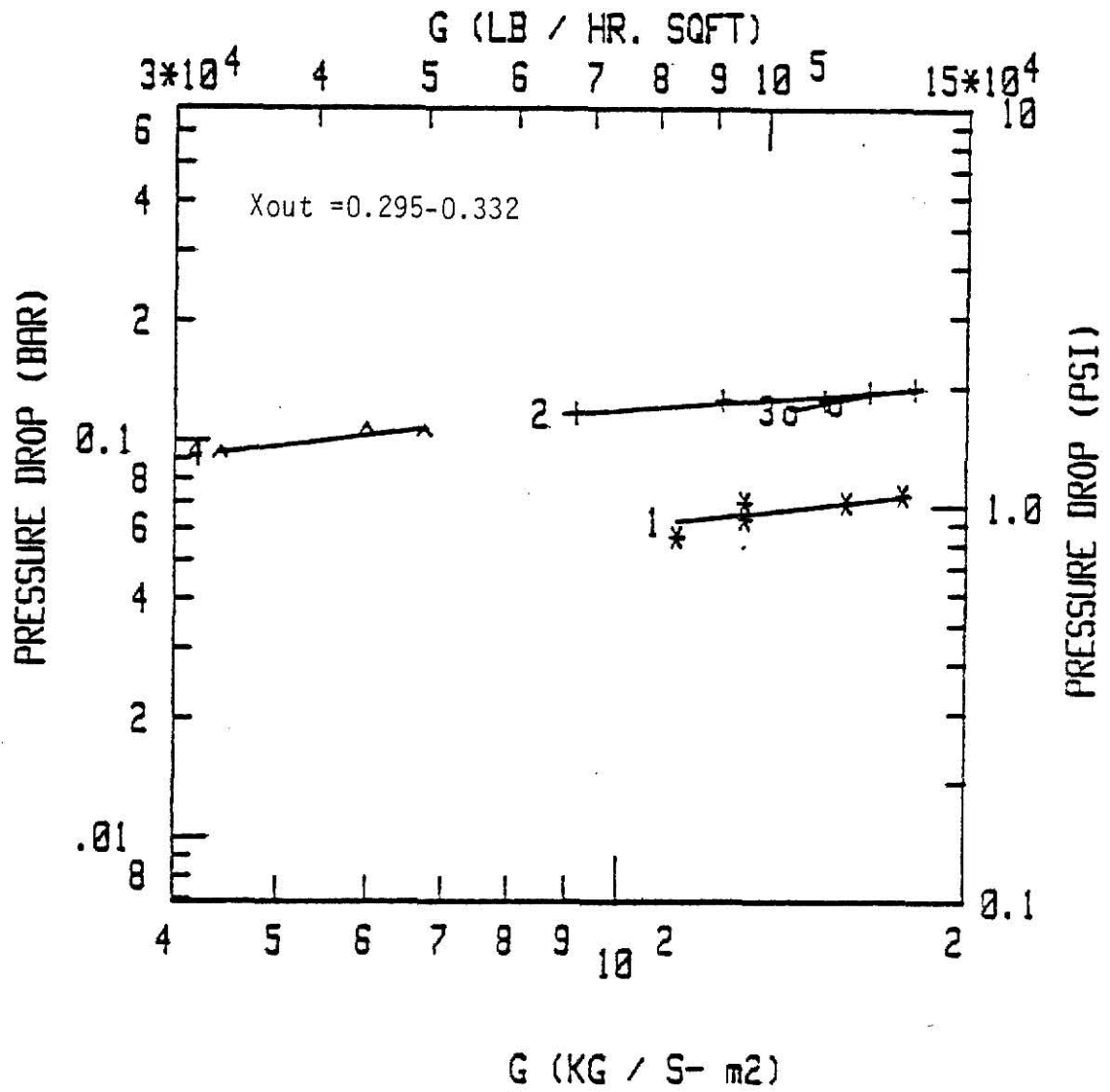


Fig. 4.8 Experimental Pressure Drop Versus Mass Flux ,
($X_{out} = 0.295-0.332$).

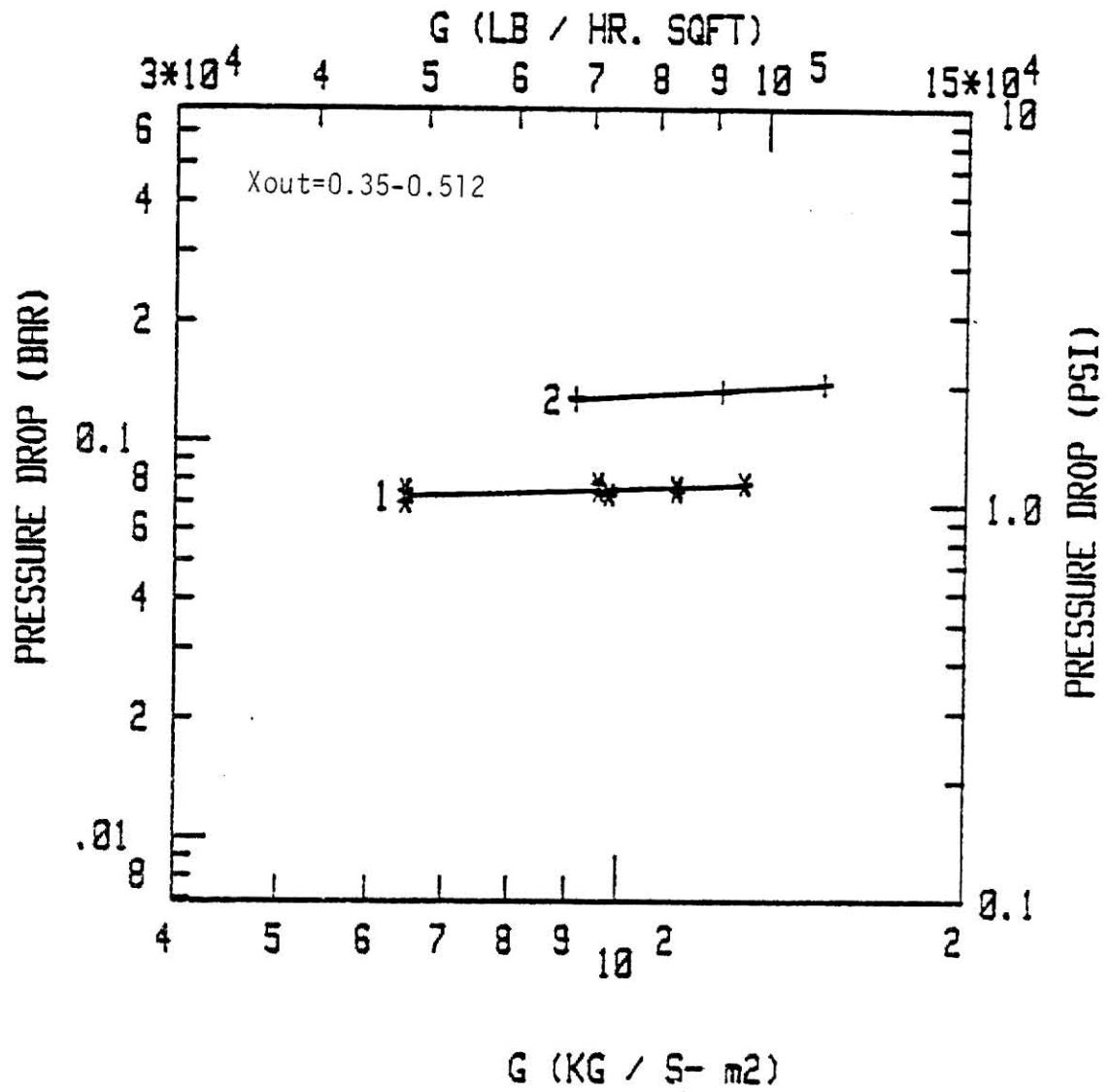


Fig. 4.9 Experimental Pressure Drop Versus Mass Flux ,
($X_{out} = 0.35-0.512$).

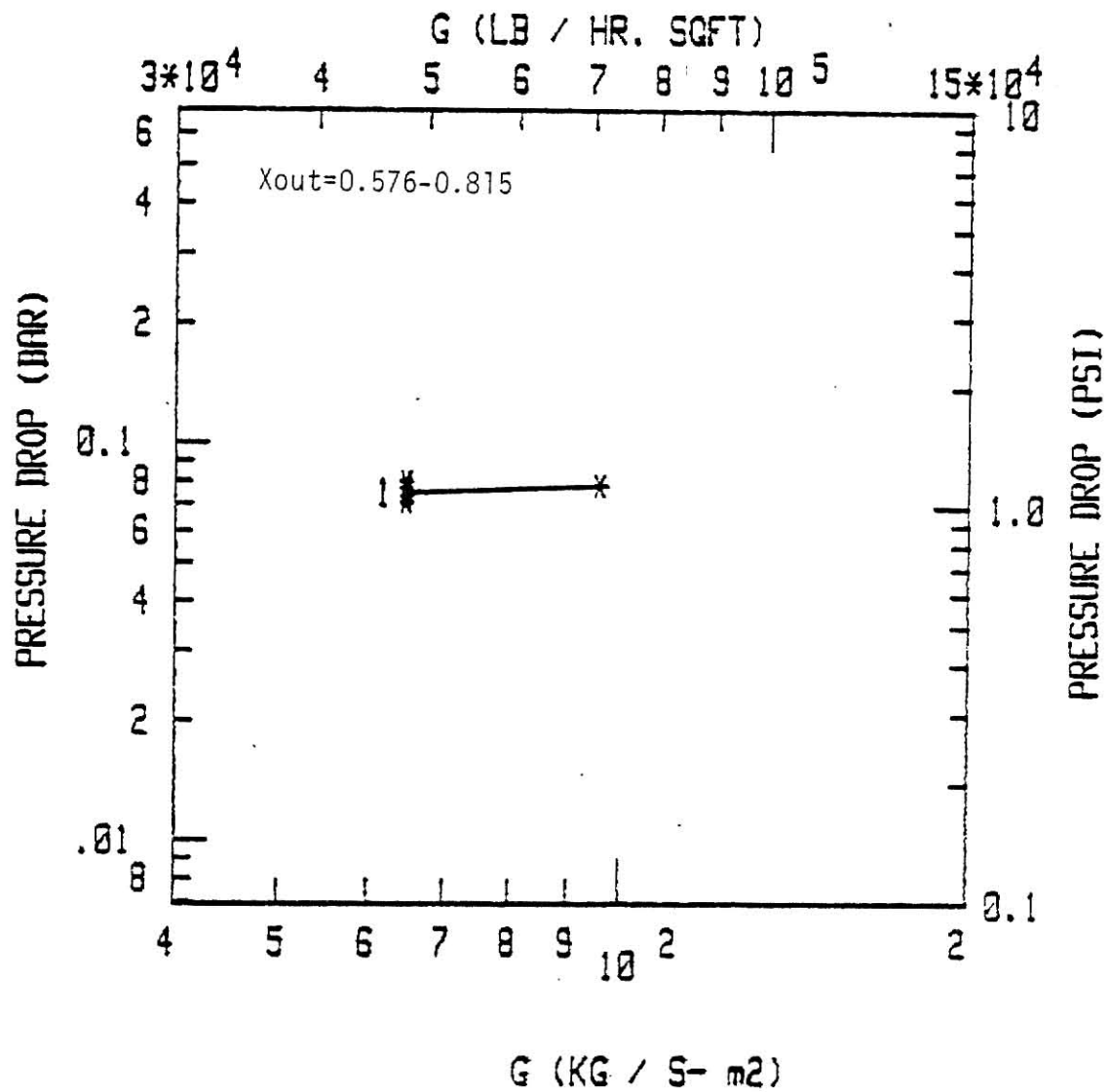


Fig.4.10 Experimental Pressure Drop Versus Mass Flux ,
($X_{out} = 0.576-0.815$).

tube (tube 2), when compared to the other tubes, with the pressure drop increases ranging from 72% to 107% over that of the smooth tube. The spiral finned tube (tube 3) gave pressure drop values that were 66% to 84% higher than the smooth tube.

The pressure drop results were correlated by the following equation:

$$\Delta P = C' G^{n'} \quad (4.4)$$

where C' and n' are given in Table E.2 of Appendix E.

Table 4.3 gives the percentage increase in the pressure drop values of tubes 2 and 3, over the smooth tube (tube 1).

The percentage increase in pressure drop for the three arbitrarily selected mass fluxes was calculated from the following relation:

$$\% \text{ Increase in } \Delta P = \frac{(\Delta P_{\text{finned tube}} - \Delta P_{\text{smooth tube}}) \times 100\%}{\Delta P_{\text{smooth tube}}} \quad (4.5)$$

The ΔP values were obtained from the correlating equations for the different ranges of exit qualities and for the selected values of the mass flux.

TABLE 4.3. Summary of Increases in Pressure Drop

Tube No.	ΔX	% Pressure Drop Increase at Different Mass Velocities, lb/hr. sq.ft.		
		80,000	100,000	180,000
1)	0.170 - 0.231			
Tube 2		95	85	72
Tube 3		76	71	66
2)	0.243 - 0.285			
Tube 2		96	89	81
Tube 3		78	74	69
3)	0.295 - 0.332			
Tube 2		107	95	82
Tube 3		76	80	84

CHAPTER V

CORRELATION OF EXPERIMENTAL DATA

5.1 INTRODUCTION

Design correlations were developed for predicting the heat transfer and pressure drop during saturated boiling inside internally finned tubes. This was achieved by first identifying correlations for predicting the heat transfer and pressure drop inside smooth tubes. Modifiers, based on the geometric parameters of the finned tubes, were then identified and applied to the smooth tube correlations to bring about the best agreement between the experimental measurements and predictions of the modified correlations.

5.2 HEAT TRANSFER

5.2.1 Smooth Tube Correlations

The literature survey showed that there are several correlations available for predicting the two phase local and/or overall average heat transfer coefficients during boiling inside tubes. None of the available correlations seem to predict well the data of different investigators.

A summary of these correlations follows.

The following equation was recommended by Pierre [26] for calculating the average heat transfer coefficient of evaporating refrigerants in a horizontal tube.

$$Nu = 0.00097 (Re^2 k_f)^{0.5} \quad (5.1)$$

valid for $(10^9 \leq Re^2 k_f \leq 0.7 \times 10^{12})$

where,

$$k_f = J \Delta X h_{fg} \frac{g_c}{Lg} \quad (5.2)$$

$$Re_L = GD_i / \mu_L$$

From the above equation for Nusselt number, the average \bar{h} is given by:

$$\bar{h}_{TP} = 0.00097 (Re^2 k_f)^{0.5} \frac{k_L}{D_i} \quad (5.3)$$

The local heat transfer correlation of Dengler and Addoms [27] is given by

$$h_{TP} = \frac{3.5}{(x_{tt})^{0.5}} h_L' \quad (5.4)$$

where h_L' is obtained from Dittus Boelter equation.

$$h_L' = 0.023 \frac{k_L}{D_i} \left(\frac{D_i G}{\mu_L} \right)^{0.8} \left(\frac{C_{pL} \mu_L}{K_L} \right)^{0.4} \quad (5.5)$$

for turbulent single phase fluid flow, and,

$$x_{tt} = \left(\frac{1-x}{x} \right)^{0.9} \left(\frac{\mu_L}{\mu_g} \right)^{0.1} \left(\frac{V_f}{V_g} \right)^{0.5} \quad (5.6)$$

The correlation suggested by Guerrieri and Talty [28] is given by

$$h_{TP} = 3.4 \left(\frac{1}{x_{tt}} \right)^{0.45} h_L \quad (5.7)$$

where,

$$h_L = 0.023 * \frac{k_L}{D_i} \left[D_i \frac{G(1-x)}{\mu_L} \right]^{0.8} \left(\frac{C_{pL} \mu_L}{k_L} \right)^{0.4} \quad (5.8)$$

The effect of nucleate boiling superimposed on convective heat transfer was accounted for by a nucleate boiling correction factor:

$$\text{NBCF} = 0.187 \left(\frac{r^*}{\delta} \right)^{-5/9} \quad (5.9)$$

where, r^* = radius of bubble, δ = liquid film thickness.

One limit of the above equation is that NBCF cannot be less than unity. This limit occurs at $\frac{r^*}{\delta}$ equal to 0.049. A value of $\frac{r^*}{\delta}$ greater than 0.049 is physically interpreted to mean that the liquid is moving swiftly enough to prevent bubble nucleation in the wall cavities at the existing film temperature difference.

Bennett et al. [29] suggested the following correlation for local two phase heat transfer coefficient, due to forced convective boiling.

$$\frac{h_{TP}}{h_{L'}} = 0.64 \left(\frac{1}{x_{tt}} \right)^{0.74} \times \left(\frac{q}{A} \right)^{0.11} \quad (5.10)$$

where,

$$h_{L'} = (1-x)^{0.8} \left[0.023 \left(\frac{GD}{\mu_L} \right)^{0.8} Pr_L^{0.4} \frac{k_L}{D_i} \right] \quad (5.11)$$

The local heat transfer coefficient correlation of Chen [30] is given by

$$h_{TP} = h_{mac} + h_{mic} \quad (5.12)$$

h_{mac} = contribution due to convection, h_{mic} = contribution due to nucleate boiling.

$$h_{mac} = 0.023 \left[\frac{G(1-x)D}{\mu_L} \right]^{0.8} Pr_L^{0.4} \left(\frac{k_L}{D} \right) F \quad (5.13)$$

where,

$$F = \begin{cases} 1 & \text{for } \frac{1}{x_{tt}} \leq 0.1 \\ 2.35 \left(\frac{1}{x_{tt}} + 0.213 \right)^{0.736} & \text{for } \frac{1}{x_{tt}} > 0.1 \end{cases} \quad (5.14)$$

and,

$$h_{mic} = \frac{0.00122 k_L^{0.79} c_p^{0.45} \rho_L^{0.49} \Delta T_{SAT}^{0.24} \Delta P_{SAT}^{0.75}}{\sigma^{0.5} \mu_L^{0.29} h_{fg}^{0.24} \rho_g^{0.24}} S \quad (5.15)$$

S = suppression factor (which is the ratio of the mean superheat seen by the growing bubble to the wall superheat T_{SAT})

S is approximated by

$$S = 1 / [1 + 2.53 \times 10^{-6} (Re_L \times F^{1.25})] \quad (5.16)$$

where F is given by Eq. (5.14).

Shah [31] suggested the following correlation for local heat transfer coefficient.

$$h_{TP} = \psi * h_L \quad (5.17)$$

where ψ is a dimensionless parameter and is calculated as shown below.

The convective Boiling and Froude numbers are defined initially as

$$C_o = \left(\frac{1}{x} - 1 \right)^{0.8} \left(\frac{\rho_g}{\rho_L} \right)^{0.5} \quad (5.18)$$

$$B_o = q / (G i_{fg}) \quad (5.19)$$

$$F_{rL} = \frac{G^2}{\rho_L^2 g D} \quad (5.20)$$

and the single phase heat transfer coefficient is given by

$$h_L = 0.023 \left[\frac{G(1-x)D}{\mu_L} \right]^{0.8} P_{rL}^{0.4} \frac{k_L}{D} \quad (5.21)$$

A dimensionless parameter N is defined as shown below:

For vertical tubes at all values of F_{rL} and for horizontal tubes with

$$F_{rL} \geq 0.04$$

$$N = C_o . \quad (5.22)$$

For horizontal tubes with $F_{rL} \leq 0.04$

$$N = 0.38 F_{rL}^{-0.3} C_o . \quad (5.23)$$

a) For $N > 1.0$

$$\psi_{nb} = 230 B_o^{0.5} , \quad B_o > 0.3 \times 10^{-4} \quad (5.24)$$

$$\psi_{nb} = 1 + 46 B_o^{0.5} , \quad B_o < 0.3 \times 10^{-4} \quad (5.25)$$

$$\psi_{cb} = \frac{1.8}{N^{0.8}} \quad (5.26)$$

If $\psi_{nb} > \psi_{cb}$, then $\psi = \psi_{nb}$.

If $\psi_{cb} > \psi_{nb}$, then $\psi = \psi_{cb}$.

b) For $0.1 < N \leq 1.0$

$$\psi_{bs} = F B_o^{0.5} \text{Exp} (2.74 N^{-0.1}) \quad (5.27)$$

ψ_{cb} is obtained from Eq. (5.26). ψ is equal to the larger value of

ψ_{bs} and ψ_{cb} .

c) If $N \leq 0.1$

$$\psi_{bs} = F B_o^{0.5} \exp(2.47 N^{-0.15}) \quad (5.28)$$

ψ_{bs} is obtained from Eq. (5.26).

ψ equals the larger of ψ_{cb} and ψ_{bs}

F is obtained as follows:

$$B_o \geq 11 \times 10^{-4}, \quad F = 14.7$$

$$B_o < 11 \times 10^{-4}, \quad F = 15.43$$

Schrock and Grossman [32] proposed the following equation for both convective and nucleate boiling regions of heat transfer.

$$\frac{h_{TP}}{h_L} = \lambda \left[\frac{q/A}{G i_{fg}} + m \left(\frac{1}{x_{tt}} \right)^n \right] \quad (5.29)$$

h_{TP} being the local heat transfer coefficient where,

$$\lambda = 7.39 \times 10^3, \quad m = 1.5 \times 10^{-4}$$

$$n = 0.66$$

and,

$$h_L = 0.023 \left(\frac{k_L}{D_i} \right) Re_L^{0.8} Pr_L^{1/3}$$

where,

$$Re_L = \frac{GD(1-x)}{\mu_L}$$

Sani [33] modified Schrock and Grossman's [32] correlation by a factor of 2. Therefore, his correlation of local heat transfer coefficient is given by

$$\frac{h_{TP}}{h_L} = 14,700 \left[\frac{q/A}{Gi_{fg}} + 1.5 \times 10^{-4} (X_{tt})^{-2/3} \right] \quad (5.30)$$

All the above correlations, except that of Pierre [26] predict local values of heat transfer coefficients, and therefore the overall average values were evaluated from the following equation

$$\bar{h} = \frac{1}{(X_{out} - X_{in})} \int_{X_{in}}^{X_{out}} h_{local} dx . \quad (5.31)$$

The comparison between the predictions of the above correlations and the experimental smooth tube measurements are shown in Figs. 5.1 through 5.8.

The results of the comparison are summarized in the following:

- 1) Sani's [33] correlation given by Eq. (5.30) correlated all the experimental values of heat transfer coefficient to within $\pm 30\%$.
- 2) The remaining correlations predicted values lower than the measured values.

On the basis of these results Sani's [33] correlation was selected as the basis for developing the finned tube correlations. In addition, the attempt was also made to use the correlation parameters of Pierre's [26] correlation to develop a heat transfer correlation for the finned tubes. The reason was due to the fact that the correlation of Pierre is among the most commonly used correlations. Also, a third correlation equation was developed using the Martinelli-Nelson [34] parameter.

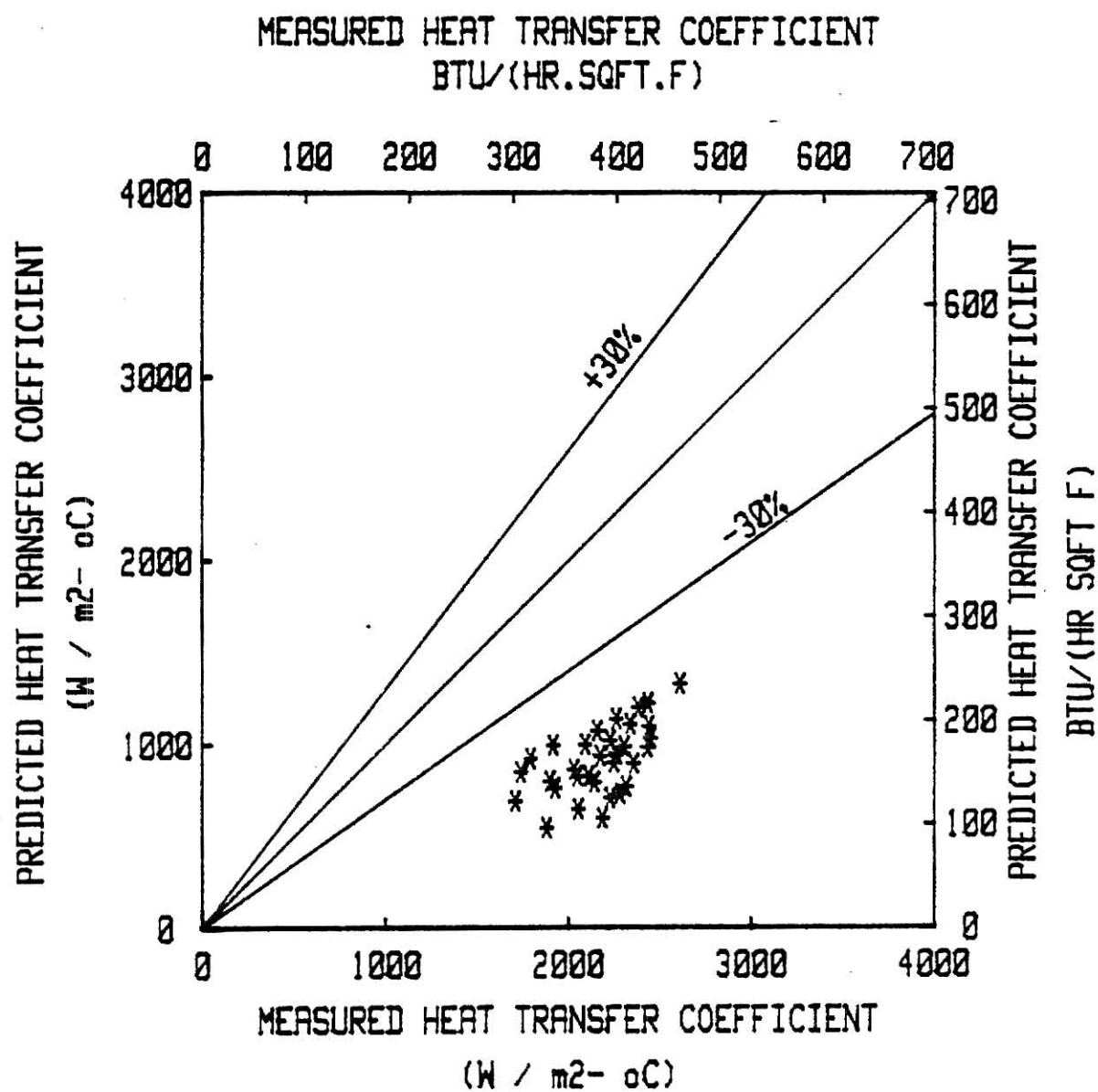


Fig. 5.1 Comparison of Experimental Overall Average Heat Transfer Coefficients With Predictions of Pierre's Correlation, Eq (5.3), Tube 1.

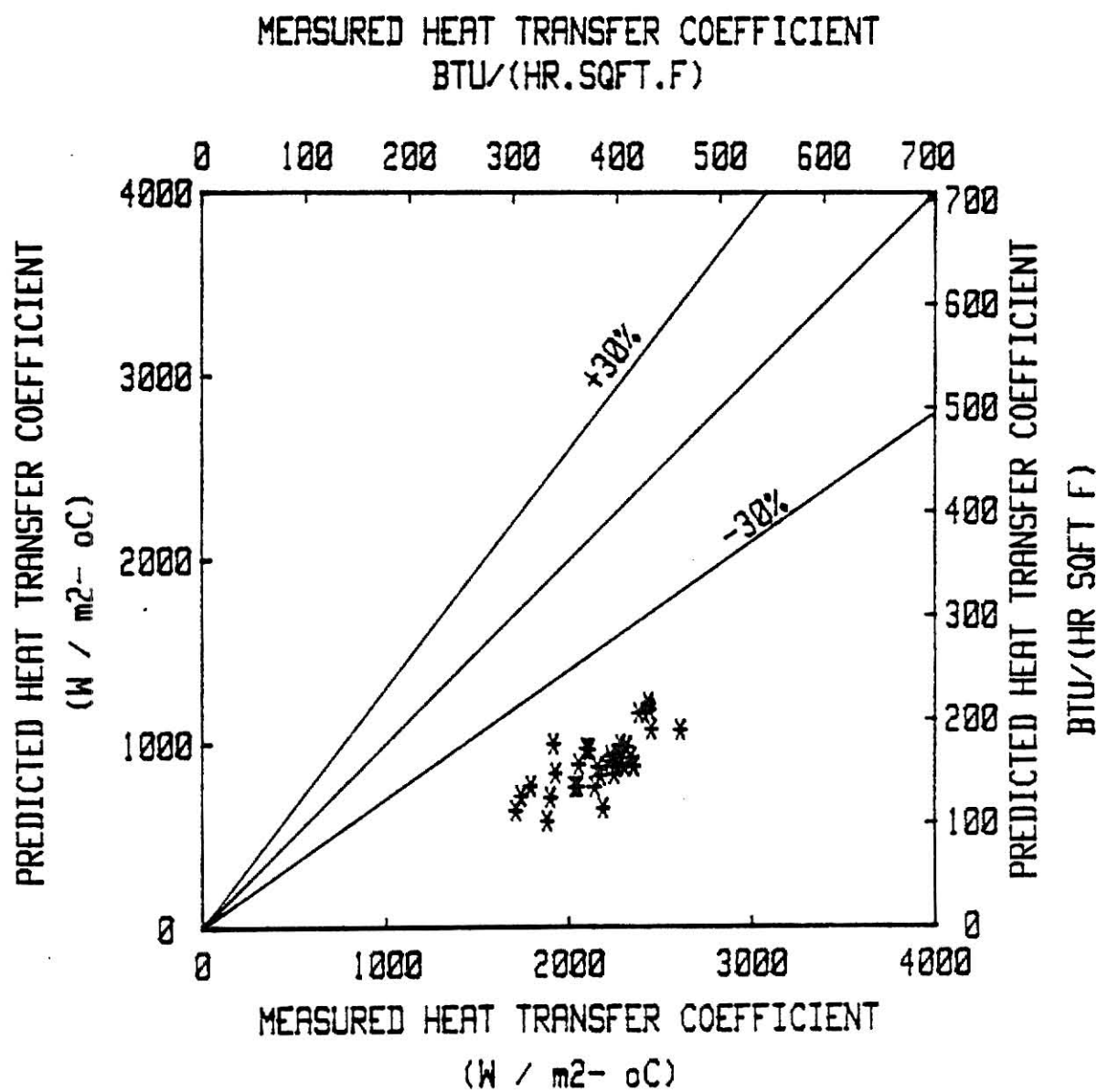


Fig. 5.2 Comparison of Experimental Overall Average Heat Transfer Coefficients With Predictions of Dengler and Addoms Correlation, Eq (5.4), Tube 1.

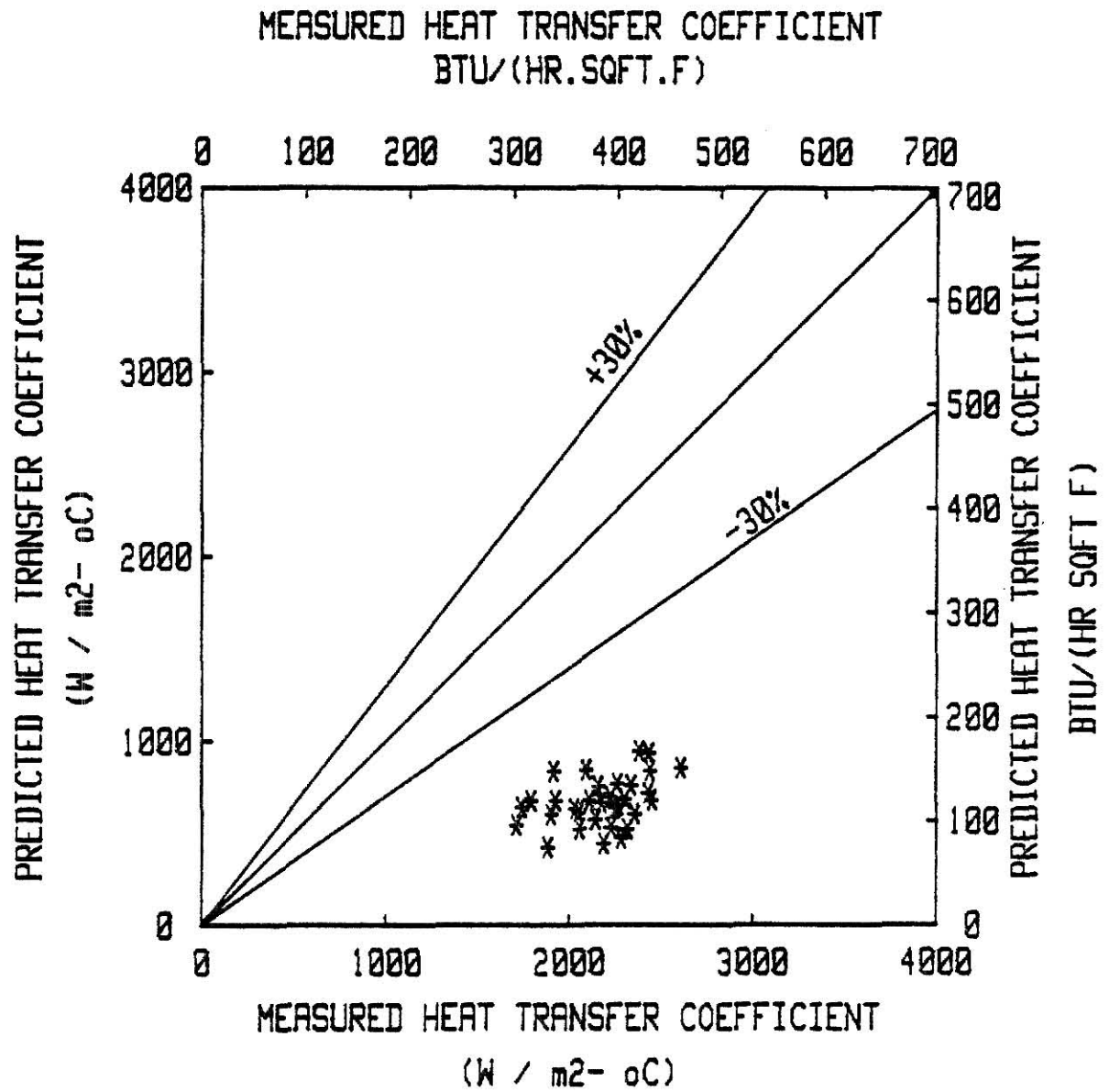


Fig. 5.3 Comparison of Experimental Overall Average Heat Transfer Coefficients With Predictions of Guerrieri and Talty Correlation, Eq (5.7), Tube 1.

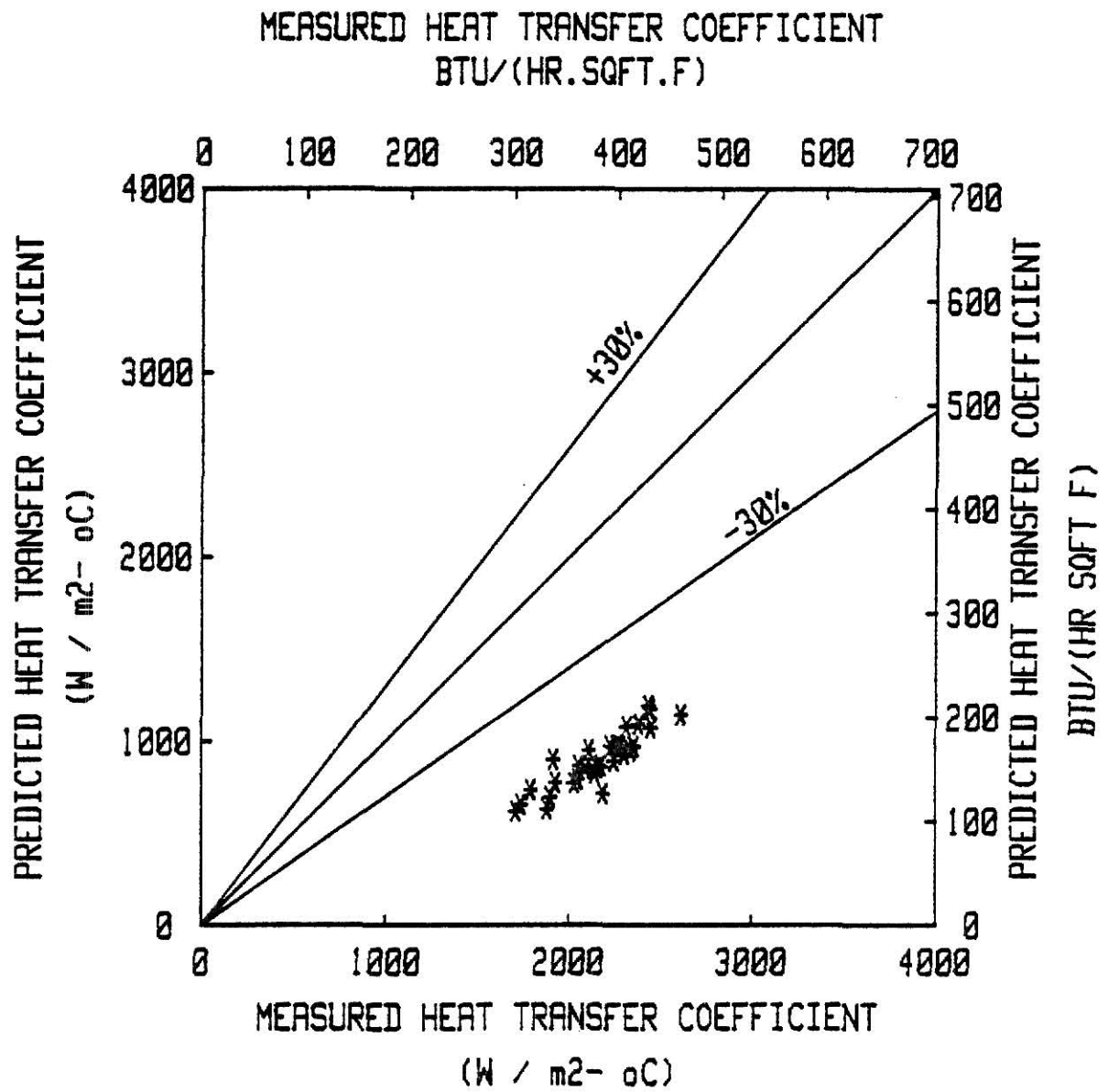


Fig. 5.4 Comparison of Experimental Overall Average Heat Transfer Coefficients With Predictions of Bennett et al. Correlation, Eq (5.10), Tube 1.

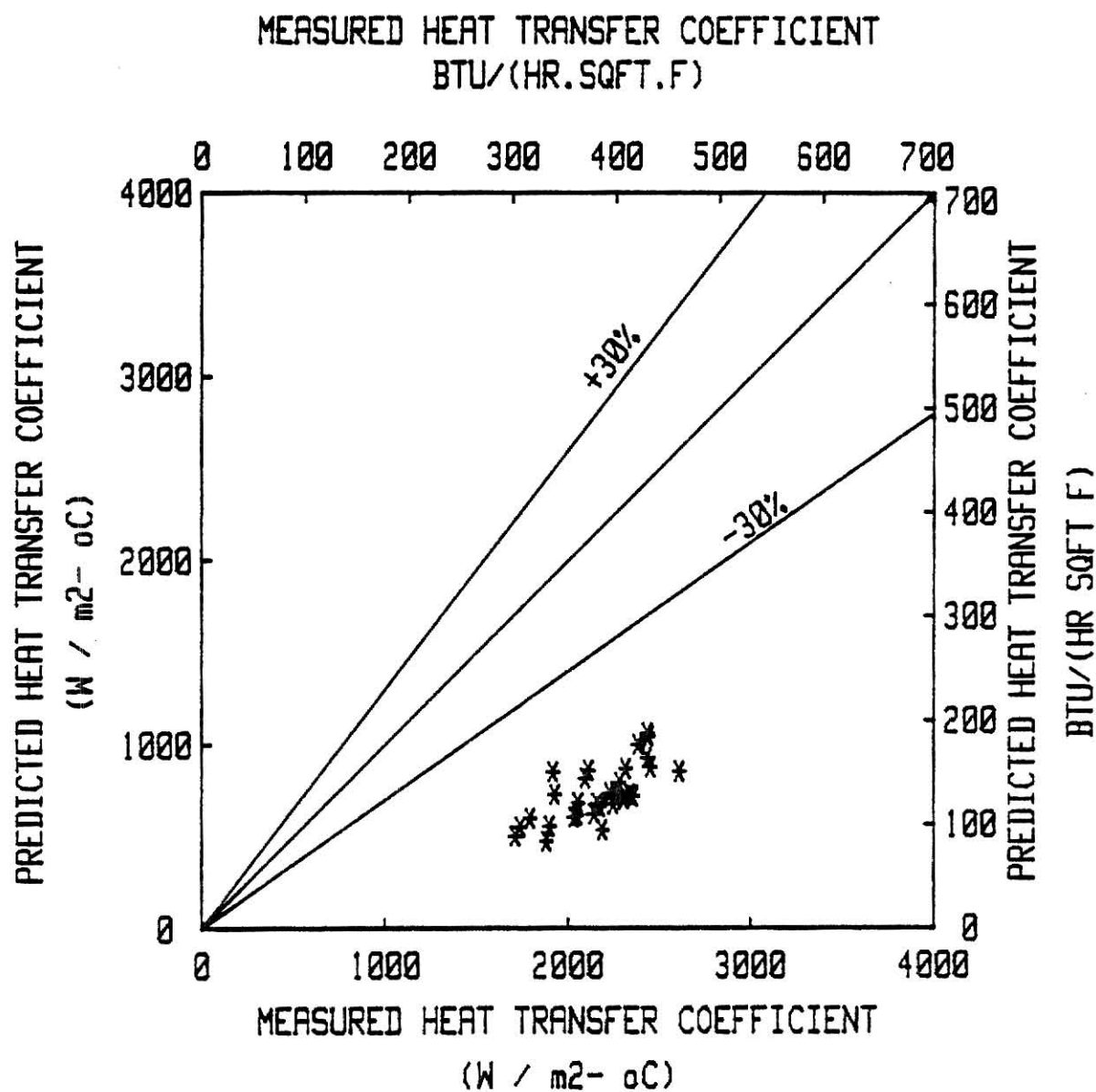


Fig. 5.5 Comparison of Experimental Overall Average Heat Transfer Coefficients With Predictions of Chen's Correlation, Eq (5.12), Tube 1.

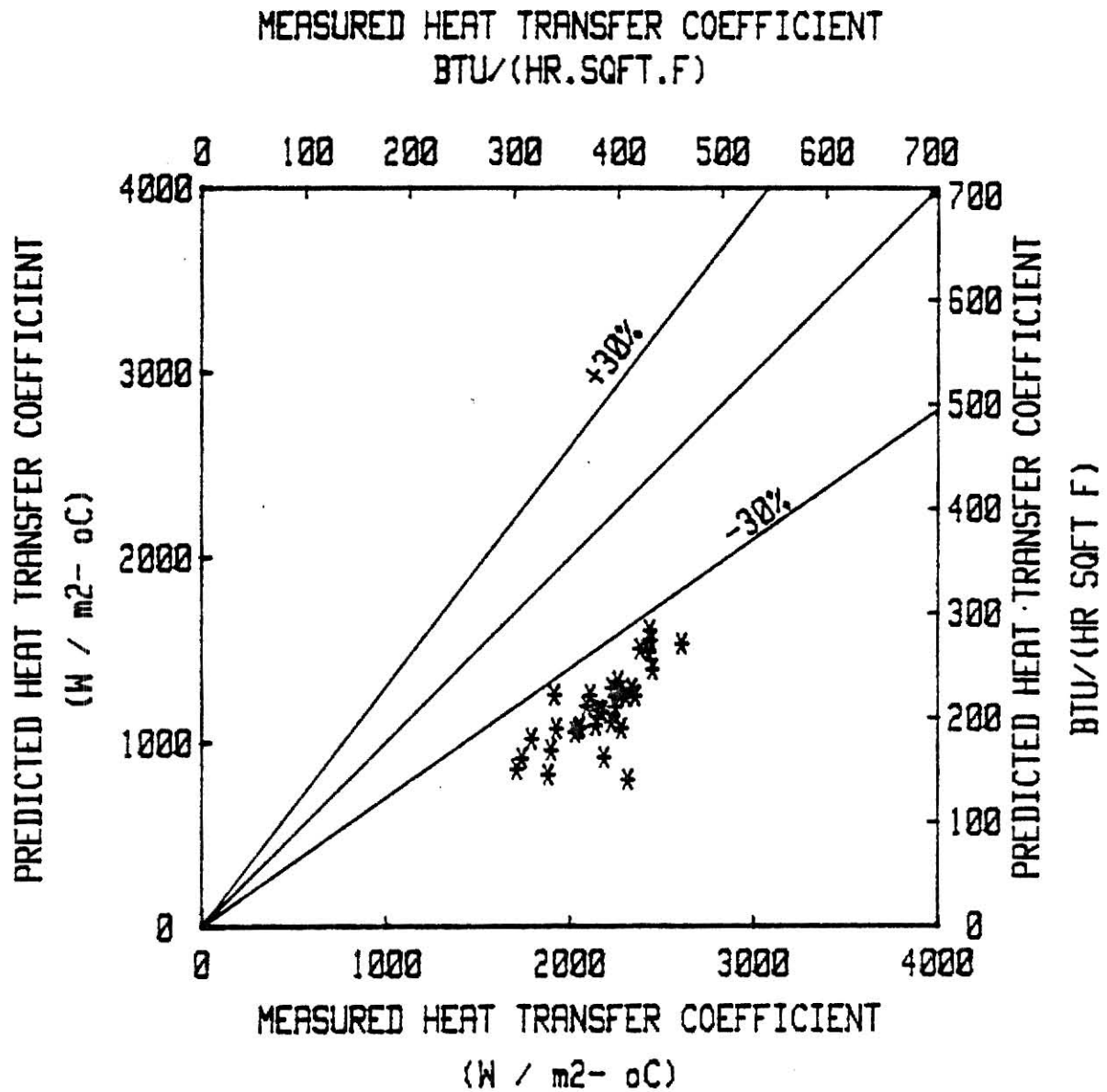


Fig. 5.6 Comparison of Experimental Overall Average Heat Transfer Coefficients With Predictions of Shah's Correlation, Eq (5.17), Tube 1.

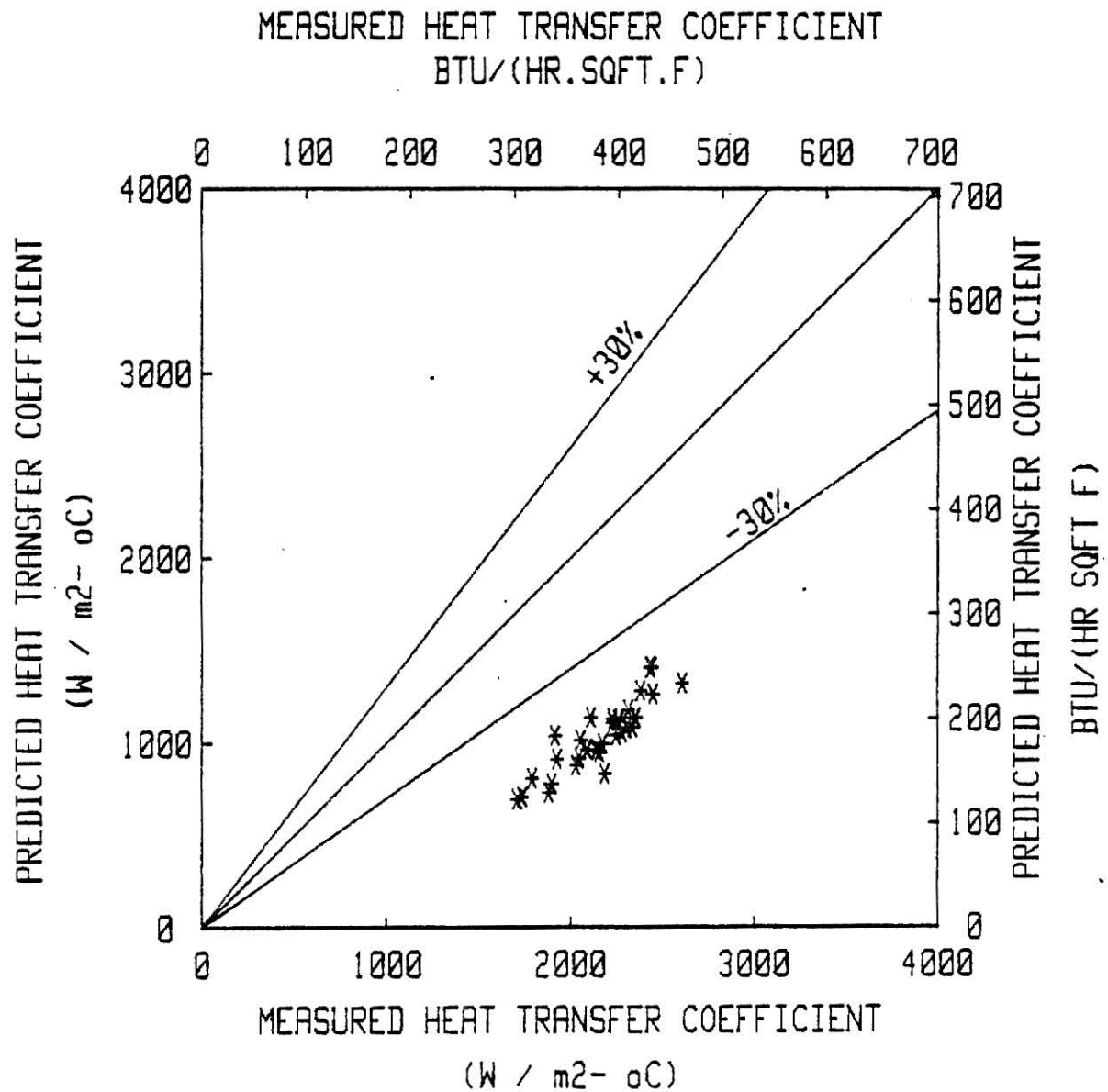


Fig. 5.7 Comparison of Experimental Overall Average Heat Transfer Coefficients With Predictions of Schrock and Grossman Correlation, Eq (5.29), Tube 1.

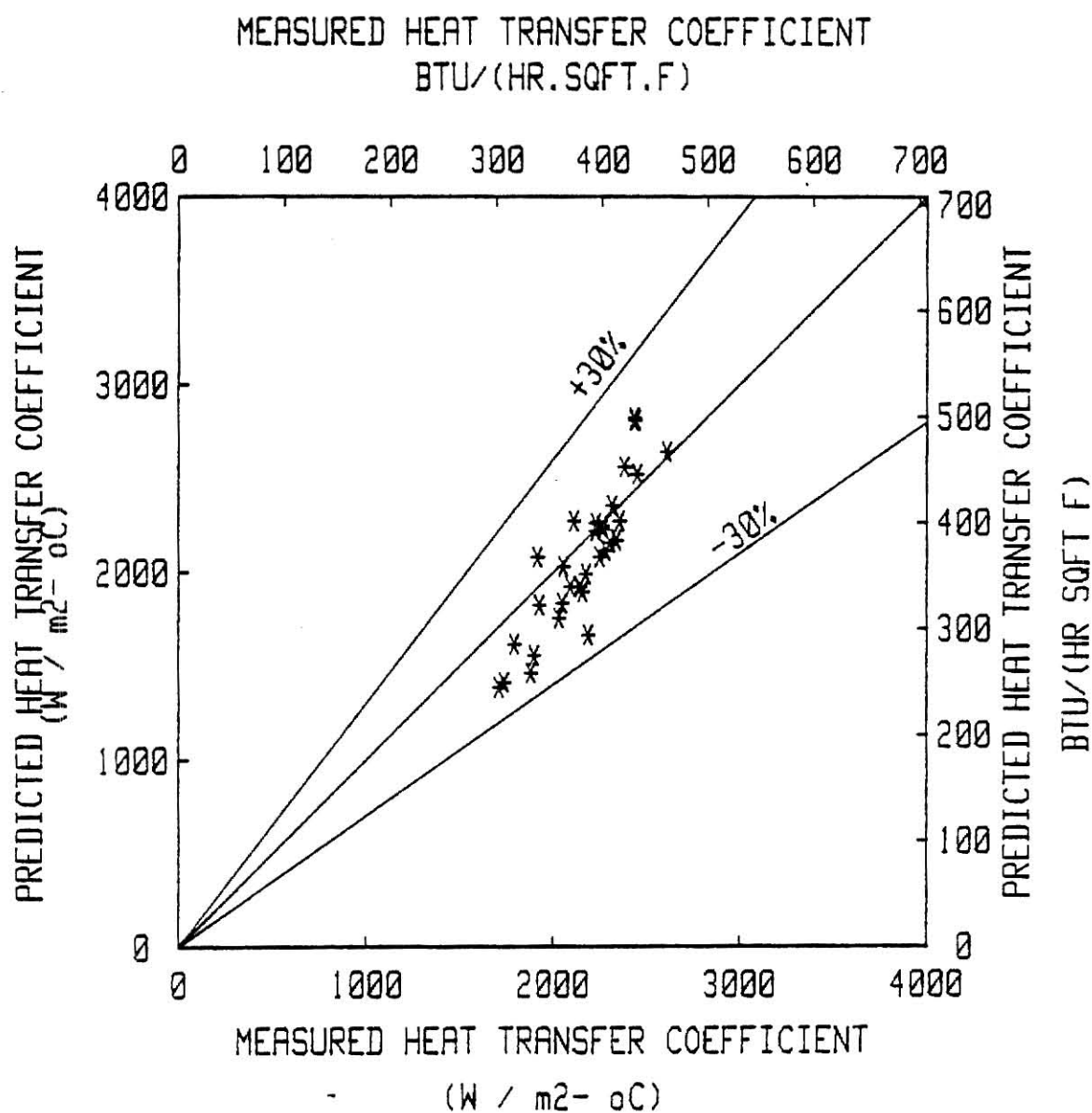


Fig. 5.8 Comparison of Experimental Overall Average Heat Transfer Coefficients With Predictions of Sani's Correlation, Eq (5.30), Tube 1.

5.2.2 Existing Finned Tubes Correlations

At the present time no correlations exist for predicting the heat transfer coefficient during saturated boiling inside finned tubes. Most of the existing finned tube correlations were developed for single phase flow. They were all based on applying modifying factors to the smooth tube correlations. For single phase turbulent flow, Watkinson et al. [8] proposed the use of $\left(\frac{W}{D_e}\right)$ for straight fins and $\left(\frac{W}{D_e}\right)$ and $\left(\frac{H}{D_e}\right)$ for spiral fins. The use of the ratio of the fin spacing to the equivalent diameter $\left(\frac{W}{D_e}\right)$ was suggested by Ornatskii et al. [35].

The heat transfer performance for heating water and air was individually determined, in turbulent flow, by Carnavos [22]. He correlated the experimental data using the hydraulic diameter and the average bulk physical properties. All heat transfer data were correlated by

$$\frac{Nu}{Pr^{0.4}} = 0.023 Re^{0.8} (F) \quad (5.32)$$

where,

$$F = (F_1)^{0.1} (F_2)^{0.5} (F_3)^3 \quad (5.33)$$

The parameters in the modifying factor F are defined as follows:

$$F_1 = \frac{A_{fa}}{A_{fc}} \quad (5.34)$$

$$F_2 = \frac{A_n}{A_a} \quad (5.35)$$

$$F_3 = \sec \alpha \quad (5.36)$$

where

$$A_{fa} = \text{actual free flow area, } \frac{\pi D_e^2}{4}, \text{ cm}^2,$$

$$A_{fc} = \text{open core free flow area, } \frac{\pi D_c^2}{4}, \text{ cm}^2,$$

$$A_n = \text{nominal heat transfer area based on } D_i \text{ as if fins were not present, cm}^2/\text{cm},$$

$$A_a = \text{actual heat transfer area, cm}^2/\text{cm},$$

$$A_{fn} = \text{nominal flow area based on } D_i \text{ as if fins were not present, } \frac{\pi D_i^2}{4}, \text{ cm}^2.$$

The equivalent diameter D_e and the core diameter are defined by:

$$\frac{\pi D_e^2}{4} = \frac{\pi D_i^2}{4} - n b t / \cos \alpha \quad (5.37)$$

$$\frac{\pi D_c^2}{4} = \frac{\pi}{4} (D_i - 2b)^2 \quad (5.38)$$

The hydraulic diameter was also defined by:

$$D_h = \frac{4A_{fa}}{A_a} \quad (5.39)$$

Using the above definitions, it can be shown that:

$$\begin{aligned} F_1 = \frac{A_{fa}}{A_{fc}} &= \frac{\left[\frac{D_e}{D_i} \right]^2}{\left[1 - (2b/D_i) \right]^2} \\ &= \frac{[1 - (4nbt)/(\pi D_i^2 \cos \alpha)]}{[1 - 2b/D_i]^2} \end{aligned} \quad (5.40)$$

$$F_2 = A_n/A_a = (D_i D_h / D_e^2) = \frac{\pi D_i}{[\pi D_i + 2nb/\cos \alpha]} \quad (5.41)$$

n = number of fins
 α = helix angle of the fin

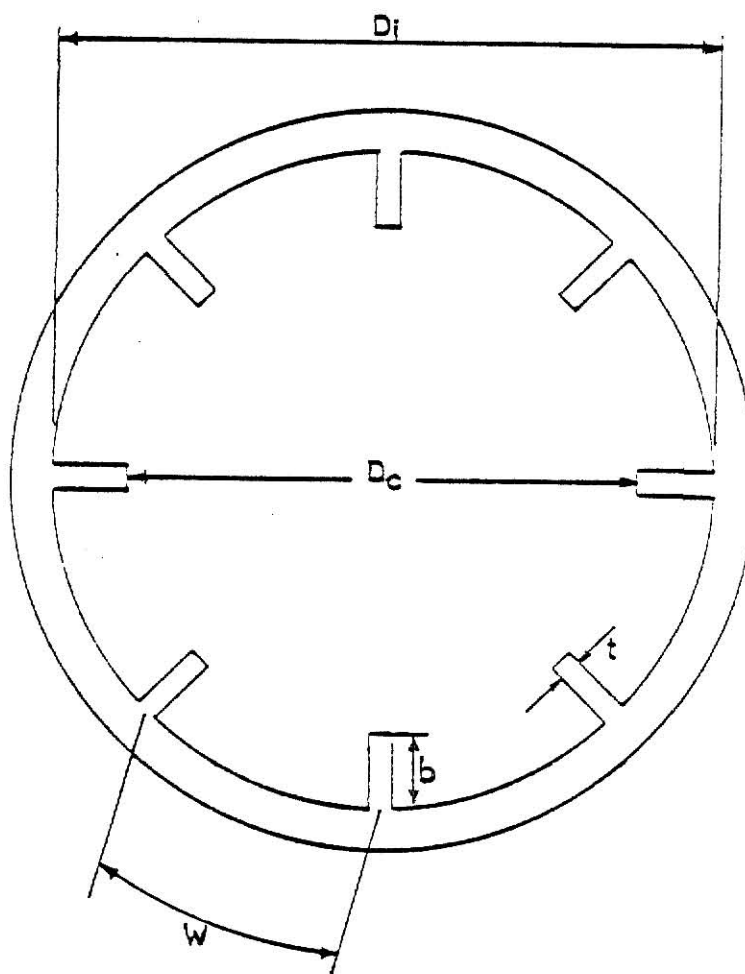


Fig. 5.9 Cross Section of Internally Finned Tube

5.2.3 New Finned Tubes Correlations

For saturated boiling, the attempt was made to use the same modifiers suggested by Carnovas [22] to the smooth tube correlations to obtain a general correlation for all the internally finned tubes. These modifiers include all the geometric parameters, D_i , w , b , t , n and α of the internally finned tubes. These parameters are defined in Fig. 5.9.

The values of F_1 , F_2 , and F_3 obtained for the finned tubes, are given in Table 5.1.

Table 5.1. Computed Values of F_1 , F_2 , and F_3 .

F Value	2	Tube Tested 3	4
F_1	1.515	1.1464	1.464
F_2	0.6678	0.5061	0.5667
F_3	1.000	1.0413	1.0236

In the following sections three different heat transfer correlations were developed. The developments of these correlations is given in the following sections.

a) Correlation Based on Pierre's Parameter ($Re^2 k_f$)

Nusselt number results of all tubes tested were correlated with Pierre's parameter [26]. Using the least square regression analysis it was possible to develop the following regression equations.

Tube 1

$$Nu = 12.24 * (Re^2 k_f)^{0.1458} \quad (5.42)$$

$$(1.46 * 10^{10} < Re^2 k_f < 7.37 * 10^{10})$$

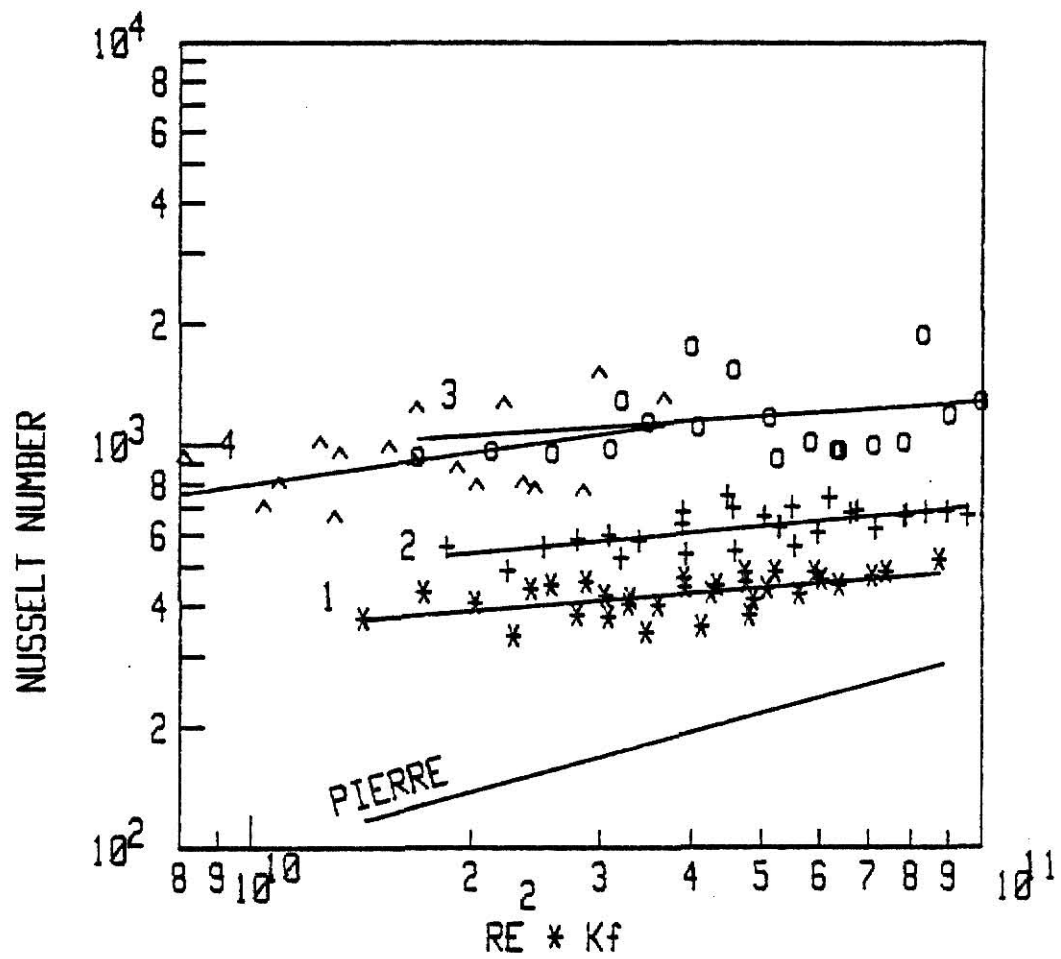


Fig.5.10 Nusselt Number Versus the Pierre Parameter ($Re^2 Kf$)

Tube 2

$$\begin{aligned} \text{Nu} &= 10.144 * (\text{Re}^2_{k_f})^{0.1678} & (5.43) \\ &(1.85 * 10^{10} < \text{Re}^2_{k_f} < 9.54 * 10^{10}) \end{aligned}$$

Tube 3

$$\begin{aligned} \text{Nu} &= 59.66 * (\text{Re}^2_{k_f})^{0.1213} & (5.44) \\ &(1.69 * 10^{10} < \text{Re}^2_{k_f} < 9.97 * 10^{10}) \end{aligned}$$

Tube 4

$$\begin{aligned} \text{Nu} &= 1.949 * (\text{Re}^2_{k_f})^{0.2614} & (5.45) \\ &(8.10 * 10^9 < \text{Re}^2_{k_f} < 3.66 * 10^{10}) \end{aligned}$$

Figure 5.10 shows a plot of Nusselt number versus $\text{Re}^2_{k_f}$ for all the tubes. From the plot one can infer that the Nusselt number increased with the increase in $\text{Re}^2_{k_f}$. For a particular value of $\text{Re}^2_{k_f}$, the Nusselt number is greater for the finned tubes than for the smooth tube. Tube 3 had the highest Nusselt number.

After developing the above regression equations, the ratios of $\frac{\text{Nu}_{\text{fin}}}{\text{Nu}_{\text{sm}}}$ were then calculated for the three internally finned tubes, over the common range of $\text{Re}^2_{k_f}$ ($1.85 \times 10^{10} < \text{Re}^2_{k_f} < 3.66 \times 10^{10}$).

After several trials of using modifying factors involving F_1 , F_2 , and F_3 discussed in the previous section, and by using the least regression analysis the following equation was developed

$$\frac{\text{Nu}_{\text{fin}}}{\text{Nu}_{\text{sm}}} = 1 + 0.00242 (F_1)^{3.715} * (F_2)^{-8.884} \quad (5.46)$$

where Nu_{sm} is calculated from Eq. (5.42).

Figures 5.11 through 5.13 show comparisons between the predictions of Eq. (5.46) and the experimental measurements of the finned tubes.

The results in Fig. 5.11 show that Eq. (5.46) correlated the experimental data of tube 2 to within $\pm 30\%$.

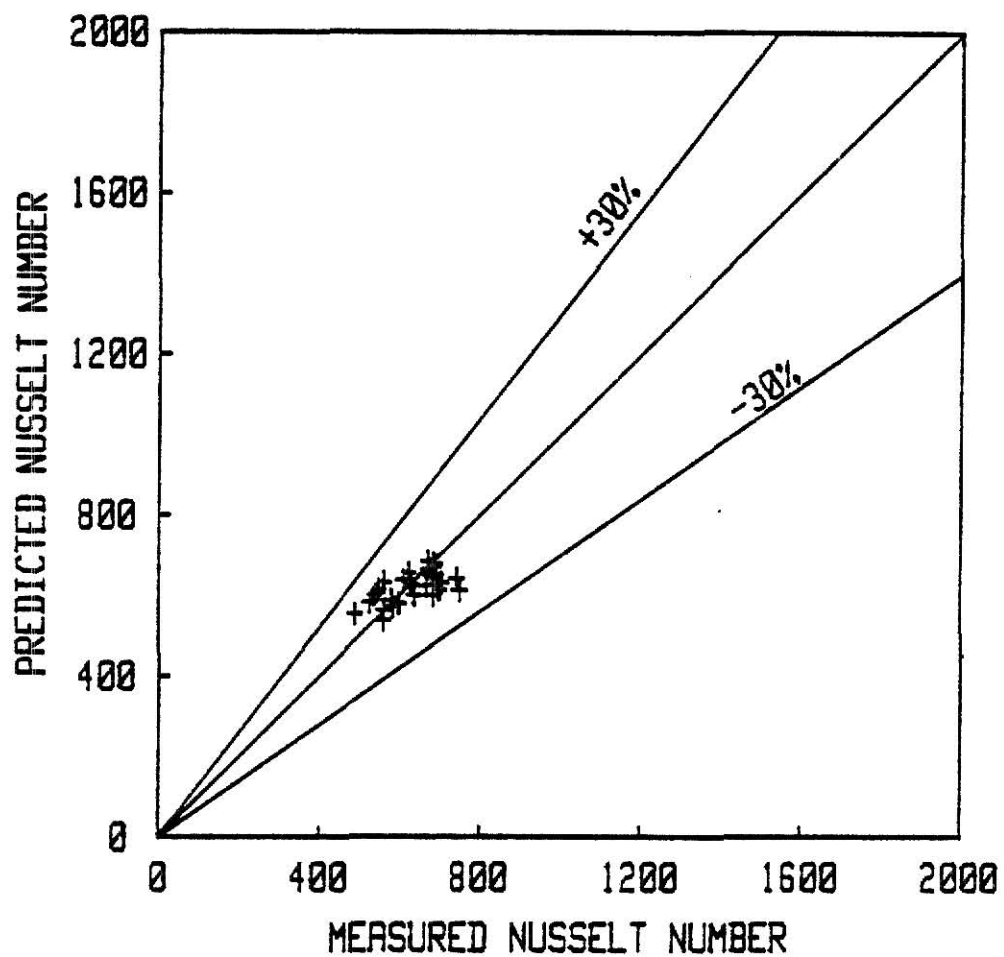


Fig. 5.11 Comparison of Experimental Values of Nusselt Number With Predictions of Modified Pierre's Type of Correlation, Eq(5.46), Tube 2.

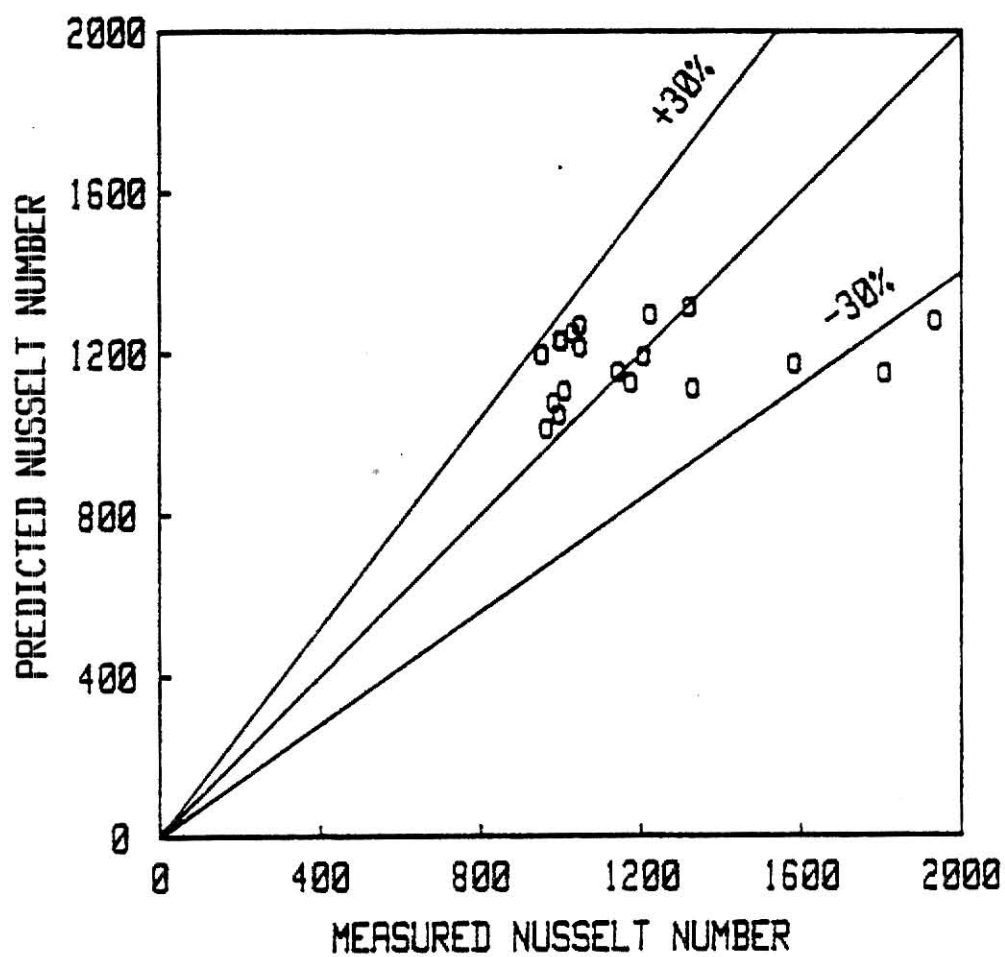


Fig. 5.12 Comparison of Experimental Values of Nusselt Number With Predictions of Modified Pierre's Type of Correlation, Eq(5.46), Tube 3.

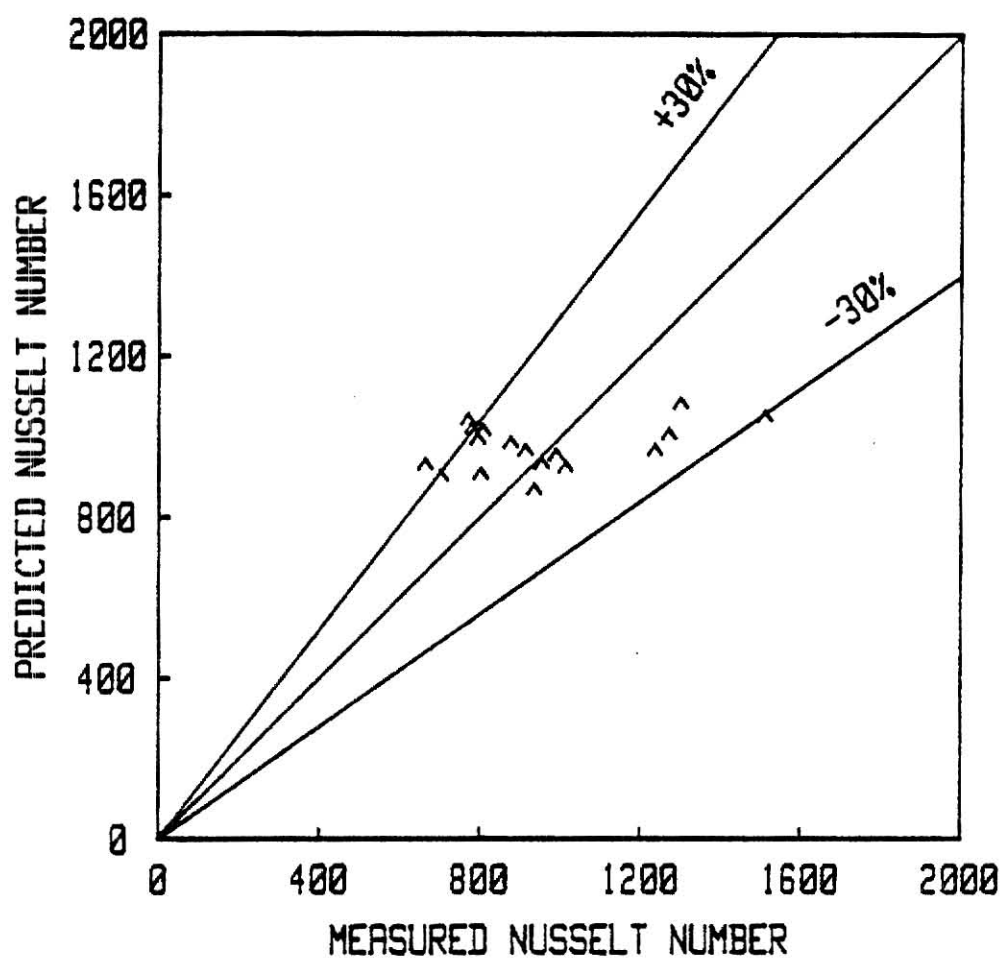


Fig. 5.13 Comparison of Experimental Values of Nusselt Number With Predictions of Modified Pierre's Type of Correlation, Eq (5.46), Tube 4.

Figure 5.12 shows a plot of the values of Nusselt number predicted by Eq. (5.46) versus the experimental values of Nusselt number for the spiral finned tube (tube 3). All the data points, except two, fall within $\pm 30\%$ range of deviation.

Figure 5.13 shows a comparison between the experimental values of Nusselt number of the spiral finned tube (tube 4), and the predictions of Eq (5.46). It shows that 88% of the data points lie within the $\pm 30\%$ disagreement range.

b) Finned Tube Correlation Based on Sani's [33] Smooth Tube Correlation

Sani [33] modified the Schrock and Grossman [32] correlation to correlate his own data points, and arrived at the following correlation.

$$\frac{h_{TP}}{h_L(1-x)^{0.8}} = 14700 \left[\frac{q/A}{Gh_{fg}} + 1.5 \times 10^{-4} \left(\frac{1}{x_{tt}} \right)^{0.66} \right] \frac{k_L}{D_i} \quad (5.47)$$

After several trials and by using the least regression analysis the following equation was developed for predicting the heat transfer coefficient for finned tubes.

$$\frac{\bar{h}_{TP \text{ fin}}}{\bar{h}_{TP \text{ sm}}} = \left[1 + 0.00137 * (F_1)^{4.635} * (F_2)^{-9.863} \right] \quad (5.48)$$

where $\bar{h}_{TP \text{ sm}}$ is calculated from Eq. (5.47).

Figures 5.14 through 5.16 show comparisons between the predicted heat transfer coefficient obtained from Eq. (5.48) and the experimental values of heat transfer coefficient.

The results show that 100% of the data points of tube 2, 64% of the data points of tube 3, and 53% of the data points of tube 4 agree with the proposed correlation to within $\pm 30\%$.

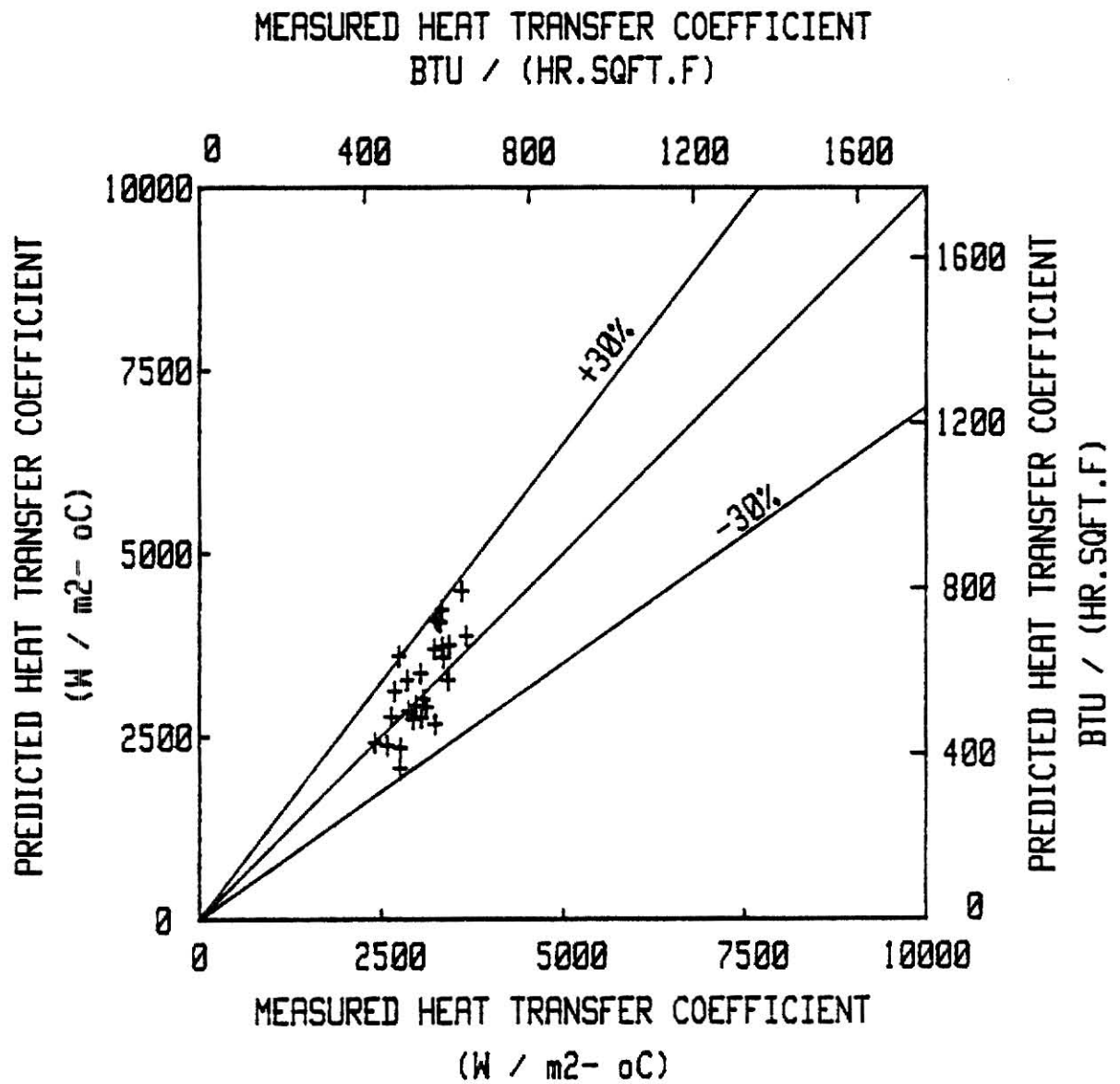


Fig. 5.14 Comparison of Experimental Overall Average Heat Transfer Coefficients With Predictions of Modified Sani's Correlation, Eq (5.48), Tube 2.

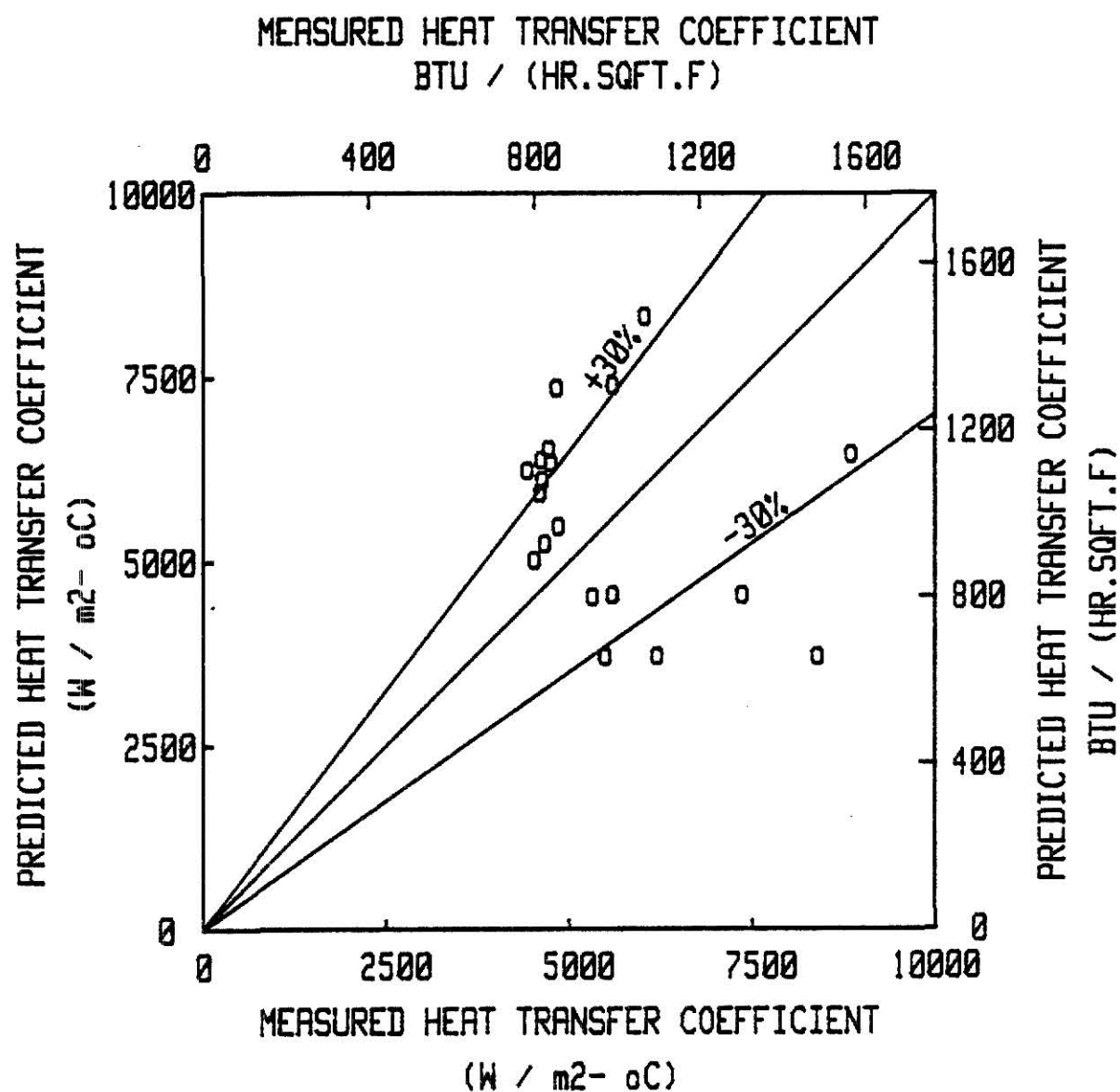


Fig. 5.15 Comparison of Experimental Overall Average Heat Transfer Coefficients With Predictions of Modified Sani's Correlation, Eq(5.48), Tube 3.

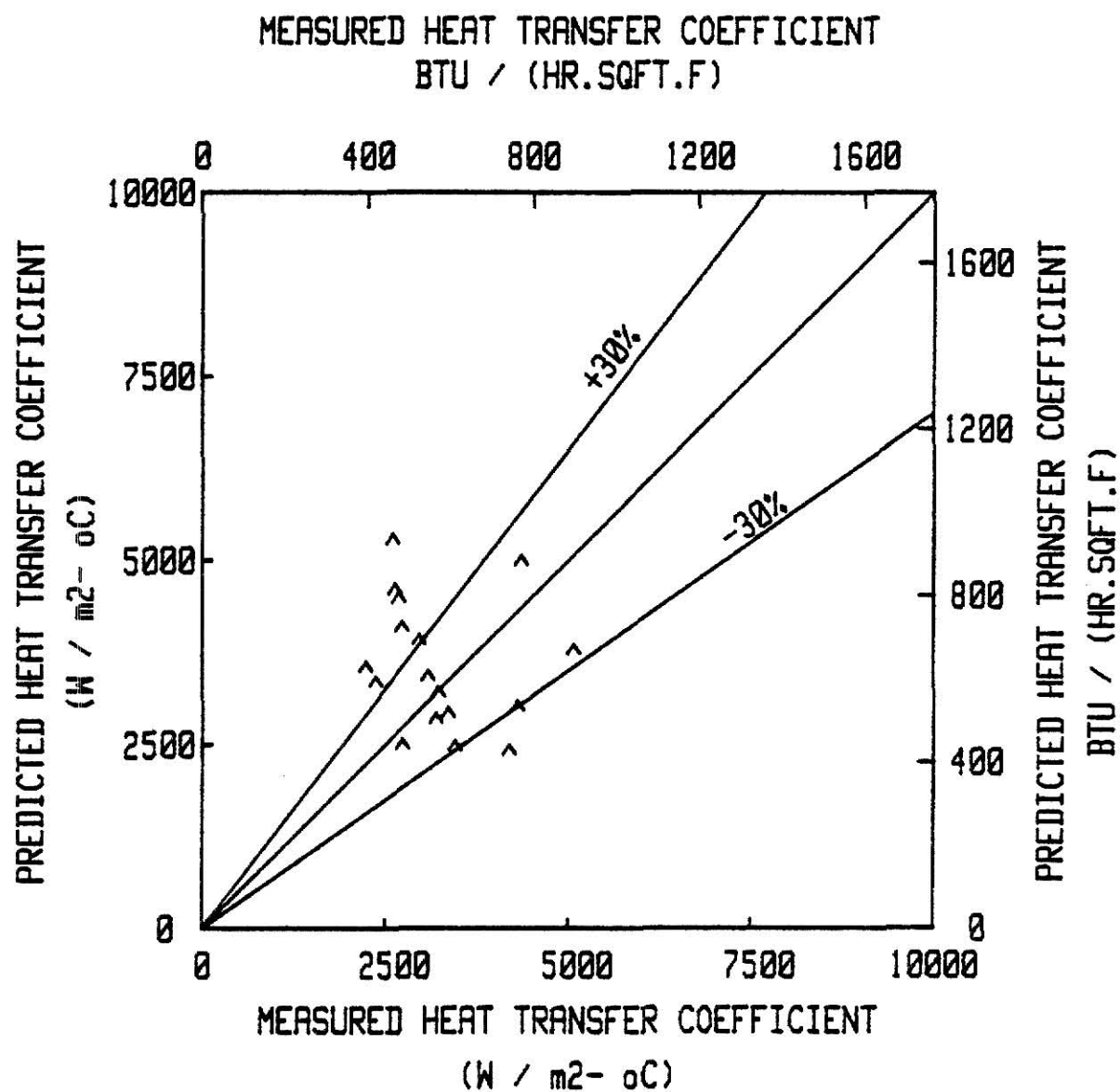


Fig. 5.16 Comparison of Experimental Overall Average Heat Transfer Coefficients With Predictions of Modified Sani's Correlation, Eq (5.48), Tube 4.

c) *Finned Tube Correlation Based on Martinelli-Nelson Parameter, X_{tt}*

Proceeding on the same lines of case (a), individual correlations were obtained for all the tubes, for the ratio of the two phase heat transfer coefficient h_{TP} to h_L' , as a function of $\frac{1}{X_{tt}}$. The general correlation equation was of the form:

$$\frac{\bar{h}_{TP}}{h_L'} = C''' \left(\frac{1}{X_{tt}} \right)^{n'''} \quad (5.49)$$

where C''' and n''' were constants that were determined for the individual tubes tested, and

$$h_L' = 0.023 \frac{k_L}{D_i} \left(\frac{D_i G}{\mu_L} \right)^{0.8} \left(\frac{C_{PL} \mu_L}{k_L} \right)^{0.4} (1-x)^{0.8} \quad (5.50)$$

The following equations were obtained for all the tubes:

Tube 1

$$\frac{\bar{h}_{TP \text{ sm}}}{h_L'} = 4.992 * \left(\frac{1}{X_{tt}} \right)^{0.8023} \quad (5.51)$$

Tube 2

$$\frac{\bar{h}_{TP \text{ fin}}}{h_L'} = 8.39 * \left(\frac{1}{X_{tt}} \right)^{0.7079} \quad (5.52)$$

Tube 3

$$\frac{\bar{h}_{TP \text{ fin}}}{h_L'} = 20.9 * \left(\frac{1}{X_{tt}} \right)^{0.5603} \quad (5.53)$$

Tube 4

$$\frac{\bar{h}_{TP \text{ fin}}}{h_L'} = 40.51 * \left(\frac{1}{X_{tt}} \right)^{0.0135} \quad (5.54)$$

The ratio of $\bar{h}_{TP \text{ fin}}/\bar{h}_{TP \text{ sm}}$ was calculated for the same $\frac{1}{X_{tt}}$ and its value was determined in terms of the parameters F_1 and F_2 . After several trials and by using the least square regression analysis, the following

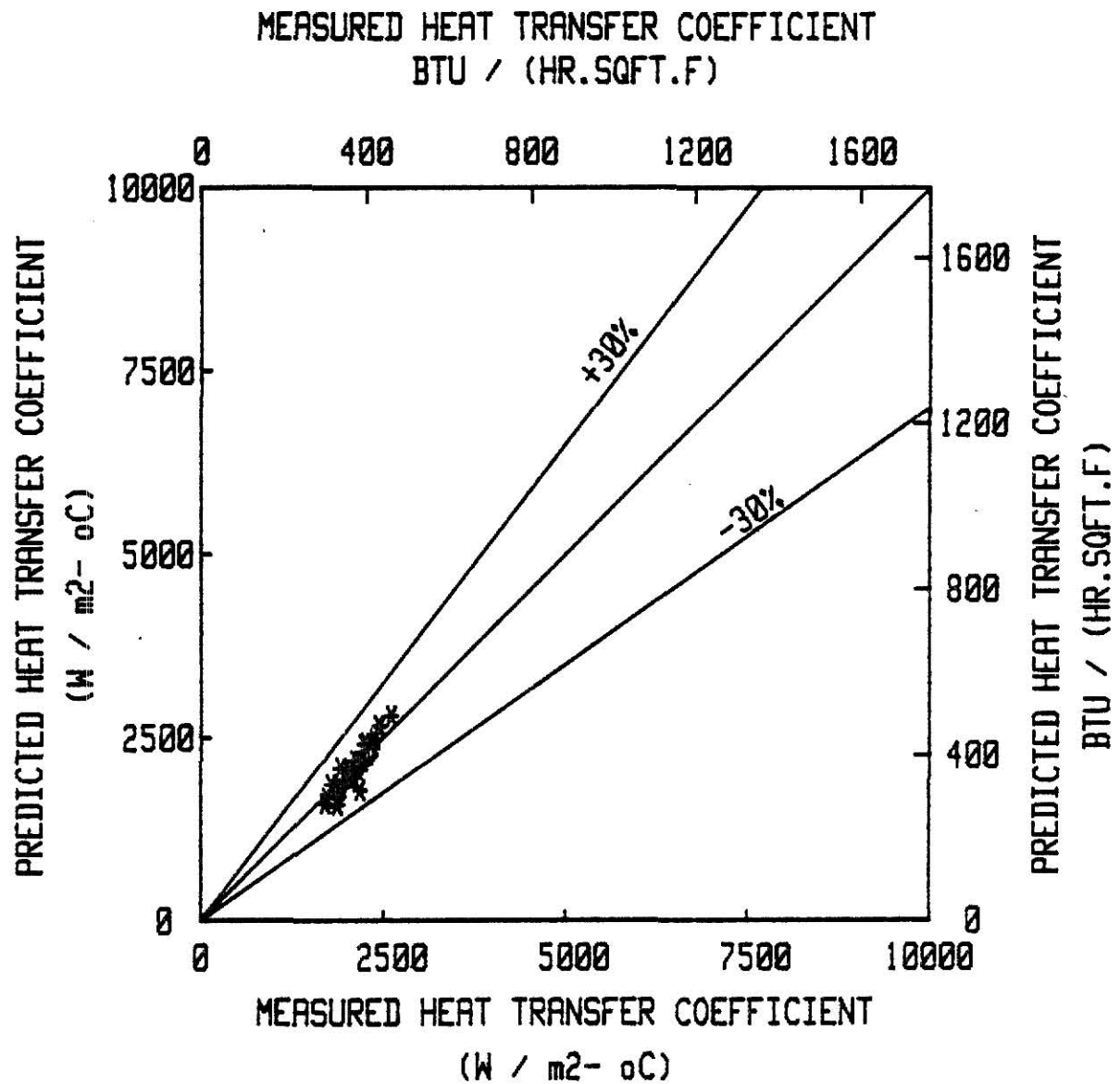


Fig. 5.17 Comparison of Experimental Overall Average Heat Transfer Coefficients With Predictions of Eq(5.51), Tube 1.

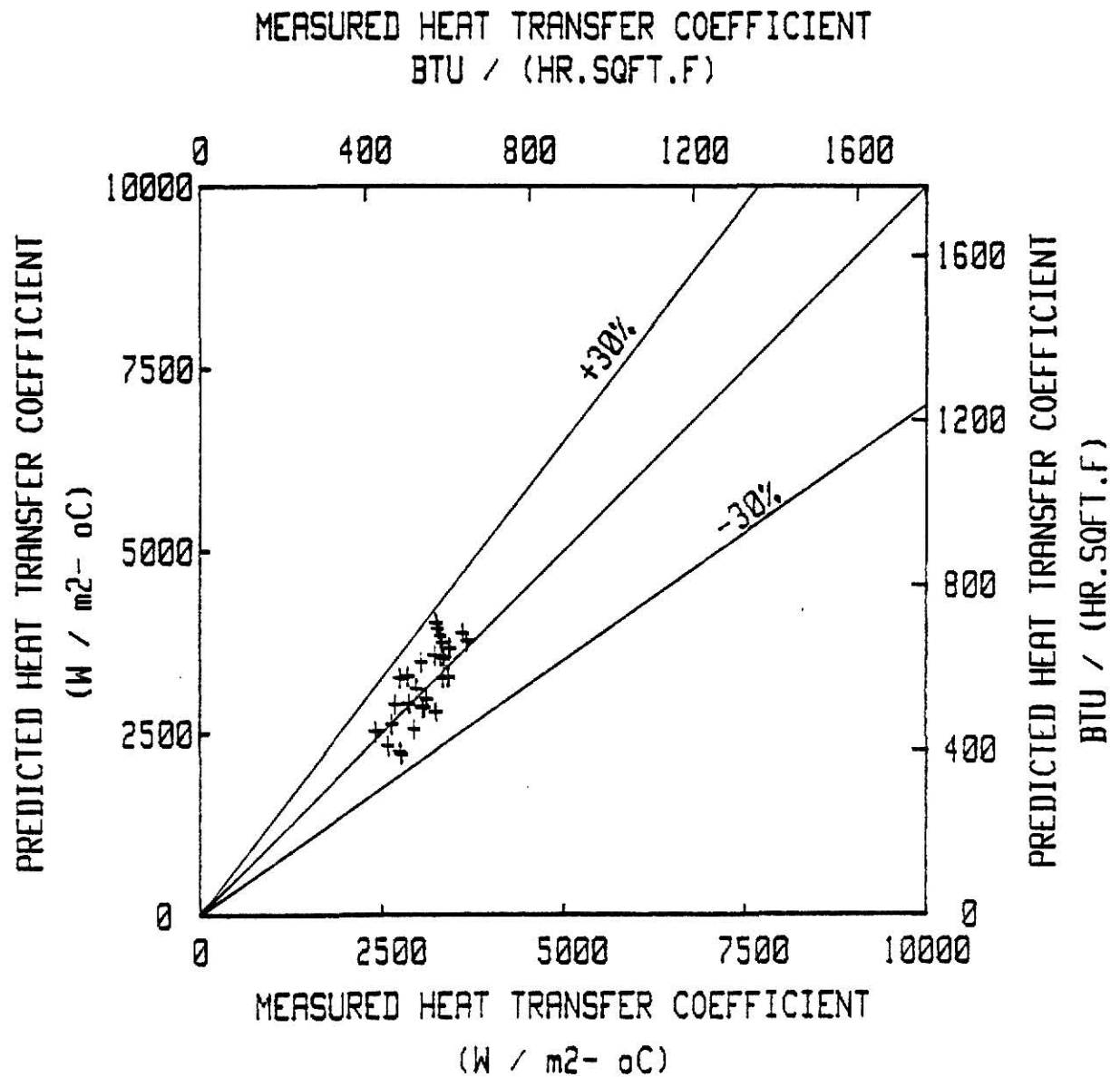


Fig. 5.18 Comparison of Experimental Overall Average Heat Transfer Coefficients With Predictions of Eq(5.55), Tube 2.

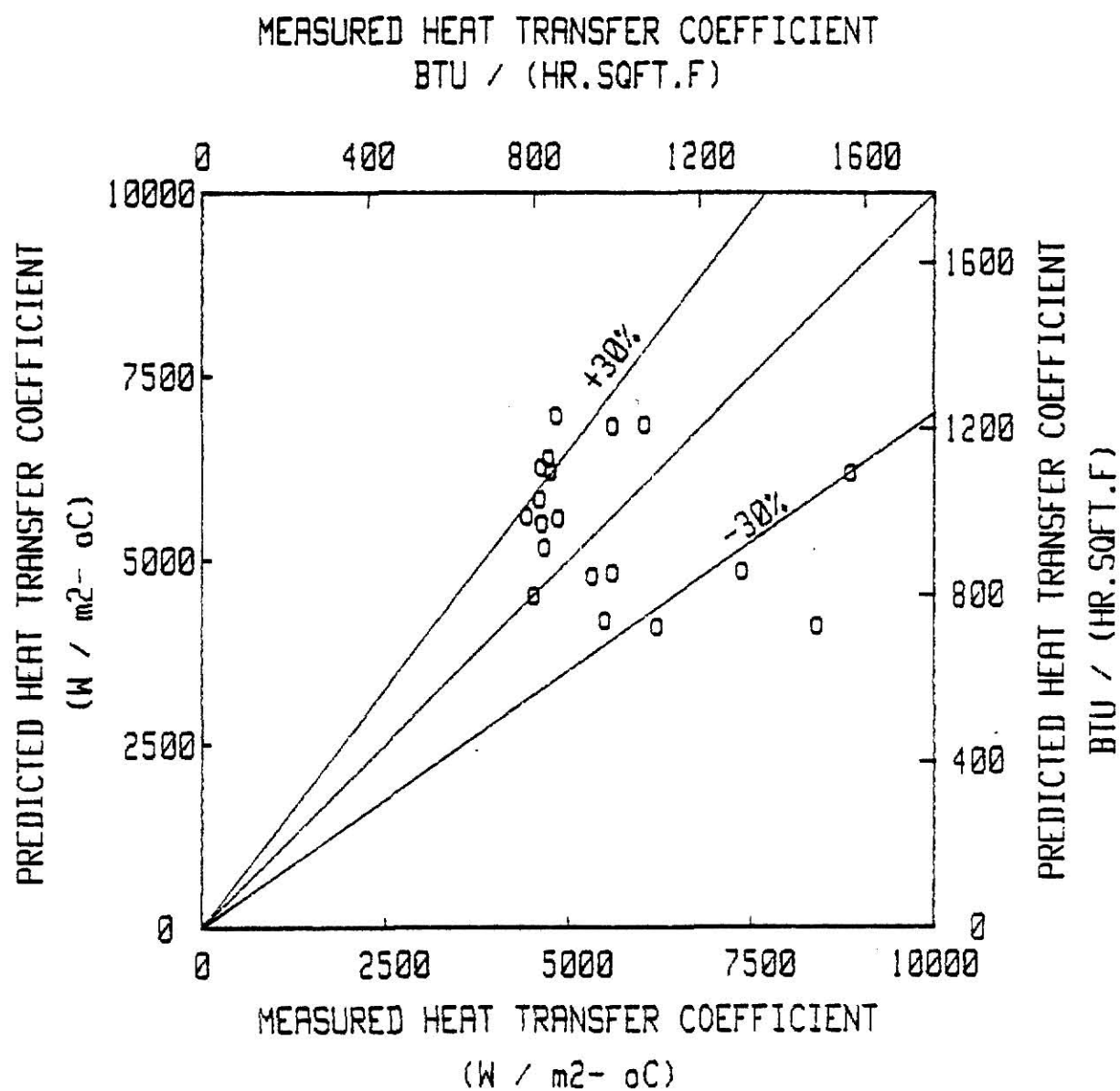


Fig. 5.19 Comparison of Experimental Overall Average Heat Transfer Coefficients With Predictions of Eq(5.55), Tube 3.

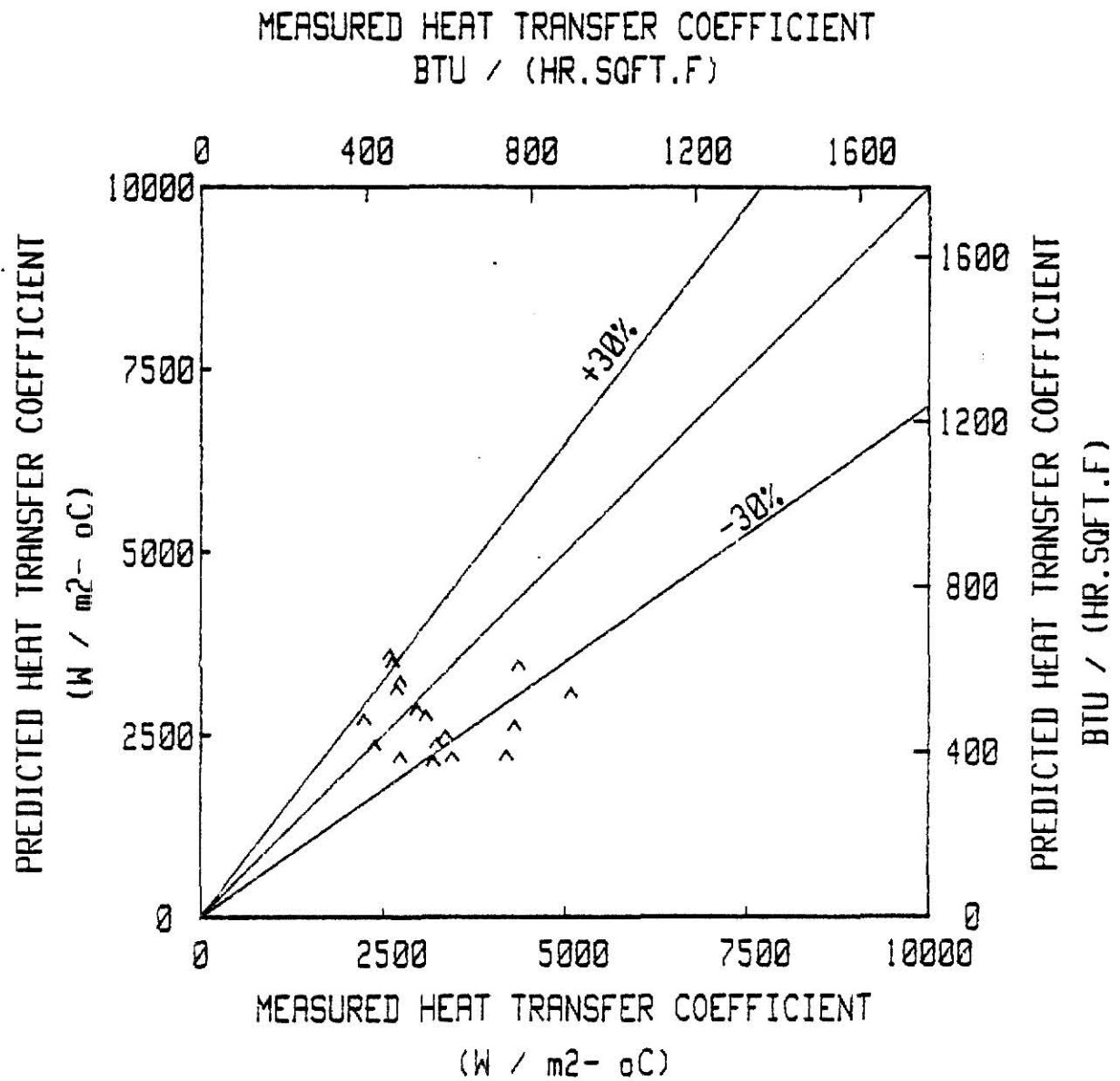


Fig. 5.20 Comparison of Experimental Overall Average Heat Transfer Coefficients With Predictions of Eq (5.55), Tube 4.

equation resulted.

$$\frac{\bar{h}_{TP \text{ fin}}}{\bar{h}_{TP \text{ sm}}} = 0.0711 * (F_1)^{2.425} (F_2)^{-5.073} \quad (5.55)$$

Figure 5.17 shows a comparison between the predictions of Eq. (5.51) for tube 1 and the experimental values of the heat transfer coefficient. Figures 5.18, 5.19 and 5.20 also show comparison between the predictions of Eq. (5.55) and the experimental heat transfer coefficient measurements of tubes 2, 3 and 4, respectively. The results show that the proposed correlation predicts to within $\pm 30\%$, except for a few data points for tubes 3 and 4, the experimental measurements.

5.3 PRESSURE DROP

5.3.1 Smooth Tube Correlations

Among all the existing correlations for pressure drop, the correlations of Pierre [26] and Martinelli and Nelson [34] were selected for predicting the two phase pressure drop.

The two phase pressure drop correlation of Pierre [26] is given by

$$\frac{\Delta P_{TP}}{L} = \left[f_m + \frac{D_i \Delta x}{x_m L} \right] \frac{G^2 v_m}{g_c D_i} \quad (5.56)$$

where,

$$f_m = 0.0185 \left[\frac{k_f}{Re} \right]^{0.25} \quad \text{for} \quad \left[\frac{Re}{k_f} \right] > 1 \quad (5.57)$$

$$k_f = \frac{(\Delta x) h_{fg}}{L} \cdot \frac{g_c}{g} \quad (5.58)$$

$$Re = \frac{GD}{\mu_l}$$

$$v_m = \frac{x_m}{\rho_g} + \frac{1 - x_m}{\rho_l} \quad (5.59)$$

and

$$x_m = \frac{x_{in} + x_{out}}{2} \quad (5.60)$$

To predict the total pressure drop during boiling inside the smooth tube for each experimental run, the distance between the two pressure taps was divided into 10 equal incremental lengths. By applying an energy balance, the quality of R-113 at the exit of each incremental length was determined. Pierre's correlation was then used to calculate the pressure

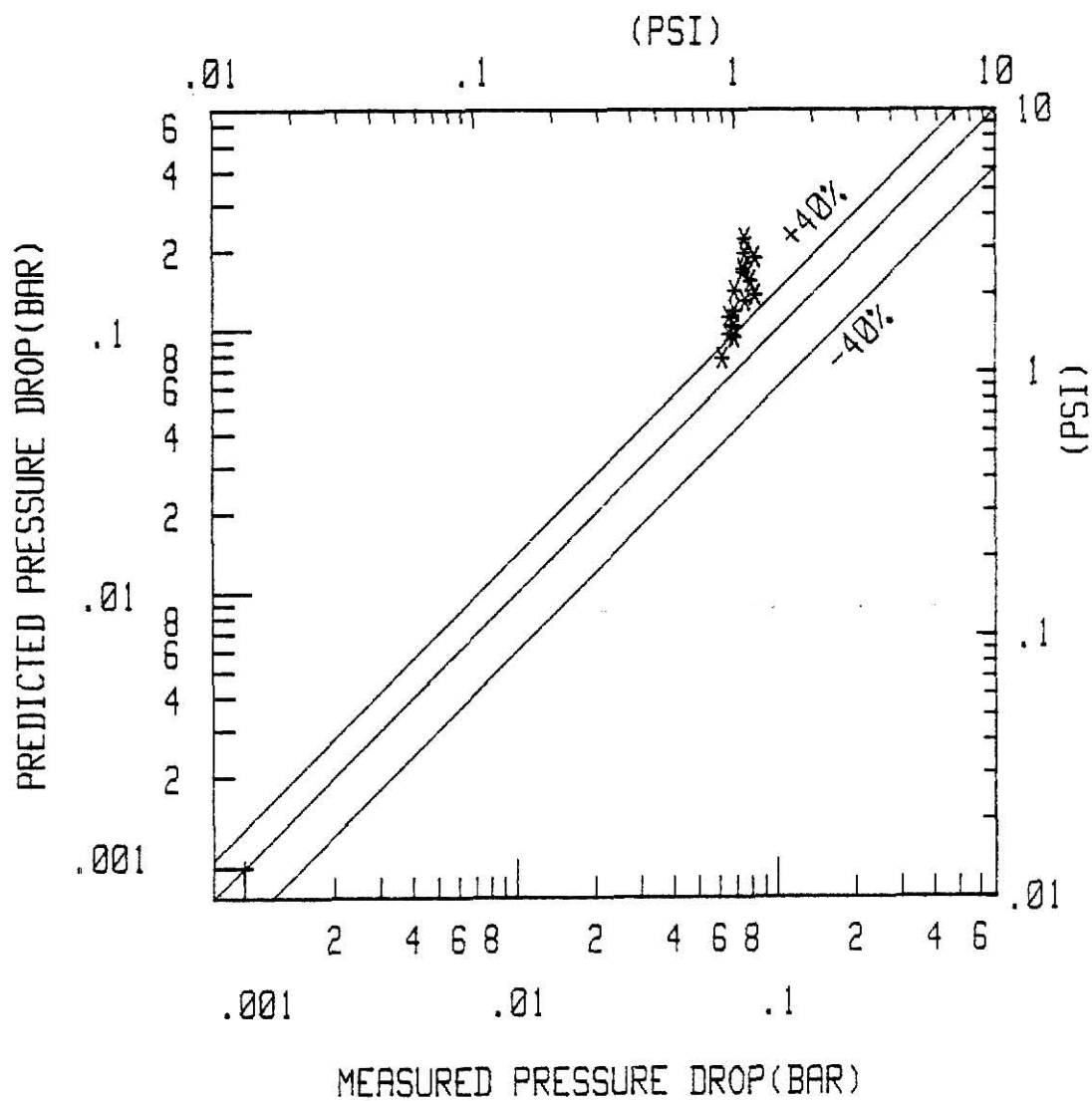


Fig. 5.21 Comparison of Experimental Pressure Drop With Predicted Values Obtained From Pierre's Correlation, Eq (5.56), Tube 1.

gradient $\frac{\Delta P}{\Delta L}$, for each subsection and the overall pressure drop was obtained by integrating the above results for the entire test section. This scheme was implemented in a digital computer program.

Fig. 5.21 compares the predicted values of ΔP obtained from Eq. (5.56) with that of the experimental values.

The results show that the pressure drop predictions of Pierre's correlation are higher than the experimental measurements.

According to the correlation proposed by Martinelli and Nelson [34], the pressure drop consists of the sum of the frictional pressure drop and the pressure drop due to the momentum change of the accelerating vapor. The pressure drop is given by

$$\Delta P_{TP} = (\Delta P_o) \left(\frac{\Delta P_{TPF}}{\Delta P_o} \right) + r_2 \left(\frac{G^2}{g} \right) \quad (5.61)$$

where ΔP_o is the single phase pressure drop, when only liquid flows into the tube, and $\frac{\Delta P_{TPF}}{\Delta P_o}$ is determined from the plot derived by Martinelli and Nelson [34], for the ratio of ΔP_{TPF} to ΔP_o as a function of exit vapor quality and pressure, for zero percent inlet quality.

r_2 is also a multiplier obtained from a plot derived by Martinelli and Nelson [34], for r_2 versus pressure and exit vapor quality for zero percent inlet quality.

ΔP_o was calculated from

$$\Delta P_o = f * \frac{\rho V_L^2}{2gD} \quad (5.62)$$

where,

$$f = 0.079 \left[\frac{GD}{\mu} \right]^{-1/4} \quad (5.63)$$

and,

$$\frac{1}{\bar{\mu}} = \frac{x_o}{\mu_g} + \frac{(1 - x_o)}{\mu_f} \quad (5.64)$$

x_o is the outlet dryness fraction.

Figure 5.22 compares the values of pressure drop predicted by Eq. (5.61) with the experimental measurements of the present study. The results show that the Martinelli-Nelson correlation was a better predictor of the experimental pressure drop measurements of the smooth tube than the correlation of Pierre [26].

5.3.2 Existing Finned Tube Correlations

The literature survey revealed that no two phase pressure drop correlation for saturated boiling exists at the present time for internally finned tubes. Among the existing correlations for single phase pressure drop inside internally finned tubes, the correlations proposed by Carnavos [22] appear to be quite promising.

Carnavos [22] proposed the correlation of Eq. (5.65) for the Fanning friction factor for single phase turbulent flow of air inside internally finned tubes.

$$f = \frac{0.046}{(Re)^{0.2}} (F_3)^{0.50} (F_4)^{0.50} \quad (5.65)$$

where, Re is Reynolds number based on the hydraulic diameter, and

$$F_3 = \cos \alpha, \text{ and } F_4 = \frac{A_{fa}}{A_{fn}}$$

Computed values of F_4 for tubes 2, 3, and 4 of the present study were 0.9174, 0.9376, and 0.9502, respectively.

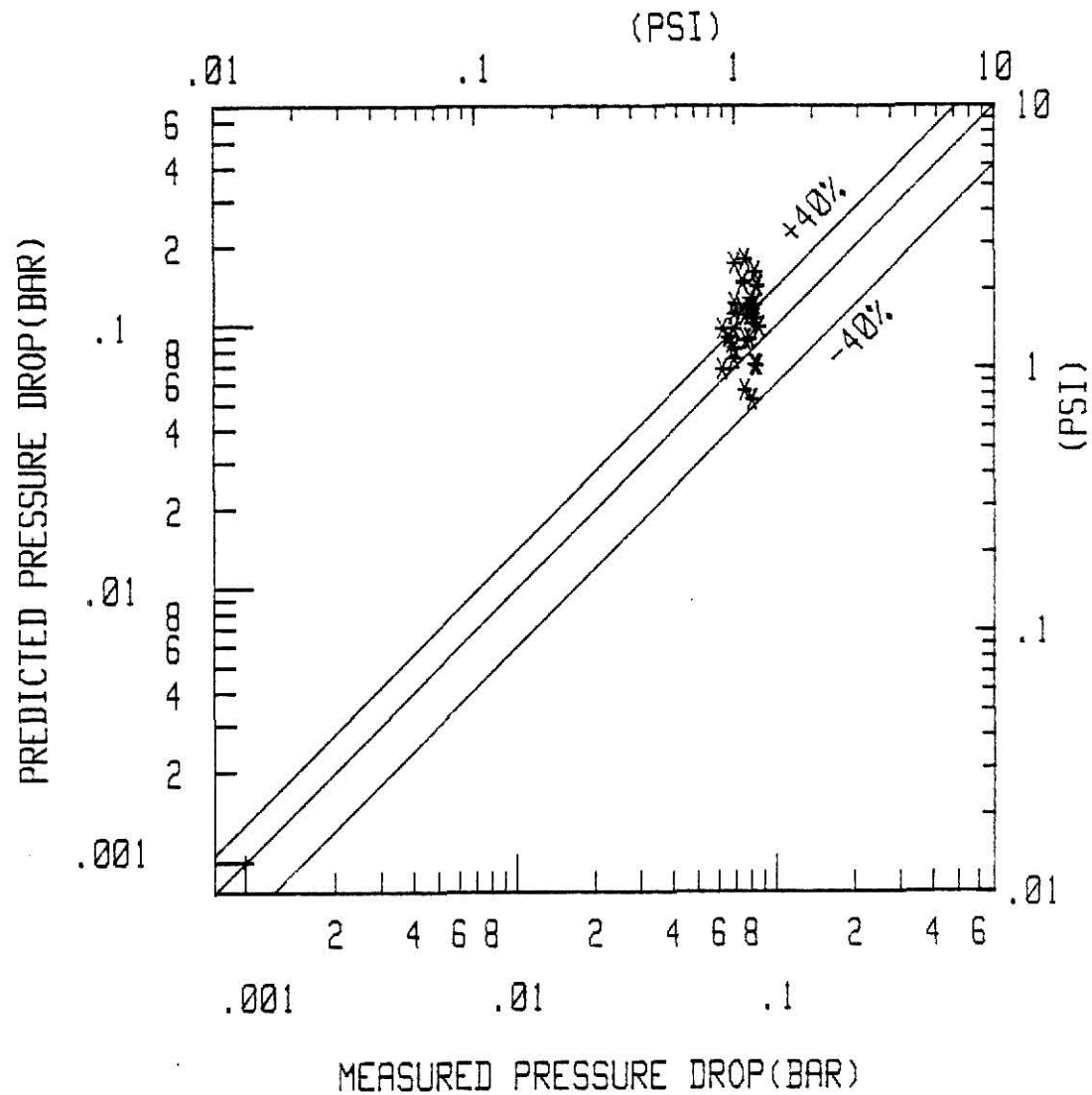


Fig. 5.22 Comparison of Experimental Pressure Drop With Predicted Values Obtained From Martinelli-Nelson Correlation, Eq (5.61), Tube 1.

Carnavos [22] also proposed the following correlation for the friction factor based on his work with single phase turbulent flow of water in internally finned tubes.

$$f = \frac{0.046}{Re^{0.2} (F^*)} \quad (5.66)$$

where,

$$F^* = \frac{(F_4)^{0.5}}{(F_3)^{0.75}} \quad (5.67)$$

The above correlation is somewhat similar to his preceding correlation, except for the term accounting for the effect of the helix angle F_3 .

5.3.3 New Finned Tubes Correlation for Saturated Boiling

Despite the fact that the Martinelli-Nelson [34] two phase pressure drop correlation was a better predictor of the smooth tube pressure drop than the Pierre [26] correlation, the latter was selected as the basis for developing the finned tubes correlation. This was due to the fact that Pierre's correlation is a widely used correlation.

Individual correlations were obtained for all the tubes, for the friction factor as a function of $\frac{Re}{k_f}$, in the form

$$f = c'' \left(\frac{Re}{k_f} \right)^{n''} \quad (5.68)$$

where, c'' and n'' were obtained using the least square regression analysis. The results for all the tubes were as follows:

Tube 1

$$f = 0.0011 * \left(\frac{k_f}{Re} \right)^{0.112} \quad (5.69)$$

Tube 2

$$f = 0.0148 * \left(\frac{k_f}{Re} \right)^{0.245} \quad (5.70)$$

Tube 3

$$f = 0.0235 * \left(\frac{k_f}{Re} \right)^{0.28} \quad (5.71)$$

Tube 4

$$f = 0.1045 * \left(\frac{k_f}{Re} \right)^{0.525} \quad (5.72)$$

In developing Eqs. (5.69) through (5.72) from Eq. (5.56), the same scheme of dividing the tube into 10 equal sections and calculating the pressure drop for each section was used.

The ratio of $\frac{(\Delta P)_{fin}}{(\Delta P)_{sm}}$ was calculated for the same $\left(\frac{Re}{k_f} \right)$ and correlated in terms of the parameters F_3 and F_4 . After several trials and by using the least square regression analysis, the following equation resulted.

$$\frac{(\Delta P)_{fin}}{(\Delta P)_{sm}} = 0.628 * (F_3)^{4.887} (F_4)^{-12.285} \quad (5.73)$$

$(\Delta P)_{sm}$ is obtained from Eq. (5.56).

Figure 5.23 shows a comparison between the experimental values of pressure drop and the values predicted by using Eq. (5.56) and the friction factor obtained from Eq. (5.69).

Figures 5.24 through 5.26 also show comparisons between the predictions of Eq. (5.73) and the experimental pressure drop values of tubes 2, 3, and 4, respectively. It is seen from Figs. 5.24 through 5.26, that 86% of the data points for tube 2, 68% for tube 3 and 70% for tube 4 lie within $\pm 40\%$ disagreement range.

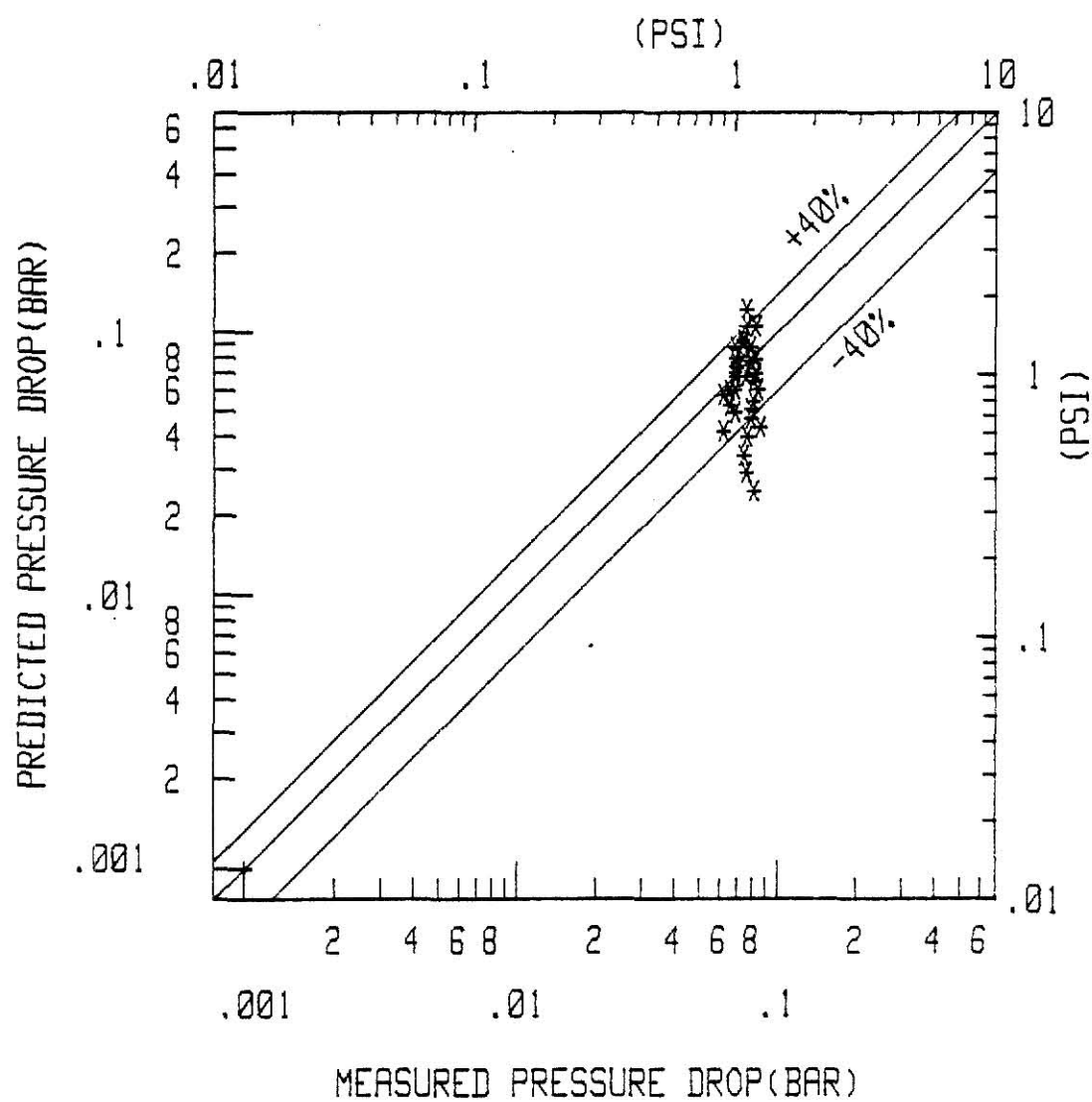


Fig. 5.23 Comparison of Experimental Values of Pressure Drop With Predicted Values of Modified Pierre's Correlation, Tube 1.

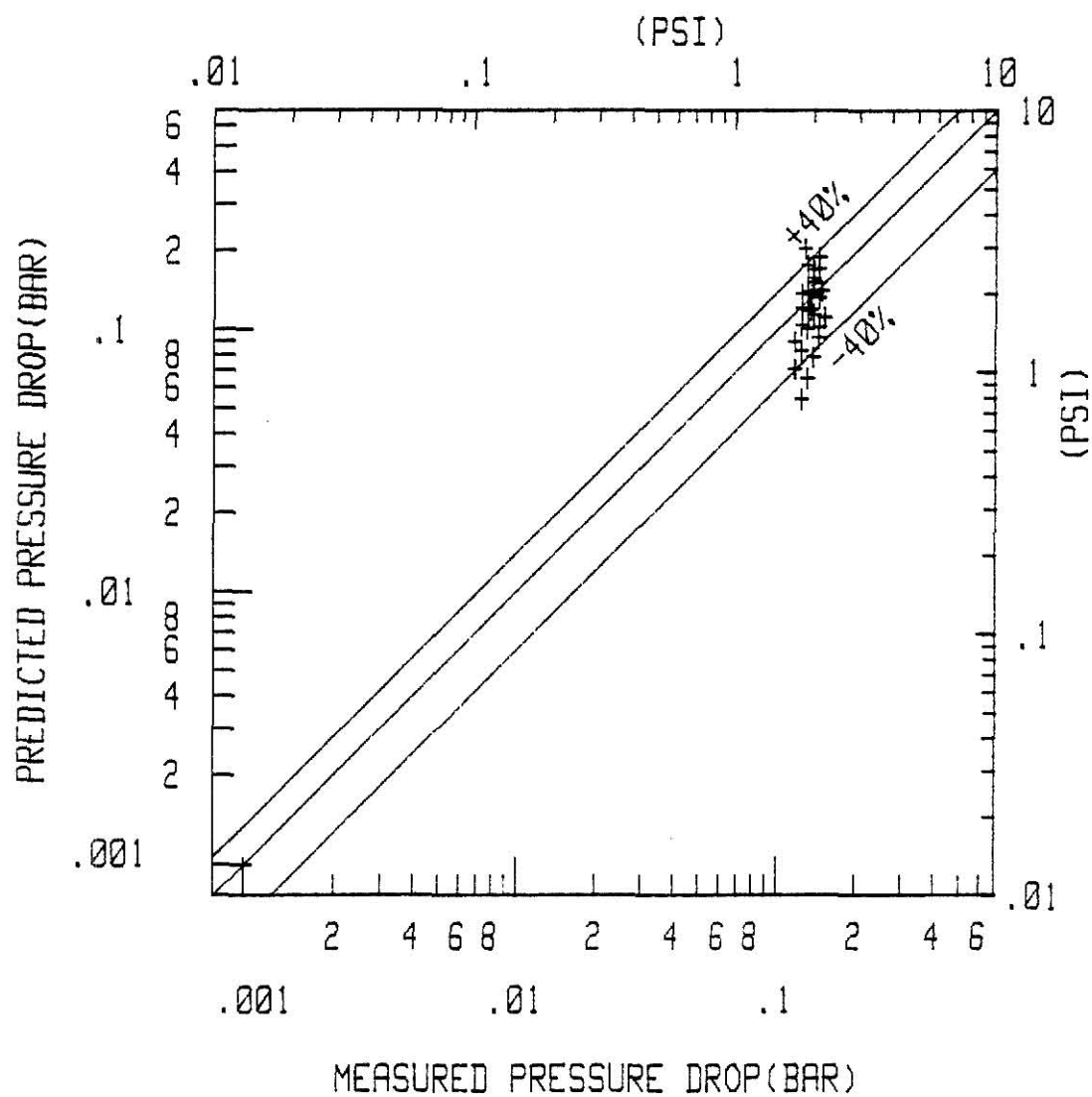


Fig. 5.24 Comparison of Experimental Values of Pressure Drop With Predicted Values of Eq (5.73), Tube 2.

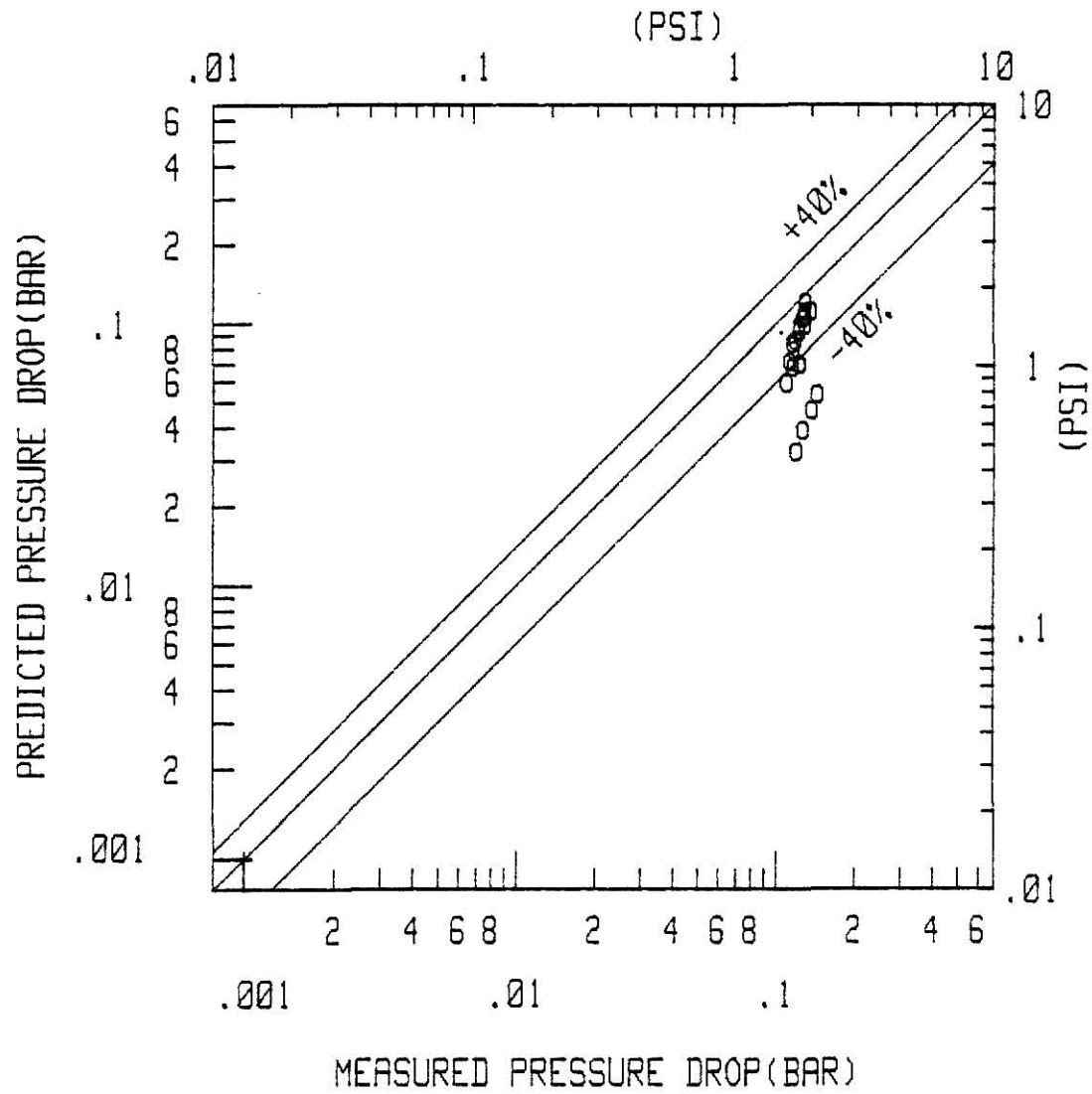


Fig. 5.25 Comparison of Experimental Values of Pressure Drop With Predicted Values of Eq (5.73), Tube 3.

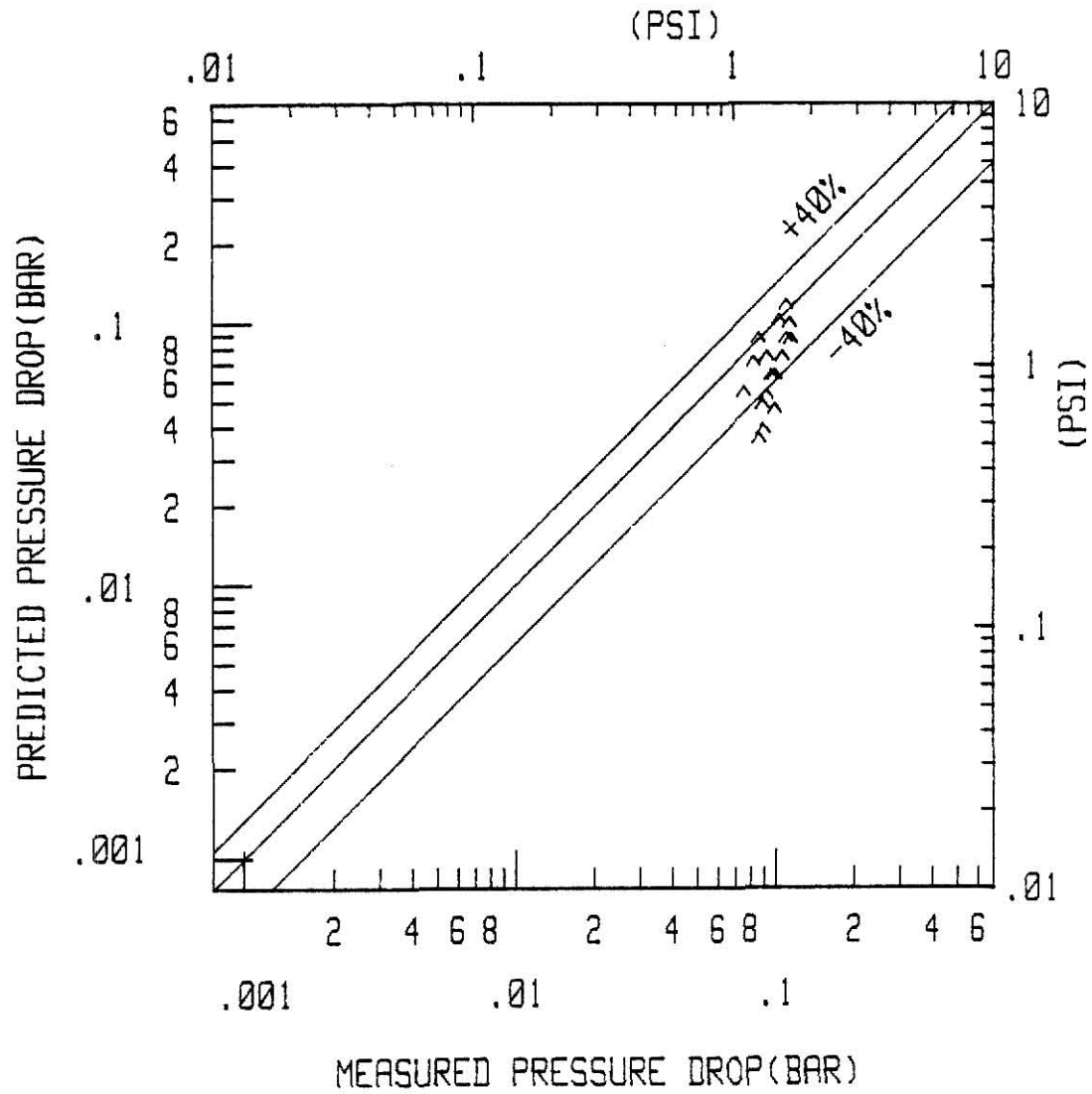


Fig. 5.26 Comparison of Experimental Values of Pressure Drop With Predicted Values of Eq (5.73), Tube 4.

CHAPTER VI

PERFORMANCE EVALUATION OF AUGMENTED TUBES

6.1 INTRODUCTION

In Chapter IV a comparison was made between the heat transfer performance of the smooth tube and the finned tubes. On a nominal area basis, tubes 2 and 3 enhanced the heat transfer by 59% and 230% respectively, above the smooth tube values. In carrying out a performance evaluation of the finned tubes, it is essential to consider the penalty of the increase in the pressure drop, associated with the enhancement of heat transfer.

6.2 PERFORMANCE INDICES

Each performance evaluation index is determined as the ratio of certain parameters of interest for the augmented and smooth surface, subject to certain constraints.

Bergles et al. [36, 37] suggested nine performance evaluation indices for heat transfer augmentation in single phase flow. Four of the performance indices were directed towards the use of promoters for improvement of existing heat exchangers; the basic geometry was fixed and analytical relationships were obtained considering the increase in heat duty or decrease in pumping power, which can be obtained under various process restrictions. Four additional indices were presented to evaluate the advantages of using promoters in the design of new heat exchangers; length and number of tubes were free, with the heat duty along with either pumping power, flow rate, or pressure drop being fixed and the objective was to reduce the exchanger's size. Finally, a performance index was presented for economic evaluation of enhanced tubes.

Royal [38] adapted two of the above indices to evaluate the performance of internally finned tubes and tubes with twisted tape inserts in augmenting the condensation heat transfer of steam. These indices were the condenser size reduction index R_h and the pressure drop index $R_{\Delta P}$, and they are given by

$$R_h = (A_{aug}/A_{sm}) = (h_{sm}/h_{aug}) \quad (6.1)$$

and,

$$R_{\Delta P} = (\Delta P_{aug}/\Delta P_{sm}) \quad (6.2)$$

R_h and $R_{\Delta P}$ were evaluated under the constraints of fixed heat duty, nominal diameter, and constant temperature difference. The same indices were used by Luu and Bergles [39, 40] in evaluating the performance of internally finned tubes and tubes with twisted tape inserts in augmenting the condensation of R-113. These indices were developed assuming that external resistance of the condensing surface is negligible or the condensing side thermal resistance controls the flow.

Azer et al, [41], Lin [42], and Said [43] used the ratio of the pumping power to the rate of heat transfer P/Q , as an evaluation index, in determining the performance of static in-line mixers, in augmenting condensation heat transfer inside horizontal tubes. The pumping power was obtained from the product of volume flow rate of the liquid at the circulating pump and the pressure drop across the test section. The constraints under which P/Q was evaluated were: the same mass flow rate, the same inlet temperature, and the same geometry. The same index of evaluation was used in the present study.

Only the smooth tube 1, straight finned tube 2 and the spiral finned tube 3 satisfied the constraint of fixed geometry, which required that the length and the inside diameter of the tube, augmented or unaugmented, be

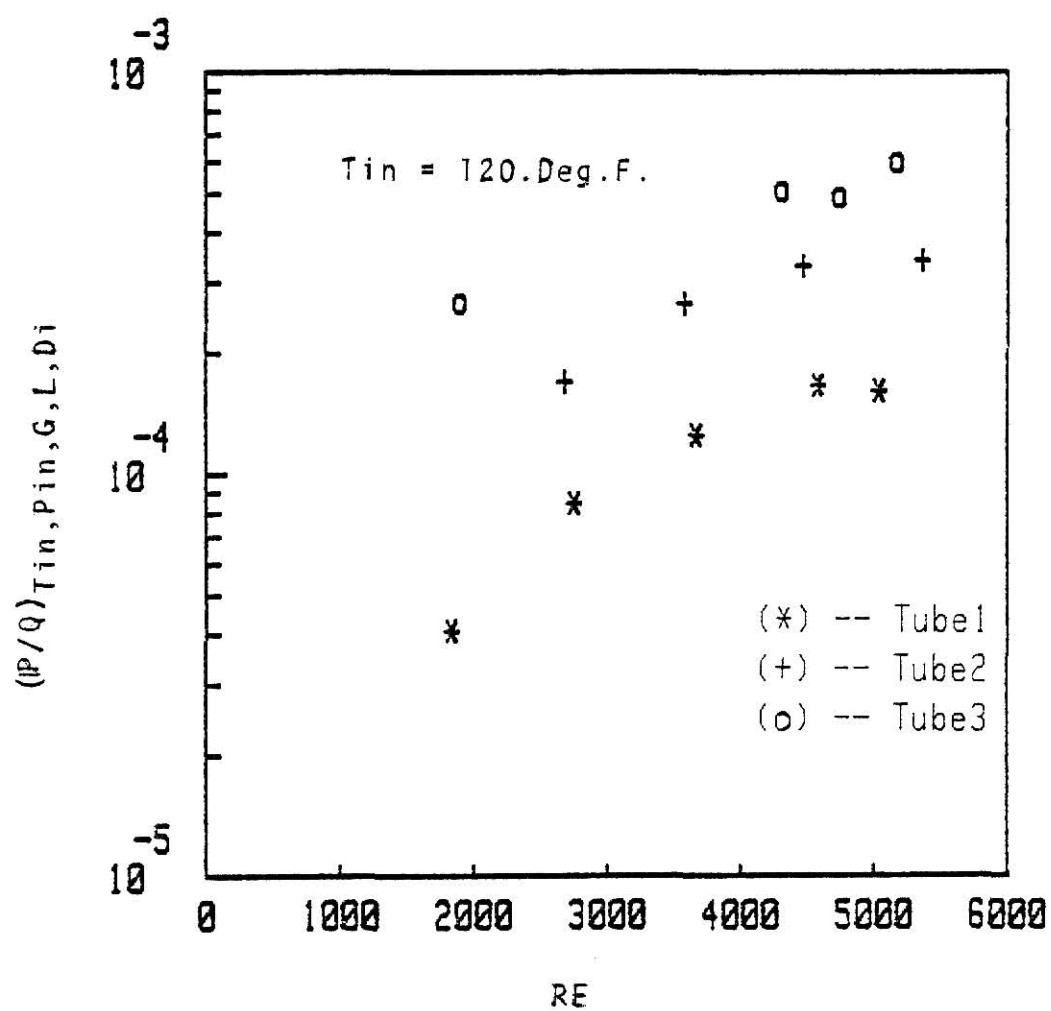


Fig. 6.1 Pumping Power per Unit Heat Transfer Rate Versus the Reynolds No. at $T_{in} = 120 \text{ F (49 C)}$.

the same. Therefore, they were the three tubes that were evaluated.

Fig. 6.1 is a plot of P/Q versus Re for tube 1, 2 and 3 at $T_{in} = 120^{\circ}F$. Re was based on the total flow rate, the inside nominal diameter D_i , and the dynamic viscosity of the liquid. The lower this index is, the lower is the power demand per unit heat transfer. It is clear from the plot of P/Q versus Re that the smooth tube performed the best, followed by tube 2 and tube 3.

It is obvious that the enhancement of heat transfer is always accompanied by an increase in pressure drop. The maximum enhancement of heat transfer was obtained with the spiral finned tube 3, which resulted in a considerable amount of power demand, well above the values obtained for that of the smooth tube 1, and the straight finned tube 2.

CHAPTER VII

SUMMARY, CONCLUSIONS AND RECOMMENDATIONS

Heat transfer and pressure drop data were taken during saturated boiling of R-113 inside a smooth, a straight finned and two spiral finned tubes. The smooth tube results were used to identify among the existing smooth tube heat transfer correlations, the best predictors of the experimental measurements of the present study. Appropriate modifiers were identified and applied to the smooth tube correlations to bring about the best agreement between the measurements and predictions.

The results are summarized in the following.

1. The heat transfer coefficients for all the tubes increased with the increase in mass flux, for a fixed range of exit dryness fraction.
2. The Nusselt number increased with Pierre's parameter (Re^{2k_f}) for all the tubes.
3. The spiral finned tube 3 gave the maximum heat transfer enhancement of 230% over the smooth tube 1 on a nominal area basis.
4. The pressure drop increased with increase in mass flux for all the tubes, for a fixed range of exit dryness fraction.
5. The straight finned tube 2 gave the maximum increase in pressure drop of 107% over the smooth tube 1.
6. The spiral finned tube 3 had the greatest pumping power demand per unit heat transfer rate for a fixed value of inlet temperature, mass flux, length, inner diameter.
7. Three new correlations were developed for predicting the saturated boiling heat transfer coefficient for finned tubes. Among the correlations

developed, the one based on Pierre's parameter was the best predictor of the experimental measurements.

8. A new correlation was developed for the pressure drop during saturated boiling heat transfer inside internally finned tubes. The correlation, based on Pierre's correlation, was a good predictor of the experimental measurements.

Recommendations for Future Studies

1. Additional studies need to be performed using different fluids and tube diameters to verify the general applicability of the correlations developed in the present study.

2. More reliable pressure drop correlations need to be developed for boiling inside smooth tubes under different flow patterns.

3. There are several performance evaluation criteria for single phase flow. More reliable and attainable performance evaluation criteria need to be defined for two phase flow.

4. Many of augmentation techniques tested in the laboratory have not been adopted for full scale industrial application. It is therefore recommended that promising techniques be considered for application in commercial equipment.

ACKNOWLEDGEMENTS

I wish to express my sincere gratitude to Dr. N.Z. Azer for his guidance and help during the course of the present investigation.

The help offered by Messrs. S.A. Said, Bud Shirley and Gary Thornton in the construction of the experimental system is gratefully acknowledged.

Thanks are due to Dr. C.L. Huang and Dr. Leonard E. Fuller for being on my examination committee and a note of appreciation to the former, for all the personal advice rendered.

Thanks are also extended to Dr. Paul L. Miller, Chairman, Dept. of Mechanical Engineering, for providing financial and moral support during my period of study.

I wish to thank Mrs. Rose Day for her efficient handling of the typing.

The author wishes to dedicate this work to his family in Madras, for their constant encouragement and inspiration.

SELECTED BIBLIOGRAPHY

1. Bergles, A.E., "Research Workshop on Augmentation of Convective Heat Transfer," Final Report HTL-8, ISU-ERI-AMES-76026 (1975).
2. Bergles, A.E., Webb, R.L., Junkhan, G.H., and Jensen, M.K., "Bibliography on Augmentation of Convective Heat and Mass Transfer," Engineering Research Institute, Iowa State University, HTL-19, ISU-ERI-AMES-79206, (1979).
3. Bergles, A.E. and Webb, R.L., "Augmentation of Convective Heat Transfer and Mass Transfer," Presented at the Winter Annual Meeting of ASME, New York, Dec. 2 (1970).
4. Boling, C.W., et al., "Heat Transfer of Evaporating Freon with Inner Fin Tubing," Refrigerating Engineering, 61, pp. 1338-1340 (1953).
5. Bernstein, E., Petrek, J.P., and Meregian, J., "Evaluation and Performance of Once-through Zero-Gravity Boiler Tubes with Two-Phase Water," PWAC-428 (1964).
6. Kidd, G.J., Jr., "The Heat Transfer and Pressure Drop Characteristics of Gas Flow inside Spirally Corrugated Tubes," ASME Transactions, J. of Heat Transfer, Paper No. 69-WA/HT-3.
7. Lipets, Au., Zholudov, Ya.S., Antonov, Ya.S. and Gromov, G.V., "The Temperature Regime and Hydraulic Resistance of Tubes with Internal Longitudinal Fins," Heat Transfer, Soviet Research, Vol. 1, No. 5, Sept. (1969).
8. Watkinson, A.P., Milette, D.L. and Tarasoff, P., "Turbulent Heat Transfer and Pressure Drop in Internally Finned Tubes," AIChE Symposium Series, 69, No. 131, (1973), pp. 94-103.
9. Withers, J.G. and Habdas, E.P., "Heat Transfer Characteristics of Helical Corrugated Tubes for In-tube Boiling of Refrigerants R-12," AIChE Symp. Series, 70, (1974), pp. 98-106.
10. Ornatskiy, A.P., Shcherbakov, V.K., and Semena, M.G., "A Method for Computing the Temperature and Selecting the Cross Section Geometry of Pipes with Internal Fins," Heat Transfer - Soviet Research, Vol. 7, No. 5, Sept.-Oct. (1975).
11. Watkinson, A.P., Milette, D.L., and Kubanek, G.R., "Heat Transfer and Pressure Drop of Internally Finned Tubes in Turbulent Air Flow," ASHRAE Transactions, Vol. 81, Part 1, (1975), pp. 330-349.
12. Masliyah, J.H. and Nandakumar, K., "Heat Transfer in Internally Finned Tubes," J. of Heat Transfer, Vol. 98, (1976), pp. 257-261.
13. Masliyah, J.H. and Nandakumar, K., "Fluid Flow and Heat Transfer in Internally Finned Helical Coils," The Canadian J. of Chemical Engineering, Vol. 55, Feb. (1977), pp. 27-36.

14. Nandakumar, K. and Masliyah, J.H., "Fully Developed Viscous Flow in Internally Finned Tubes," *The Chemical Eng. J.*, Vol. 10 (1975), pp. 113-120.
15. Soliman, H.M. and Feingold, A., "Heat Transfer, Pressure Drop and Performance Evaluation of a Quintuplex Internally Finned Tube," ASME Paper 77-HT-46, Presented at the AIChE-ASME Heat Transfer Conference, Salt Lake City, Utah, Aug. (1977).
16. Vander Mast, V.C., Read, S.M., and Bromley, L.A., "Boiling of Natural Sea Water in Falling Film Evaporators," *Desalination*, 18 (1976), pp. 71-94.
17. VanRooyen, R.S. and Kröger, D.G., "Laminar Flow Heat Transfer in Internally Finned Tubes with Twisted Tape Inserts," *Intl. Heat Transfer Conf.*, 1978, Vol. 2, pp. 577-581.
18. Marner, W.J. and Bergles, A.E., "Augmentation of Tube Side Laminar Flow Heat Transfer by Means of Twisted-Tape Inserts, Static Mixer Inserts, and Internally Finned Tubes," Presented at Sixth International Heat Transfer Conference, Toronto, Canada, Aug. 1978.
19. Patankar, S.V., Ivanovic, M. and Sparrow, E.M., "Analysis of Turbulent Flow and Heat Transfer in Internally Finned Tubes and Annuli," *J. of Heat Transfer*, Feb. 1979, Vol. 101, pp. 29-37.
20. Minchenko, F.P. and Shvartsman, G.S., "Heat Transfer Enhancement in Finned Steam Generating Tubes," *Heat Transfer-Soviet Research*, Vol. 11, No. 2, March-April 1979, pp. 14-23.
21. Kubanek, G.R., and Milette, D.L., "Evaporative Heat Transfer and Pressure Drop Performance of Forge-Fin Tubes with R-22," Internal Report No. 340, Noranda Research Centre, Point Claire, Quebec, July 1976.
22. Carnavos, T.C., "Heat Transfer Performance of Internally Finned Tubes in Turbulent Flow," *Heat Transfer Engineering*, Vol. 1, No. 4, April-June (1980), pp. 32-37.
23. Carnavos, T.C., "Cooling Air in Turbulent Flow Multi-Passage Internally Finned Tubes," ASME Paper 78-WA/HT-52. Presented at the Winter Annual Meeting, San Francisco, Calif., Dec. 10-15 (1978).
24. Carnavos, T.C., "Cooling Air in Turbulent Flow with Internally Finned Tubes," Presented at the 17th Natl. Heat Transfer Conf., Salt Lake City, Utah, AIChE Paper 4, Aug. 14-17 (1977). Also *Heat Transfer Engineering* Vol. 1, No. 2, Oct.-Dec. (1979), pp. 41-46.
25. Soliman, H.M., Chan, T.S. and Trupp, A.C., "Analysis of Laminar Heat Transfer in Internally Finned Tubes with Uniform Outside Wall Temperature," *J. of Heat Transfer*, Vol. 102, Nov. 1980, pp. 598-604.
26. Pierre, B., "The Coefficient of Heat Transfer for Boiling Freon-12 in Horizontal Tubes," *Heating and Air Treatment Engineer*, pp. 302-310, Dec. (1956).

27. Dengler, C.E., and Addoms, J.N., "Heat Transfer Mechanism for Vaporization of Water in Vertical Tubes," Chemical Engineering Progress Symposium Series, Vol. 52, No. 18, 1956, pp. 95-103.
28. Guerrieri, S.A. and Talty, R.D., "A Study of Heat Transfer to Organic liquids in Single Tube Natural Circulation Boilers," Chemical Engineering Progress Symposium Series, "Heat Transfer," Louisville, No. 18, Vol. 52, 1956, pp. 69-77.
29. Bennett, J.A.R., Collier, J.G., Pratt, H.R.C., and Thornton, J.D., "Heat Transfer to Two Phase Gas-Liquid Systems, Part I," Transactions of the Institution of Chemical Engineers, England, Vol. 39, 1961, pp. 113-126.
30. Chen, J.C., "A Correlation for Boiling Heat Transfer to Saturated Fluids in Convective Flow," I and EC Process Design and Development, Vol. 5, No. 3, July 1966, pp. 322-329.
31. Shah, M.M., "A New Correlation for Heat Transfer During Boiling Flow Through Pipes," ASHRAE Transactions, Vol. 82, Part 2, 1976, pp. 66-86.
32. Schrock, V.E., and Grossman, L.M., "Forced Convection Boiling in Tubes," Nuclear Science and Engg., Vol. 12, 1962, pp. 474-481.
33. Sani, R.L., "Downflow Boiling and Non-Boiling Heat Transfer in a Uniformly Heated Tube," University of California at Berkeley, Report UCRL 9023, 1960.
34. Martinelli, R.C., and Nelson, D.B., "Prediction of Pressure Drop During Forced Circulation Boiling of Water," Trans. ASME, Aug. 1948, pp. 695-702.
35. Ornatskii, A.P., Shcherbakov, V.K., and Semena, M.G., "Investigation of Velocity Distribution in Tubes with Internal Longitudinal Fins," Thermal Engineering (USSR), 17, (2), (1970), 108.
36. Bergles, A.E., Bunn, R.L. and Junkhan, G.H., "Extended Performance Evaluation Criteria for Enhanced Heat Transfer Surfaces," Letters in Heat and Mass Transfer, Vol. 1, 1974, pp. 113-120, Int. J. of Heat and Mass Transfer.
37. Bergles, A.E., Blumenkrantz, A.R. and Tuborek, J., "Performance Evaluation Criteria for Enhanced Heat Transfer Surfaces," 13th Natl. Heat Transfer Conf., AIChE, ASME, Denver, Col., Aug. 6-9, 1972.
38. Royal, J., "Augmentation of Horizontal In-Tube Condensation of Steam," Ph.D. Dissertation, Iowa State University, Ames, Iowa, 1975.
39. Luu, M., "Augmentation of In-Tube Condensation of R-113," Ph.D. Dissertation, Dept. of Mech. Engg., Iowa State University, Ames Iowa, (1980).
40. Luu, M. and Bergles, A.E., "Augmentation of In-Tube Condensation of R-113," ASHRAE - Project RP-219, HTL-23, ISU-ERI-Ames-20157, Project 1309, Jan. (1980).

41. Azer, N.Z., Fan, L.T., and Lin, S.T., "Augmentation of Condensation Heat Transfer with In-Line Static Mixers," Proceedings of the 1976 HTFMI, (1976): 512-526.
42. Lin, S.T., "Augmentation of Two Phase Heat Transfer with In-Line Static Mixers," Ph.D. Dissertation, Dept. of Mechanical Engg., Kansas State University, Manhattan, Kansas, 1979.
43. Said, S.A.M., "Augmentation of Condensation Heat Transfer of R-113 by Internally Finned Tubes and Twisted Tape Inserts," Ph.D. Dissertation, Dept. of Mechanical Engg., Kansas State University, Manhattan, Kansas, 1982.
44. Kline, S.J., and McClintock, F.A., "Describing Uncertainties in Single Sample Experiments," Mechanical Engineering 75, January (1953): 3-8.

NOMENCLATURE

Symbol

A	Flow Cross-sectional area, m^2 and Heat Conduction area, m^2
A_a	Actual heat transfer area, m^2/m^2
A_{fa}	Actual free flow area, m^2
A_{fc}	Open core free flow area, m^2
A_{fn}	Nominal flow area based on inside tube diameter as if fins were not present, m^2
A_n	Nominal heat transfer area based on inside tube diameter as if fins were not present, m^2/m
b	Fin height, m
B_o	Boiling number, Eq. (5.19)
C	Constant in Eq. (4.2)
C'	Constant in Eq. (4.4)
C''	Constant in Eq. (5.69)
C'''	Constant in Eq. (5.49)
C_o	Convection number Eq. (5.18)
$C_{p\ell}$	Specific heat of liquid, $W.hr/kg.^{\circ}C$
D_e	Equivalent diameter, m
D_h	Hydraulic diameter ($D_h = 4 A_{fa}/A_a$), m
D_i	Inside tube diameter, m
D_o	Outside tube diameter, m
f_m	Friction factor
F	Factor defined in Eqs. (5.14) and (5.33)
F_1	Parameter defined in Eq. (5.34)
F_2	Parameter defined in Eq. (5.35)
F_3	Parameter defined in Eq. (5.36)

Fr_L	Froude Number, Eq. (5.20)
g_c	Gravitational constant, $g_c = 9.81 \frac{\text{kg} \cdot \text{m}/\text{sec}^2}{\text{N}}$
G	Mass flux, $\text{kg}/\text{hr} \cdot \text{m}^2$
h	Heat Transfer coefficient $\text{W}/\text{m}^2 \text{ } ^\circ\text{C}$
h_L	Single phase heat transfer coefficient $\text{W}/\text{m}^2 \text{ } ^\circ\text{C}$
h_L'	Single phase liquid heat transfer coefficient $\text{W}/\text{m}^2 \text{ } ^\circ\text{C}$
\bar{h}_{TP}	Average heat transfer coefficient $\text{W}/\text{m}^2 \text{ } ^\circ\text{C}$
h_{TP}	Local heat transfer coefficient, $\text{W}/\text{m}^2 \text{ } ^\circ\text{C}$
H	Fin pitch (length per turn), $\text{m}/360^\circ$
h_f	Enthalpy of saturated liquid J/kg
h_g	Enthalpy of saturated vapor J/kg
h_{mac}	Heat transfer coefficient due to convection $\text{W}/\text{m}^2 \text{ } ^\circ\text{C}$
h_{mic}	Heat transfer coefficient due to nucleate boiling
h_{fg}	Latent heat of vaporization, J/kg
k_L	Thermal conductivity of saturated liquid, $\text{W}/\text{m} \text{ } ^\circ\text{C}$
k	Thermal conductivity of copper, $\text{W}/\text{m} \text{ } ^\circ\text{C}$
k_f	Pierre Parameter defined in Eq. (5.2)
L	Length of test section, m
m	Constant in Eq. (5.29)
M_f	Mass flow rate of R-113, kg/hr
n	Constant in Eqs. (4.2) and (5.24) or number of internal fins.
n'	Constant in Eq. (4.4)
n'''	Constant in Eq. (5.49)
N	Dimensionless parameter, Eq. (5.22)
NBCF	Nucleate Boiling Correction Factor
Nu	Nusselt Number

P	System pressure, bar
ΔP_{SAT}	Pressure difference between inlet pressure and saturation pressure, bar
Pr_L	Prandtl number of saturated liquid
q/A	Heat Flux applied to tube, W/m^2
Q	Electric input to test section, W
r^*	radius of bubble, m
r_o	Outer radius of tube, m
r_i	Inner radius of tube, m
$R_{\Delta p}$	Pressure drop index for the performance evaluation, Eq. (6.2)
R_h	Reduction condenser size index for the performance evaluation, Eq. (6.1)
Re	Reynolds number, $(\frac{G D_i}{\mu_L})$
Re_L	Reynolds number based on liquid on liquid phase alone flowing in the tube ($Re_L = G(1-x) D_i / \mu_L$)
S	Suppression factor in Eq. (5.16)
T	Temperature, $^{\circ}C$
T_{av}	Average of inlet and outlet temperatures of R-113, $^{\circ}C$
ΔT	Temperature differences, $^{\circ}C$
T_{WL}	Average inside wall temperature, $^{\circ}C$
ΔT_{SAT}	Wall superheat, $^{\circ}C$
V_f	Specific volume of saturated liquid, m^3/kg
V_g	Specific volume of saturated vapor, m^3/kg
V_m	Mean specific volume of the two phase fluid, m^3/kg
W	Transverse pitch of internal fins ($W = \frac{\pi D_i}{n}$)
x	Dryness fraction (ratio of vapor mass to total mass)
Δx	Difference in quality between exit and inlet

Greek Letters

α	Spiral fin tube helix angle (angle between fin and tube axis) degrees
δ	Liquid film thickness, m
λ	Constant used in Eq. (5.29)
μ_L	Dynamic viscosity of saturated liquid kg/hr m
μ_V	Dynamic viscosity of saturated vapor, kg/ hr m
ν_L	Kinematic viscosity of saturated liquid, m ² /hr
ρ	Density, kg/m ³
ρ_L	Density of Saturated liquid, kg/m ³
ρ_V, ρ_g	Density of saturated vapor phase, kg/m ³
ψ	Constant in Eq. (5.17)
ψ_{nb}	Dimensionless parameter by Eqs. (5.24), (5.25)
ψ_{cb}	Dimensionless parameter Eq. (5.26)
ψ_{bs}	Dimensionless parameter, Eq. (5.27), (5.28)
σ	Surface Tension, dyne/cm

Subscripts

aug	Augmented surface
cal	Calculated
exp	Experimental
in	Inlet
out	Outlet
s	Saturated
sm	Smooth surface
finned	Finned surface
TP	two phase

APPENDIX A

SAMPLE OF DATA REDUCTION AND CALCULATION PROCEDURE
OF HEAT TRANSFER COEFFICIENTEXPERIMENTAL RUN NO. 4, SMOOTH TUBE (TUBE 1)

R-113 inlet pressure	= 2.3 psig
R-113 inlet temperature	= 120.38 ⁰ F
R-113 exit temperature	= 120.38 ⁰ F
Pump flow rate	= 0.1 gpm
Temperature at flow meter	= 98.06 ⁰ F
Pressure Drop	= 2.22 mv \approx 1.0295 psi

Surface temperature

T (26, 27)*	= 138.56 ⁰ F
T (28, 29)	= 134.33 ⁰ F
T (30, 31)	= 131.81 ⁰ F
T (32, 33)	= 133.07 ⁰ F
T (34, 35)	= 131.45 ⁰ F
T (36, 37)	= 133.79 ⁰ F
T (38, 39)	= 133.7 ⁰ F
T (40, 41)	= 135.77 ⁰ F
T (42, 43)	= 134.06 ⁰ F

*T(26, 27) is the average of thermocouples readings at a given axial location.

R-113 Density	= 95.96 lb/ft ³
---------------	----------------------------

Calculation Procedure

Mass flow rate, M_f :

$$\begin{aligned}
 M_f &= 0.1 \frac{\text{gallons}}{\text{minute}} \times 60 \frac{\text{minute}}{\text{hour}} \times 0.13368 \frac{\text{ft}^3}{\text{gallon}} \times 95.96 \frac{\text{lbm}}{\text{ft}^3} \\
 &= 76.97 \text{ lbm/hr}
 \end{aligned}$$

Enthalpy of F-113 at inlet = 33.566 Btu/lb

Enthalpy of saturated liquid at exit, h_f = 33.566 Btu/lb

Enthalpy of saturated vapor at exit, h_g = 96.467 Btu/lb

Heat Loss to the top by Conduction:

$$\begin{aligned}
 &= \frac{KA}{L} * (T(40, 41) - T(42, 43)) \\
 &= \frac{227 \times \frac{\pi}{4} \left[\left(\frac{0.624}{12} \right)^2 - \left(\frac{0.545}{12} \right)^2 \right] * [135.77 - 134.06]}{(2/12)} \\
 &= \underline{0.9214} \text{ Btu/hr}
 \end{aligned}$$

Heat loss to the bottom by conduction:

$$\begin{aligned}
 &= \frac{KA}{L} \times (T(26,27) - T(28,29)) \\
 &= \frac{227 \times \frac{\pi}{4} \left[\left(\frac{0.624}{12} \right)^2 - \left(\frac{0.545}{12} \right)^2 \right] * [138.56 - 134.33]}{(2/12)} \\
 &= \underline{2.28} \text{ Btu/hr}
 \end{aligned}$$

Total Electrical Power Supplied:

$$\begin{aligned}
 &= 54.0 \text{ vol.} \times 18.2 \text{ amp} \times 3.41 \frac{\text{B/hr}}{\text{W}} \\
 &= 3346.85 \text{ Btu/hr}
 \end{aligned}$$

Heat gained by F-113:

$$\begin{aligned}
 &= 3346.85 - (0.9214 + 2.28) \\
 &= \underline{3343.65 \text{ Btu/hr}}
 \end{aligned}$$

Dryness fraction at Exit:

$$\begin{aligned}
 3343.65 &= 76.97 [96.467 x + (1 - x) 33.566 - 33.566] \\
 \underline{x} &= \underline{0.689}
 \end{aligned}$$

Average outside surface temperature:

$$\begin{aligned}
 &= (138.56 + 134.33 + 131.81 + 133.07 + 131.45 + \\
 &\quad 133.79 + 133.7 + 135.77 + 134.06)/9.0 \\
 &= \underline{134.06^{\circ}\text{F}}
 \end{aligned}$$

Temperature drop across the wall thickness:

$$\begin{aligned}
 \Delta T &= \frac{Q \ln(r_o/r_i)}{2\pi KL} \\
 &= 3345.33 \ln\left(\frac{0.624}{0.545}\right) \\
 &= 0.0735^{\circ}\text{F}
 \end{aligned}$$

Average inside surface temperature:

$$= 134.06 - 0.0735 = \underline{133.99^{\circ}\text{F}}$$

$$\begin{aligned}
 h_i &= \frac{Q}{A\Delta T} = \frac{3345.33 \text{ B/hr}}{(\pi \times \frac{0.545}{12} \times \frac{52.5}{12}) \text{ ft}^2 \times (133.99 - 120.38)^{\circ}\text{F}} \\
 &= 393.48 \frac{\text{Btu}}{\text{hrft}^2 \text{ }^{\circ}\text{F}}
 \end{aligned}$$

$$\begin{aligned}
 G &= \frac{\dot{M}_f}{A} = \frac{76.97 \text{ lbm/hr}}{(\frac{0.545}{24})^2 \pi \text{ ft}^2} \\
 &= 47491.38 \frac{\text{lbm}}{\text{hrft}^2}
 \end{aligned}$$

APPENDIX B
COMPUTER PROGRAM FOR DATA REDUCTION

Symbols used in the Computer Program

TIN	R-113 inlet temperature
TOUT	R-113 outlet temperature
TWLM	Average inside wall temperature
GV	Total R-113 mass velocity
DT	Temperature drop across the wall and F-113
QAFN	Heat Flux
HI	Inside heat transfer coefficient
DP	Pressure drop
RE	Reynolds Number
NU	Nusselts Number
X(EXIT)	Dryness fraction at Exit

C CALCULATION OF SATURATED LIQUID ENTHALPY IN BTU/LBM FROM
 C ASHRAE TABLES
 C $HFF(X) = 8.1416 + 0.19636 * X + 0.118E-03 * X * X + 0.3816E-07 * X * X * X$

C CALCULATION OF SATURATED VAPOR ENTHALPY IN BTU/LBM FROM
 C ASHRAE TABLES

C $HGF(X) = 78.6342 + 0.14846 * X + 0.22E-05 * X * X - 0.4133E-07 * X * X * X$

C CALCULATION OF SATURATED LIQUID DENSITY LBM/CU FT AS A
 C FUNCTION OF SATURATED TEMP. DEG F (CURVE FIT FROM
 C ASHRAE TABLES)

C $LDEN(X) = 104.07 - 0.0827 * X$

```

      DIMENSION T(21),ANU(100),G(100),HI(100),AQ(100),RE(100)
      DIMENSION VM(100),GX(100),HID(100),PIN(100)
      REAL K,MYU,MF,KF
110 FORMAT(/,T7,'TABLE (2):-',/,',',6X,126(' ',/))
111 FORMAT(T7,'RUN',4X,'TYPE',8X,'TIN',15X,'TOUT',18X,'TWLM',
      *19X,'GV',15X,'DT',5X)
115 FORMAT(T7,'NO.',12X,'(OF)',4X,'(OC)',5X,'(OF)',6X,'(OC)',
      *9X,'(OF)',6X,'(OC)',2X,'(LB/HR-FT2)',2X,'(KG/S-M2)',3X,
      1'(OF)',2X,'(OC)')
120 FORMAT(' ',6X,126(' ',/))
      WRITE(6,110)
      WRITE(6,111)
      WRITE(6,115)
      WRITE(6,120)
130 FORMAT(7X,I2,4X,'SM',4X,F6.2,2X,F6.2,4X,F6.2,2X,F6.2,9X,
      *F6.2,2X,F6.2,4X,F9.2,2X,F9.2,4X,F5.2,2X,F4.2)
131 FORMAT(7X,I2,4X,'STFN',2X,F6.2,2X,F6.2,4X,F6.2,2X,F6.2,
      *9X,F6.2,2X,F6.2,4X,F9.2,2X,F9.2,4X,F5.2,2X,F4.2)
132 FORMAT(7X,I2,4X,'SP11',2X,F6.2,2X,F6.2,4X,F6.2,2X,F6.2,
      *9X,F6.2,2X,F6.2,4X,F9.2,2X,F9.2,4X,F4.2,2X,F4.2)
133 FORMAT(7X,I2,4X,'SP22',2X,F6.2,2X,F6.2,4X,F6.2,2X,F6.2,
      *9X,F6.2,2X,F6.2,4X,F9.2,2X,F9.2,4X,F4.2,2X,F4.2)
      N = 96
      DO 1 I=1,N
      READ(5,2) PFL,TINL,TOU,TFL,TAVS,T(4),T(6),T(18),T(20),V,
      *A,PRTR
2  FORMAT(F5.3,2X,10F6.3,F5.3)
      AMVLT=PRTR*2.0
      PRTR = .00626 + 0.46094*AMVLT
      CALL CCNVRT(TINL,TIN)
      CALL CCNVRT(TOU,TOUT)
      TAV = (TINL+TOU)/2.0
      IF(I.GT.79) GO TO 700
      IF (I.GT.60) GO TO 600
      IF (I.GT.32) GO TO 500
      DOUT = 0.624

```

```

    DIN = 0.545
    TL = 52.5
    S = 0.96
    GOTO800
500 DCUT = 0.624
    DIN = 0.559
    TL = 53.5
    S = 0.93
    GOTO800
600 DCUT = 0.625
    DIN = 0.579
    TL = 53.0
    S = 0.93
    GOTO800
700 DCUT = 0.8725
    DIN = 0.8025
    TL = 52.5
    S = 0.93
800 CONTINUE
    CALL CCNVRT(TAV,TFAV)
    CALL CCNVRT(TFL,TFLD)
    CALL CCNVRT(TAVS,TASUR)
    DEN = 104.07-0.0827*TFLD
    MF=PFL*60.0*0.13368*DEN
    HIN = 8.1416+0.19636*TFAV+0.118E-03*TFAV*TFAV+0.3816E-07*
    *TFAV**3
    HSL=HIN
    HSV = 78.6342+0.14846*TFAV+0.22E-05*TFAV*TFAV-0.4133E-07*
    *TFAV**3
    CALL CCNVRT(T(4),TFA)
    CALL CCNVRT(T(6),TFB)
    CALL CCNVRT(T(18),TFC)
    CALL CCNVRT(T(20),TFD)
    HTLBOT = 227*(22.0/7.0*((DCUT/24.0)**2.0-(DIN/24.0)**2.0))*
1ABS(TFA-TFB)*6.0
    HTLTCP = 227*(22.0/7.0*((DCUT/24.0)**2.0-(DIN/24.0)**2.0))*
2ABS(TFC-TFD)*6.0
    ELEC = V*A*3.41*S
    HEAT=ELEC-HTLTCP-HTLBCT
    DRY=(HEAT/MF+HIN-HSL)/(HSV-HSL)
    DELT = HEAT*ALOG(DOUT/DIN)/(2.0*22.0/7.0*227*TL/12.0)
    TAVINS=TASUR-DELT
    HI(I) = HEAT/(22.0/7.0*DIN/12.0*(TL/12.0)*(TAVINS-TFAV))
    K=0.04847-0.0000657*TFLD
    ANU(I) = HI(I)*DIN/(12.0*K)
    G(I) = MF/((DIN/24.0)**2.0*22.0/7.0)
    MYU=5.57059-0.90962*ALOG(TFLD)
    RE(I) = G(I)*(DIN/12.0)/MYU
    HFG=72.537-0.08*TFAV
    KF = DRY*HFG*778*32.2/(32.2*(TL/12.0))
    RHOV=-0.643082+9.3588*1E-3*TFAV
    VM(I)=CRY/2.0/RHOV+(1-DRY/2.0)/DEN
    AQ(I) = RE(I)**2.0*KF
    PR = PRTR*0.0705

```

```

      HIG(I) = HI(I)*5.678
      HEA = HEAT*3.1423
      GX(I) = G(I)*0.001354
      TAVI = (TAVINS-32.0)/1.8
      TAS = (TAVINS - 32.0)/1.8
      TAVP = (TIN+TOUT)/2.0
      DET = TAVI-TAS
      DEL = TAVI-TAV
      DELT = TAVINS-TAVP
      IF(I.GT.79) GOTO190
      IF(I.GT.60) GOTO180
      IF(I.GT.32) GOTO170
      IF(I.LE.32) GOTO160
160  WRITE(6,130) I,TIN,TINL,TCUT,TOU,TAVINS,TAVI,G(I),GX(I),
      *DELT,DEL
      GOTO200
170  WRITE(6,131) I,TIN,TINL,TOUT,TOU,TAVINS,TAVI,G(I),GX(I),
      *DELT,DEL
      GOTO200
180  WRITE(6,132) I,TIN,TINL,TCUT,TOU,TAVINS,TAVI,G(I),GX(I),
      *DELT,DEL
      GOTO200
190  WRITE(6,133) I,TIN,TINL,TCUT,TOU,TAVINS,TAVI,G(I),GX(I),
      *DELT,DEL
200  CONTINUE
1   CONTINUE
      STCP
      END
      SUBROUTINE CONVRT(T,TFARH)
      TFARH=T*1.8+32
      RETURN
      END

```

APPENDIX C

Table. (C.1):-

REF. NO.	TYPE	TIN		TOUT		TULM		GV		OI	
		(OF)	(OC)	(OF)	(OC)	(OF)	(OC)	(UB/AIR-T2)	(KG/S-M2)	(OF)	(OC)
1	SM	119.76	48.29	118.58	48.13	128.31	53.59	47484.91	64.29	9.64	5.35
2	SM	119.66	48.79	119.48	48.69	129.52	59.18	47484.01	64.29	9.95	5.53
3	SM	120.20	49.09	120.02	48.90	132.49	55.83	47572.41	64.41	12.38	6.88
4	SM	123.38	49.10	123.38	49.13	133.99	56.66	47491.38	64.30	13.61	7.56
5	SM	119.43	48.60	119.66	48.70	133.73	56.52	47756.60	64.66	14.16	7.37
6	SM	123.74	49.33	123.74	49.33	136.22	57.90	47596.11	64.32	15.48	8.69
7	SM	123.23	49.09	120.20	49.00	132.03	55.57	71679.00	97.05	11.83	6.57
8	SM	123.74	49.30	123.74	49.33	133.71	56.51	71513.25	96.83	12.97	7.21
9	SM	123.08	50.69	123.08	50.60	136.60	58.11	71248.96	96.47	13.52	7.51
10	SM	124.70	51.50	124.52	51.40	140.22	63.12	71458.03	96.75	14.61	8.57
11	SM	116.36	47.23	117.14	47.39	126.65	52.69	83702.94	113.33	9.80	5.40
12	SM	119.22	47.90	118.22	47.90	126.71	53.73	83806.06	113.47	10.49	5.43
13	SM	113.49	48.09	118.22	47.99	129.99	54.39	83879.59	113.56	11.59	6.44
14	SM	120.56	49.23	120.56	49.23	132.97	56.10	83677.13	113.30	12.41	6.99
15	SM	121.92	49.90	122.11	50.03	135.39	57.44	83561.13	113.14	13.43	7.49
16	SM	123.10	50.63	123.26	50.73	137.92	58.95	83574.00	113.16	14.75	8.23
17	SM	120.02	48.90	120.02	48.40	139.29	54.56	95041.63	128.69	10.18	5.60
18	SM	120.56	49.23	129.74	49.39	131.70	55.39	95115.31	128.79	11.95	6.14
19	SM	122.18	50.10	122.13	50.19	134.23	56.79	95100.56	128.77	12.05	6.69
20	SM	123.38	50.63	122.91	50.59	135.57	57.54	95109.56	128.77	12.58	6.99
21	SM	123.80	51.03	123.80	51.03	137.61	58.67	95115.31	128.79	13.81	7.67
22	SM	124.52	51.40	124.70	51.53	139.16	59.53	95115.31	128.79	14.55	8.08
23	SM	120.72	48.93	120.92	48.99	139.01	59.45	119225.69	161.43	9.99	5.59
24	SM	122.00	50.03	122.00	50.03	133.36	56.31	114938.80	160.91	11.36	6.31
25	SM	121.10	49.59	121.64	49.33	135.77	56.54	119133.59	161.31	12.49	6.89
26	SM	124.52	51.40	124.52	51.40	136.95	58.33	118820.40	160.88	12.43	6.91
27	SM	125.69	52.90	125.69	52.90	139.01	59.45	113746.89	169.78	13.41	7.45
28	SM	126.59	52.53	126.59	52.53	143.04	61.46	118832.03	169.86	14.34	7.99

Table. (C-1)-(Continued)

RUG NO.	TYPE	TIN		TOUT		TUM		GV		DI	
		(OF)	(OC)	(OF)	(OC)	(OF)	(OC)	(LUB/HR-F12)	(KG/S-M2)	(OF)	(OC)
29	SM	122.36	50.20	122.54	50.30	132.79	55.99	133965.70	177.33	10.34	5.74
30	SM	123.62	53.90	123.80	51.00	135.17	57.32	133965.70	177.33	11.46	6.37
31	SM	125.24	51.80	125.06	51.70	130.96	58.92	130884.70	177.22	12.91	7.17
32	SM	127.40	53.00	127.53	53.10	141.71	60.95	130823.90	177.14	14.22	7.93
33	STFN	119.10	48.50	119.48	48.60	125.14	51.74	68333.19	92.52	5.75	3.19
34	STFN	119.30	40.50	119.48	48.60	127.36	52.98	68291.19	92.47	7.97	4.44
35	STFN	120.30	49.10	120.55	49.20	128.73	53.74	68218.69	92.40	8.26	4.54
36	STFN	121.28	40.60	121.28	49.60	131.31	55.17	68207.13	92.35	10.03	5.57
37	STFN	123.08	50.60	122.90	50.50	132.65	55.91	68049.56	92.14	9.66	5.36
38	STFN	124.98	51.60	125.06	51.70	134.93	57.18	68091.63	92.20	9.96	5.53
39	STFN	121.28	49.60	121.28	49.60	127.95	52.80	90970.94	123.17	5.77	3.20
40	STFN	122.72	50.40	122.72	50.40	129.26	54.03	90844.88	123.00	6.54	3.63
41	STFN	123.80	51.00	123.98	51.10	131.58	55.32	90676.81	122.78	7.68	4.27
42	STFN	125.24	51.80	125.06	51.70	133.30	56.28	90634.75	122.72	8.15	4.53
43	STFN	126.50	52.50	126.32	52.40	136.38	57.82	90550.75	122.61	9.67	5.37
44	STFN	128.66	53.70	128.48	53.60	138.71	59.28	90410.69	122.42	10.14	5.63
45	STFN	121.64	49.80	121.82	49.90	128.03	53.35	112855.80	152.81	6.30	3.50
46	STFN	123.62	50.90	123.80	51.00	131.12	55.97	113241.00	153.33	7.41	4.12
47	STFN	124.70	51.50	124.70	51.50	133.13	56.18	113188.40	153.26	8.43	4.68
48	STFN	126.14	52.30	126.14	52.30	135.96	57.75	113713.30	153.92	9.82	5.45
49	STFN	129.32	53.90	128.84	53.80	138.36	59.09	112938.30	152.88	9.43	5.24
50	STFN	130.82	54.90	130.82	54.90	142.31	61.12	112785.80	152.71	11.16	6.22
51	STFN	128.30	53.50	128.12	53.40	136.89	57.16	124950.10	169.18	6.08	3.71
52	STFN	129.30	54.10	129.30	54.10	136.75	58.19	124796.00	168.97	7.37	4.09
53	STFN	132.80	56.00	132.80	56.00	141.13	60.63	124545.60	168.63	8.33	4.63
54	STFN	131.88	56.60	133.70	56.50	143.68	62.04	124372.30	168.40	9.99	5.49
55	STFN	135.60	57.60	135.68	57.60	146.54	63.63	124295.30	168.30	10.86	6.13
56	STFN	124.52	51.40	124.52	51.40	131.56	55.31	135721.10	183.77	7.34	3.91
57	STFN	126.38	51.60	126.38	51.60	133.97	56.15	135847.10	183.94	8.19	4.55
58	STFN	126.14	52.20	126.32	52.10	136.72	57.62	135734.10	183.85	9.49	5.27

Table. (C-1) - (Continued)

RUN NO.	TYPE	TIN (OF)	TIN (OC)	TCUF (OF)	TCUF (OC)	THLM (OF)	THLM (OC)	GV (LB/HR-FT ²)	GV (KG/S-M ²)	DT (OF)	DT (OC)
59	STFN	129.38	54.10	129.10	54.10	139.23	59.57	135574.00	183.57	9.85	5.47
60	STFN	131.36	55.20	131.59	55.30	142.76	61.53	135364.00	183.28	11.31	6.28
61	SP11	127.95	53.31	127.95	53.31	132.03	55.57	46364.32	62.78	4.08	2.27
62	SP11	129.19	53.99	129.19	53.99	134.08	56.71	46378.68	62.80	4.89	2.72
63	SP11	129.52	54.18	129.31	54.06	135.41	57.45	46378.68	62.80	6.91	3.53
64	SP11	130.75	54.86	130.75	54.86	137.66	58.70	46443.30	62.88	6.91	3.89
65	SP11	131.96	55.48	131.45	55.25	134.92	56.68	105683.40	143.10	2.55	1.31
66	SP11	133.30	56.28	132.89	56.35	136.55	58.08	105634.50	143.03	3.46	1.92
67	SP11	134.74	57.08	134.62	57.01	139.91	59.95	105585.50	142.96	5.23	2.91
68	SP11	136.00	58.22	136.59	58.11	162.66	61.48	105618.10	143.01	5.96	3.31
69	SP11	139.27	59.59	139.47	59.71	146.14	63.41	105569.20	142.94	6.77	3.76
70	SP11	130.13	54.52	130.13	54.52	132.82	56.91	116413.20	157.62	2.68	1.49
71	SP11	133.71	56.51	133.51	56.39	136.13	57.85	116197.80	157.33	2.52	1.60
72	SP11	136.30	57.99	136.10	57.88	141.92	60.57	115910.60	156.94	4.74	2.53
73	SP11	138.98	59.43	138.77	59.32	144.62	62.57	115623.40	156.55	5.74	3.19
74	SP11	144.62	62.57	144.62	62.57	150.52	65.75	115246.50	156.74	5.80	3.22
75	SP11	136.95	57.19	136.74	57.38	136.61	58.11	126330.60	171.05	1.75	0.77
76	SP11	146.13	57.88	135.98	57.76	139.49	59.67	126311.00	171.03	3.32	1.85
77	SP11	137.62	58.68	137.62	58.68	142.49	61.38	126232.60	173.92	4.36	2.71
78	SP11	143.51	61.95	143.51	61.95	146.63	63.68	126017.30	173.63	3.12	1.71
79	SP11	145.56	63.09	145.77	63.21	151.99	66.12	125841.00	173.39	5.37	2.99
80	SP22	123.63	59.90	123.42	59.79	126.50	52.50	32942.20	44.60	2.97	1.65
81	SP22	129.30	54.10	129.20	54.00	136.98	56.71	32891.23	44.53	4.79	2.66
82	SP22	130.64	54.80	130.46	54.70	136.83	58.24	32850.46	44.48	6.29	3.43
83	SP22	123.34	51.02	123.89	51.02	127.12	52.91	49463.71	59.53	3.48	1.93
84	SP22	127.58	53.10	127.49	53.00	123.88	56.94	44160.79	59.79	3.30	1.89
85	SP22	129.92	53.99	129.02	53.90	133.46	56.35	44133.61	59.76	4.62	2.45
86	SP22	129.92	54.40	130.11	54.51	130.12	57.35	44113.21	59.73	6.11	3.41
87	SP22	131.00	55.60	130.62	54.99	130.32	59.36	44140.40	59.77	7.91	4.11
88	SP22	124.96	51.59	124.66	51.48	127.41	53.26	44466.84	66.98	2.75	1.53

Table. (C-1)-(Continued)

PUR NO.	TYPE	TIN (°F)	(°C)	TEMP (°F)	(°C)	TEMP (°F)	(°C)	GV (11.0/11.0-11.2)	(KG/S-42)	DI (11.1)	(10.1)
89	SP22	127.04	52.80	126.86	52.73	130.36	54.65	40803.23	67.43	3.41	1.99
90	SP22	128.30	53.53	128.30	53.50	133.07	56.12	40757.36	67.37	4.72	2.62
91	SP22	129.56	54.29	129.74	54.39	135.86	57.70	40696.19	67.29	6.21	3.15
92	SP22	131.36	55.20	131.36	55.20	139.08	59.99	40665.61	67.25	7.72	4.29
93	SP22	127.13	52.85	127.13	52.85	129.37	54.39	65915.00	85.25	2.24	1.24
94	SP22	128.77	53.76	128.77	53.76	131.58	55.32	65078.06	89.47	2.81	1.56
95	SP22	132.09	56.05	133.10	56.16	130.05	57.81	65904.75	89.24	3.06	1.70
96	SP22	135.36	57.42	135.36	57.42	130.63	59.79	65822.81	89.10	4.27	2.37

Table. (C-2):-

PHI NO.	TYPE	(0.710.FT2)	QAN	(0.022)	(0.710.FT2.0F)	III	(W/M2.0C)	PSIG	DP	BAR	RE	NU	X (EX11)
1	SH	2000.58	6286.43		332.43		1387.52	1.1895		0.0768	1542.84	359.34	0.4115
2	SH	2400.24	7542.28		386.24		2193.64	1.0233		0.0719	1542.84	417.61	0.4942
3	SH	2805.68	8816.21		362.94		2060.78	1.1125		0.0784	1523.67	391.03	0.5769
4	SH	3343.65	10506.75		393.48		2234.29	1.1295		0.0726	1541.24	425.21	0.6889
5	SH	3565.16	11202.79		413.11		2284.84	1.1586		0.0817	1483.91	431.25	0.7298
6	SH	3955.35	12428.89		499.05		2322.59	1.1664		0.0752	1533.04	441.79	0.8150
7	SH	2705.75	8785.37		373.63		2148.74	1.0664		0.0752	2216.35	404.40	0.3816
8	SH	3521.24	9453.54		372.91		2117.38	1.0895		0.0764	2252.06	493.17	0.4135
9	SH	3516.43	11349.68		416.25		2364.36	1.1356		0.0801	2309.46	449.80	0.4844
10	SH	4189.36	13164.23		429.83		2443.38	1.1356		0.0801	2263.99	461.86	0.5763
11	SH	5109.93	5813.94		392.27		1716.27	0.8369		0.0589	2569.11	322.47	0.2155
12	SH	2229.89	7006.96		343.32		1932.34	0.9281		0.0654	2546.96	362.26	0.2597
13	SH	2629.13	8233.14		361.92		2054.98	0.9369		0.0589	2533.12	384.72	0.3050
14	SH	3078.79	9674.50		397.19		2255.25	1.0895		0.0768	2574.65	423.97	0.3601
15	SH	3369.06	10586.61		400.30		2272.91	1.1125		0.0764	2599.61	428.36	0.3952
16	SH	3909.29	12535.27		433.01		2458.63	0.9973		0.0703	2556.84	463.24	0.4885
17	SH	2133.93	6703.86		335.69		1634.91	0.6829		0.0622	3069.69	362.14	0.2195
18	SH	2473.61	7772.83		358.57		2035.95	0.8829		0.0622	2953.72	386.50	0.2545
19	SH	2890.20	9031.98		364.15		2181.23	1.0203		0.0719	3056.91	414.21	0.2980
20	SH	3200.66	10357.44		407.39		2313.14	0.9281		0.0654	3056.91	439.25	0.3303
21	SH	3393.92	10664.71		393.65		2235.15	1.1356		0.0801	3053.72	424.32	0.3505
22	SH	3917.98	12308.63		431.24		2448.57	0.9231		0.0654	3053.72	464.84	0.4049
23	SH	1917.96	6923.96		337.35		1745.15	0.9201		0.0654	3745.49	329.63	0.1573
24	SH	2247.09	7661.02		316.71		1798.30	0.9201		0.0654	3829.13	341.68	0.1853
25	SH	2621.63	8258.09		333.60		1921.93	0.9281		0.0654	3745.36	363.53	0.2156
26	SH	3237.12	10071.72		413.13		2346.03	0.9973		0.0703	3833.12	445.87	0.2653
27	SH	3346.37	10515.29		399.67		2269.44	0.9973		0.0793	3849.10	431.78	0.2773
28	SH	3852.07	12106.37		433.27		2463.37	1.1323		0.0719	3837.11	464.45	0.3194
29	SH	2395.55	7496.12		369.52		2094.14	1.1125		0.0734	4159.43	397.31	0.1786
30	SH	2728.55	8573.91		381.24		2167.67	1.1664		0.0752	4159.43	439.51	0.2046
31	SH	4341.96	10658.56		429.86		2396.62	1.1125		0.0784	4176.93	453.31	0.2549
32	SH	4194.63	12866.72		431.97		2517.93	1.1664		0.0752	4199.98	496.71	0.3087

Table. (C-2)-(Continued)

RUN NO.	TYPE	(B/HR.FT2)	CAFN	(W/M2)	(B/HR.FT2.DF)	HI	(W/M2.OC)	PSI	DP	BAR	HE	NU	X(EXIT)
33	STIN	1821.68		5724.26	485.52		2756.78	1.6656		0.1174	2116.37	529.36	0.2477
34	STIN	2204.33		6926.66	423.63		2405.38	1.7117		0.1207	2126.12	462.40	0.2999
35	STIN	2724.51		8561.21	505.12		2068.09	1.8500		0.1304	2137.68	552.11	0.3714
36	STIN	3202.59		10314.89	501.21		2845.34	1.8500		0.1304	2144.62	548.28	0.4481
37	STIN	3714.41		11671.90	589.35		3246.36	1.8500		0.1304	2179.40	647.41	0.5091
38	STIN	4135.72		13152.78	644.03		3656.79	2.0344		0.1434	2170.12	736.68	0.5747
39	STIN	1822.07		5725.47	483.95		2747.89	1.5735		0.1109	2853.33	529.12	0.1865
40	STIN	2204.61		6927.55	516.24		2931.19	1.6656		0.1174	2381.12	565.83	0.2263
41	STIN	2722.17		8648.15	548.13		3112.39	1.7578		0.1239	2910.25	602.80	0.2834
42	STIN	3195.94		10032.61	600.44		3409.32	1.8500		0.1304	2927.55	660.88	0.3297
43	STIN	3808.44		11907.27	603.14		3624.62	1.9422		0.1365	2946.16	664.96	0.3938
44	STIN	4193.14		13176.11	633.72		3598.17	1.9883		0.1402	2977.24	700.64	0.4353
45	STIN	1865.97		5863.43	453.89		2577.18	1.5735		0.1109	3756.60	533.09	0.1540
46	STIN	2237.04		7332.20	462.61		2626.69	1.6656		0.1174	3671.06	509.60	0.1845
47	STIN	2547.53		8130.79	470.47		2671.34	1.7578		0.1239	3682.70	518.73	0.2136
48	STIN	3005.27		9694.84	481.54		2736.17	1.7578		0.1239	3721.55	532.39	0.2555
49	STIN	3577.46		11241.44	531.35		3300.93	1.8500		0.1304	3744.91	643.83	0.2975
50	STIN	4186.05		13153.84	573.29		3254.65	2.0344		0.1434	2772.21	636.06	0.3492
51	STIN	2442.64		7801.20	560.69		3234.71	1.8339		0.1272	3953.34	624.07	0.1864
52	STIN	2576.99		8097.67	535.99		3343.33	1.6656		0.1174	3987.95	588.46	0.1940
53	STIN	3196.48		10012.87	536.36		3328.34	1.9422		0.1369	4042.43	646.10	0.2413
54	STIN	3655.92		11688.01	560.50		3216.57	1.8500		0.1304	4080.87	625.79	0.2775
55	STIN	4137.49		12906.96	579.53		3390.58	1.9422		0.1269	4097.98	640.91	0.3127
56	STIN	2483.39		7833.55	540.71		3373.14	1.6656		0.1174	4442.54	596.97	0.1710
57	STIN	2796.09		8706.14	522.92		2069.12	1.8500		0.1304	4414.58	576.36	0.1924
58	STIN	3396.49		10309.98	533.59		3029.72	1.7578		0.1239	4428.55	588.61	0.2280
59	STIN	3759.13		11012.30	584.94		3321.26	1.9883		0.1402	4475.20	647.07	0.2605
60	STIN	4296.44		13217.99	669.96		3236.23	1.9883		0.1472	4521.96	632.28	0.2926
61	SP11	2341.37		7357.28	856.62		4063.88	1.6195		0.1142	1577.62	980.41	0.4415
62	SP11	2892.37		9008.68	863.19		5014.77	1.7117		0.1207	1574.31	1010.26	0.5460
63	SP11	3696.32		10507.47	873.47		4043.68	1.8500		0.1304	1574.31	995.94	0.6602

Table. (C-2)-(Continued)

NO.	TYPE	(B/10 ⁶ , J 12)	GAFF	(W/M2)	(B/10 ⁶ , J 12, 3 F)	H I	(W/M2, 3 F)	PSI	DP	EAR	RE	NU	X(EXIT)
64	SP11	4130.26	12978.50		892.38		5366.95	1.9422		0.1369	1559.47	1018.29	0.7799
65	SP11	1359.71	5043.76		1174.91		6671.14	1.4813		0.1044	3514.33	1337.57	0.1545
66	SP11	2331.31	7325.67		1006.77		5716.44	1.5274		0.1077	3525.55	1147.12	0.1941
67	SP11	2936.70	9228.90		837.62		4755.08	1.6195		0.1142	3536.77	955.18	0.2450
68	SP11	3490.25	13967.42		874.01		4962.63	1.6656		0.1174	3529.29	996.12	0.2918
69	SP11	4138.29	13903.76		912.67		5182.16	1.7578		0.1239	3540.51	1341.37	0.3472
70	SP11	1370.67	5378.29		1059.44		5937.63	1.5735		0.1199	3878.80	1181.52	0.1408
71	SP11	2355.85	7402.80		1394.19		7915.24	1.5735		0.1109	3878.10	1588.55	0.1784
72	SP11	2915.18	9169.38		918.09		5212.91	1.6656		0.1174	3944.03	1050.77	0.2220
73	SP11	3453.27	10851.21		898.02		5098.96	1.7117		0.1207	4010.24	1032.43	0.2644
74	SP11	4110.34	12915.91		1357.43		6034.11	1.9500		0.1304	4057.69	1222.94	0.3177
75	SP11	1366.36	5864.66		1587.59		9325.68	1.6656		0.1174	4329.64	1822.38	0.1302
76	SP11	2356.37	7434.43		1358.76		6011.64	1.5735		0.1109	4334.15	1214.15	0.1646
77	SP11	2954.36	9969.26		876.35		4975.89	1.6656		0.1174	4352.21	1036.10	0.1999
78	SP11	3532.45	11005.76		1675.08		9311.13	1.7394		0.1226	4401.98	1929.37	0.2473
79	SP11	4134.91	12898.37		1143.57		6476.17	1.7578		0.1239	4442.82	1316.85	0.2910
80	SP22	1678.36	5115.34		595.82		3483.35	1.1586		0.0817	1542.41	943.56	0.2238
81	SP22	1956.13	6146.73		443.73		2519.49	1.2347		0.0849	1558.65	774.68	0.2711
82	SP22	2512.59	7581.98		417.69		2312.79	1.3433		0.0547	1571.68	665.15	0.3352
83	SP22	1635.64	5119.66		517.75		2967.04	1.2047		0.0869	2043.57	837.49	0.1685
84	SP22	1834.94	5923.34		633.94		3423.62	1.2503		0.0882	1981.10	946.99	0.1942
85	SP22	2343.02	7362.46		576.72		3774.01	1.3430		0.0947	1989.70	905.46	0.2419
86	SP22	2816.12	3848.77		533.98		2444.58	1.4352		0.1312	1996.15	787.21	0.2912
87	SP22	3391.93	17501.34		493.77		2736.61	1.5453		0.1393	1987.55	770.31	0.3457
88	SP22	1678.79	5118.14		654.92		2661.34	1.3233		0.0719	2296.59	1319.32	0.1493
89	SP22	1769.61	6135.96		627.27		3561.22	1.2969		0.0914	2193.12	979.27	0.1797
90	SP22	2402.44	7509.17		553.77		3149.28	1.2508		0.0882	2204.59	866.35	0.2198
91	SP22	2909.75	9153.33		509.51		2934.32	1.5813		0.1344	2223.91	798.61	0.2673
92	SP22	3443.76	10811.89		464.41		2759.51	1.5274		0.1377	2233.58	760.12	0.3165

Table. (C-2)- (Continued)

RUN NO.	TYPE	(B/HR.FT2)	CAFN (W/M2)	(B/HR.FT2.OF)	HI (W/M2.OC)	PSI	DP	DAR	RE	NU	X(Exit)
93	SP22	1614.51	5073.27	783.59	4448.71	1.1125		0.0784	3075.08	1239.75	0.1114
94	SP22	2076.05	6523.57	803.75	4563.73	1.1586		0.0817	3023.29	1266.12	0.1431
95	SP22	2669.68	8388.92	948.44	5385.23	1.3891		0.3979	3078.32	1501.15	0.1854
96	SP22	3193.93	10036.26	813.45	4618.78	1.4813		0.1044	3110.79	1291.11	0.2227

APPENDIX D

ADDITIONAL INFORMATION ON THE INSTRUMENTATION
AND COMPONENTS USED IN THIS STUDY1) R-113 FLOW CIRCUITA. Components:

1. Refrigerant-113 Liquid Circulating Gear Pump:

Sherwood Alear Siegler Company
Bronze Rotary Gear Pump
Model: S and V series
R.P.M.: 1725
Pipe Size: 1/4"
Shaft Diameter: 1/2"
H.P.: 1/3
Dripless Mechanical Shaft Seal, Self Lubricated

2. Refrigerant-113 Liquid Circulating Pump Motor:

Dayton - Electric A.C. Motor
Model No.: 5K991
R.P.M.: 1725
H.P.: 1/2
HZ: 60

3. Refrigerant-113 Filter:

Sparlan - Catchall Refrigerant Filter
Type: C-304

4. Refrigerant-113 Liquid Receiver:

Midland-Ross Refrigerant Type Circular Tank
Serial No.: 2193
Size: 3.5 gallons
Working Pressure: Max. allowable working pressure 400 psi at
650°F

5. Refrigerant-113 Valves:

Diaphragm Packless Line Valves
Superior Brand, Solder to Solder Type
A. Model No.: 214-4S (1/4")
B. Model No.: 216-10S (5/8")

6. Refrigerant-113 Tube Connectors:

Standard Copper tube
Sweat Fitting type

7. Test Section, and preheaters, locally constructed:

Material: Copper Tubing,
Heating Element: Ribbon type chromel of $0.204 \Omega / 30.48 \text{ cm}$

Teflon tape: Saunder type S-17
Epoxy: Armstrong A-68 and B-68 types

8. Thermocouples

Copper Constantan thermocouple of type B and S 24 gauge

B. Instrumentation

1. Refrigerant-113 Flow Meters

a. Fischer-Porter Variable Area Type Flow Meter
Range: $0 \sim 0.35 \text{ gpm liquid}$
Model: 10A3565S
Serial No.: 720714733A2
Tube No.: FP-1/2-27-G-10/55

b. Fischer-Porter Variable Area Type Flow Meter
Range: $0 \sim 0.5 \text{ gpm liquid}$
Model: 10A3565S
Serial No.: 7207A4733A1
Tube No.: FP-1/2-17-G-10/55

2. Refrigerant-113 Pressure Gauge

Heise Pressure Gauge of Type H28832
Range: $0 \sim 200 \text{ psig}$

3. Pressure Transducer:

Pace Wiancko Division of Whittaker Corporation:
Model: KP15
Serial No.: 150330

4. Transducer Indicator

Pace Wiancko Division of Whittaker Corporation
Model: CD25
Serial No.: 23449

5. Voltage Regulator

Superior Electric Co.
Powerstat Variable Autotransformer

Input: 240 V, 60 Hz
Output: 0 - 280 V, 28 A, 7.8 kW

6. A.C. Ampere Meter:

Daystrom, Incorporated Weston Instruments Div.
Weston Instruments, Inc.
New York, New Jersey
Model: 433 No. 164330

7. A.C. Volt Meter:

Daystrom, Incorporated Weston Instruments Div.
Weston Instruments, Inc.
New York, New Jersey
Model: 433 No. 146652

8. Data Acquisition System:

Esterline Angus, an Esterline Company
Model: PD-2064
Type: Key Programmable.

The system can gather analog and digital data from up to 64 channels under the control of tiny microprocessor. The system outputs the measured values in engineering or scientific units through various output devices. The solid state integrated circuit microprocessor is combined with RAMS (random access memory devices), ROMS (read-only memory devices), and PROMS (programmable ROMs) to provide a keyboard-programmable system that permits the instrument to scan, measure, collect, identify, and record both analog and digital input signals.

Accuracy:

With Ambient Temperature at $77^{\circ}\text{F} \pm 9^{\circ}\text{F}$

$\pm 0.01\%$ of reading, $\pm 0.015\%$ full scale, ± 1 count on 4000 MV range;
 $\pm 0.01\%$ of reading, $\pm 0.03\%$ full scale, ± 1 count on 400 MV range;
 $\pm 0.0\%$ of reading, $\pm 0.04\%$ full scale, \pm count on 40 MV range.

Over Full Operation Ambient Temperature Range of 32°F to 122°F

$\pm 0.5 \mu\text{V}$ per $^{\circ}\text{C}$, $\pm 0.01\%$ of reading, $\pm 0.04\%$ full scale, ± 1 count on all ranges.

9. Vacuum Pump

Matheson Scientific
Division of Will Ross, Inc.

Serial No.: 1173
Power: 115 V, 60 Hz
Connections: 3 conductor power cord with 2 prong adaptor.
Inlet and outlet connector to 3/8" I.D. hose.
Function: Portable A.C. powered source of vacuum (to 686 mm/
27" Hg) or pressure (to 1.7 kg/cm², 25 psig)

2) WATER FLOW CIRCUIT

1. Cooling Water Flow Meters:

- a. Brooks Rotameter
Type: 1110 - 09H3A1B
Serial No.: 7201-74650/1
Tube No.: R-9M-25-1 BR-3/4-14G10
Range: 0 ~ 3 GPM
- b. Brooks Rotameter
Type: 1
Serial No.: R-9M-25-2
Range: 0 ~ 2 GPM

2. Cooling Water Pump:

A.O. Smith Co. Pump.
Model No.: C48L2DA11A4
Serial No.: J69
H.P.: 1
R.P.M.: 3450
Hz: 60

APPENDIX E

Table E.1. Tabulation of Statistical Information for the Curve fits to the Experimental Overall Heat Transfer Coefficient

x_{OUT}	TUBE NO.	n	c	Correlation Coefficient
0.17 -	1	0.3563	5.4	0.7527
0.231	2	0.1988	50.89	0.7550
	3	1.66	3.83×10^{-6}	0.8800
	4	0.648	0.571	0.7786
0.243 -	1	0.499	1.187	0.9796
0.285	2	0.239	34.28	0.7144
	3	1.5	2.307×10^{-5}	0.9011
	4	0.3501	11.041	0.9856
0.295	1	0.4757	1.67	0.9590
0.332	2	0.4152	4.58	0.7885
	3	1.75	1.396×10^{-6}	0.9900
	4	0.395	6.584	0.9385
0.350 -	1	0.214	35.86	0.7171
0.512	2	0.2511	38.13	0.800
0.576 -	1	0.206	5.11	0.6047
0.815				

Table E.2. Tabulation of Statistical Information for the Curve fits to the Experimental Overall Pressure Drop.

x_{OUT}	TUBE NO.	n'	c'	Correlation Coefficient
0.17 -	1	0.515	2.39×10^{-3}	0.876
0.231	2	0.257	0.086	0.766
	3	0.399	0.0155	0.7168
	4	0.293	0.0554	0.8872
0.243 -	1	0.391	0.0105	0.844
0.285	2	0.231	0.1264	0.8963
	3	0.293	0.0566	0.999
	4	0.518	0.0055	0.99
0.295 -	1	0.318	0.0249	0.67
0.332	2	0.1998	0.1859	0.961
	3	0.553	0.0029	0.999
	4	0.345	0.0377	0.933
0.35 -	1	0.099	0.3643	0.725
0.512	2	0.173	0.2718	0.9897
0.576 -	1	0.1029	0.36	0.67
0.815				

APPENDIX F

UNCERTAINTY ANALYSIS IN EXPERIMENTAL MEASUREMENTS OF
OVERALL HEAT TRANSFER COEFFICIENTThe Uncertainty Intervals for Individual Measurements

<u>Measurements</u>	<u>Run No. 17</u>	<u>Smooth Tube 1 Uncertainty Interval</u>
1. Tube radius		± 0.001 ft
2. Freon temperature		$\pm 0.6^{\circ}\text{F}$
3. Tube wall temperature		$\pm 0.6^{\circ}\text{F}$
4. Pressure		± 0.3 psi
5. Tube length		± 0.002 ft
6. Freon flow rate		$\pm 1.0\%$ of flow
7. Inlet enthalpy of R-113		± 0.15 Btu/lbm
8. Energy transfer W_Q		$\pm 6\%$ of Q
9. R-113 specific heat		± 0.01 Btu/.bm $^{\circ}\text{F}$
10. R-113 viscosity		± 0.01 lbm/ft. hr.
11. R-113 thermal conductivity		± 0.005 Btu/ft $^{\circ}\text{F}$

Uncertainty Analysis in Experimental Measurements of Average Heat Transfer Coefficient

An error analysis of the uncertainty in the experimental measurements of the heat transfer coefficient, was carried out.

The uncertainty for the smooth tube 1, Run no. 17, is estimated below, using the method of Kline and McClintock [44].

The average heat transfer coefficient is calculated by:

$$h = \frac{Q}{A(T_{WL} - T_{av})} \quad (1)$$

when T_{WL} = the average wall temperature

T_{av} = the average of the inlet and outlet temperatures.

The experimental uncertainty for the average heat transfer coefficient is given by

$$w_h = \left[\left(\frac{\partial h}{\partial Q} w_Q \right)^2 + \left(\frac{\partial h}{\partial A} w_A \right)^2 + \left(\frac{\partial h}{\partial T_{av}} w_{T_{av}} \right)^2 + \left(\frac{\partial h}{\partial T_W} w_{T_W} \right)^2 \right]^{1/2} \quad (2)$$

From (1)

$$\frac{\partial h}{\partial Q} = \frac{1}{A(T_W - T_{av})}$$

$$\frac{\partial h}{\partial A} = - \frac{Q}{A^2(T_W - T_{av})}$$

$$\frac{\partial h}{\partial T_W} = - \frac{Q}{A(T_W - T_{av})^2}$$

$$\frac{\partial h}{\partial T_{av}} = \frac{Q}{A(T_W - T_{av})^2}$$

For the particular run under consideration:

$$A = \pi D_i L = \pi \left(\frac{0.545}{12} \right) \left(\frac{52.5}{12} \right) = 0.6242 \text{ ft}^2$$

$$T_{av} = 120.02^\circ\text{F}; T_{WL} = 130.2^\circ\text{F}; m = 151 \text{ lb/hr}; Q = 2134 \text{ Btu/hr}$$

$$\frac{\partial h}{\partial Q} = \frac{1}{0.6242(130.2 - 120.02)} = 0.1574$$

$$\frac{\partial h}{\partial A} = \frac{-2134}{(0.6242)^2(130.2 - 120.02)} = -538.02$$

$$\frac{\partial h}{\partial T_W} = \frac{-2134}{(0.6242)(130.2 - 120.02)^2} = -32.99$$

$$\frac{\partial h}{\partial T_{av}} = \frac{2134}{(0.6242)(130.2 - 120.02)^2} = 32.99$$

It was estimated that the uncertainty in heat transfer Q is $\pm 6\%$, therefore $W_Q = \pm .06$. Uncertainty for energy transfer, W_Q :

$$= \frac{6}{100} \times 2134 = \pm 128.04 \text{ Btu/hr} \quad (3)$$

Uncertainty for heat transfer area:

$$(A = 2 \pi r L)$$

$$\begin{aligned} W_A &= \left\{ \left(\frac{\partial A}{\partial r} W_r \right)^2 + \left(\frac{\partial A}{\partial L} W_L \right)^2 \right\}^{\frac{1}{2}} \\ &= \{ (2\pi L W_r)^2 + (2\pi r W_L)^2 \}^{\frac{1}{2}} \end{aligned} \quad (4)$$

Substituting Eq. (3) and Eq. (4) into (2) gives the uncertainty for h as:

$$W_h^2 = \frac{1}{A^2(T_W - T_{av})^2} (W_Q)^2 + \frac{Q^2}{(T_W - T_{av})^2} \frac{1}{A^4} [(2\pi L W_r)^2 + (2\pi r W_L)^2] \\ + \frac{Q^2}{A^2(T_W - T_{av})^4} W_{TW}^2 + \frac{Q^2}{A^2(T_W - T_{av})^4} W_{Tav}^2$$

$$W_h^2 = \frac{1}{(0.6242)^2 (130.2 - 120.02)^2} \times (128.04)$$

$$+ \frac{(2134)^2}{(130.02 - 120.02)^2} \frac{1}{(0.6242)^4} [(2\pi \times \frac{52.5}{12} \times 0.001)^2$$

$$+ (2\pi \times \frac{0.545}{12} \times 0.002)^2] + \frac{(2134)^2}{(0.6242)^2 (130.02 - 120.02)^4} \times (0.6)^2$$

$$+ \frac{(2134)^2}{(0.6242)^2 (130.2 - 120.02)^4} \times (0.6)^2$$

$$= 3.171 + 218.77 + (391.79 \times 2) = 1005.52$$

$$\therefore W_h = \pm 31.709 \text{ Btu/hr ft}^2 \text{ } ^\circ\text{F}$$

$$\text{Therefore, } h = 335.49 \frac{\text{Btu}}{\text{hr ft}^2 \text{ } ^\circ\text{F}} \pm 31.709$$

$$\therefore \text{Uncertainty for this run is about } \pm \underline{\underline{9.45\%}}.$$

APPENDIX G
CALIBRATION OF PRESSURE TRANSDUCER

The pressure transducer was calibrated by a dead weight tester. Different weights were added to the dead weight tester and the corresponding voltage registered in the voltmeter, connected to the transducer indicator. A calibration curve of pressure versus the voltage was drawn as shown in Fig. G-1. The following equation was used in determining the values of the pressure drop.

$$\Delta p \text{ (psi)} = 0.00626 + 0.46094 * V \text{ (millivolts)}.$$

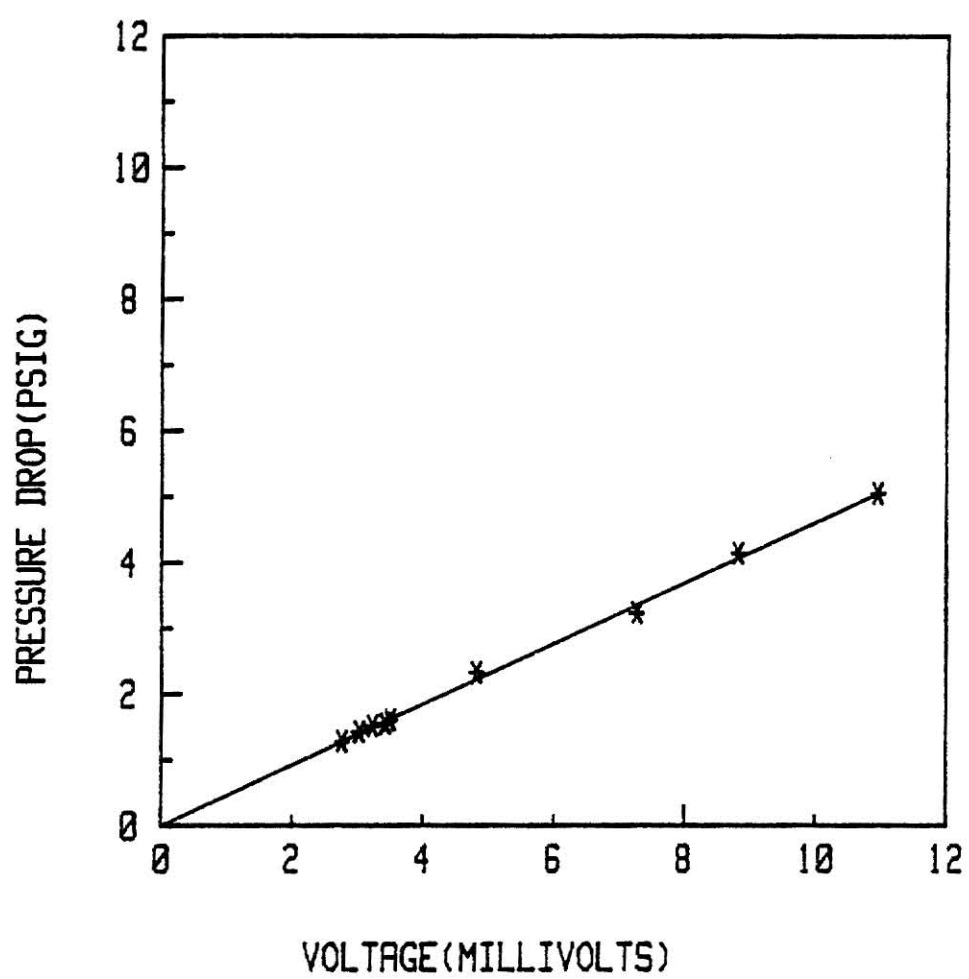


Fig. G.1 Calibration curve for Pressure Drop

CURRICULUM VITA

VISWANATHAN SIVAKUMAR

Candidate for the Degree of
Master of Science

Thesis: AUGMENTATION OF BOILING HEAT TRANSFER BY INTERNALLY FINNED TUBES

Major Field: Mechanical Engineering

Biographical:

Personal Data: Born in Salem, Tamilnadu, India, January 27, 1959.

Education: Graduated from St. Patricks High School, Madras, 1975;

Bachelor of Engineering degree with Honors, in Mechanical Engineering, College of Engineering, Guindy, University of Madras, 1980; completed requirements for Master of Science, Kansas State University, 1982.

Research Experience: Graduate Research Assistant, Dept of Mechanical Engineering, Kansas State University, 1980-1982.

AUGMENTATION OF BOILING HEAT TRANSFER
BY INTERNALLY FINNED TUBES

by

VISWANATHAN SIVAKUMAR

B.E. (Hons.), University of Madras, Madras, India, 1980

AN ABSTRACT OF MASTER'S THESIS

submitted in partial fulfillment of the

requirements for the degree

MASTER OF SCIENCE

Department of Mechanical Engineering

KANSAS STATE UNIVERSITY

Manhattan, Kansas

1982

AUGMENTATION OF BOILING HEAT TRANSFER BY INTERNALLY FINNED TUBES

ABSTRACT:

Heat transfer and pressure drop data were taken during saturated boiling inside four vertical electrically heated tubes.

One tube was smooth, and the remaining three were internally finned with different fin geometries. The smooth tube results were used to identify, among the existing smooth tube heat transfer and pressure drop correlations, the best predictors of the experimental measurements of the present study. Appropriate modifiers were identified and applied to the smooth tube correlations to bring about the best agreement between the measurements and predictions.

The results are summarized below.

1. On a nominal area basis, an enhancement in heat transfer coefficients as high as 230% over the smooth tube, was obtained with the internally finned tubes.

2. The augmentation in heat transfer was not without an increase in pressure drop, with values ranging as high as 170% over the smooth tube pressure drop values for the same mass flux.

3. Three new correlations were developed for predicting the saturated boiling heat transfer coefficients for internally finned tubes. The correlation based on Pierre's parameter was the best predictor of the experimental measurement.

4. A new correlation was developed for predicting the pressure drop during saturated boiling inside internally finned tubes.

5. The performance of the tubes tested, was evaluated by the ratio of the pumping power to the heat transfer rate, subject to the constraints of fixed geometry, inlet temperature and flow rate. The smooth tube required the least power when compared to the finned tubes.